DEVELOPMENT OF QUANTUM CHEMISTRY-BASED POLARIZABLE POTENTIAL TO DESCRIBE INTERMOLECULAR INTERACTIONS OF NONIONIC POLYMERS WITH WATER

by

Oleg N. Starovoytov

A dissertation submitted to the faculty of
The University of Utah
in partial fulfillment of the requirements for the degree of

Doctor of Philosophy

Department of Materials Science and Engineering

The University of Utah

May 2011

The University of Utah Graduate School

STATEMENT OF DISSERTATION APPROVAL

The dissertation of **Oleg N. Starovoytov**

has been approved by the following supervisory committee members:

Grant D. Smith	, Chair	**02.22.2011** Date Approved
Thomas E. Cheatham	, Member	**02.22.2011** Date Approved
Feng Liu	, Member	**02.22.2011** Date Approved
Dmitry Bedrov	, Member	**02.18.2011** Date Approved
Oleg Borodin	, Member	**02.18.2011** Date Approved

and by **Anil V. Virkar**, Chair of the Department of **Materials Science and Engineering**

and by Charles A. Wight, Dean of The Graduate School.

ABSTRACT

A new quantum chemistry-based, atomic point polarizable dipole potential was developed for molecular dynamic (MD) simulations of poly (ethylene oxide) (PEO) and poly (propylene oxide) (PPO) aqueous solutions employing a modified version of a single water molecule with four interaction sites and Drude polarizability (SWM4-DP). A two-extended charge ether model has been chosen as best describing electrostatic potential of DME. Ether/water interactions were parameterized to reproduce the binding energy of water with 1,2-dimethoxyethane (DME) that was determined from high-level quantum chemistry calculations. The DME/water nonbonded parameters were found to be transferrable to 1,2-dimethoxypropane (DMP).

An accuracy of the developed force field was justified by comparing thermodynamics properties obtained from molecular dynamics simulations with experimental data including free energy, enthalpy, and entropy of DME solvation. Free energy of DME solvation in water was obtained employing a new interface transit method (ITM) followed by calculations using perturbation theory. Simulations of DME/water solutions at room temperature using the new polarizable force field yielded enthalpy of solvation in a good agreement with experiment.

Simulations of PEO/water and PPO/water solutions improved ability of the new force field to capture, at least qualitatively, low critical solution temperature (LCST) behavior in these solutions.

The predicted miscibility of PEO and water as a function of temperature was found to be strongly correlated with the predicted free energy of solvation of DME in water for the various force fields investigated. Intermolecular pair correlations are employed to analyze phase behavior of nonionic polymers in aqueous solution.

Dedicated to my family

TABLE OF CONTENTS

ACKNOWLEDGMENTS

The author would like to gratefully acknowledge the enormous support of Professor Grant D. Smith and research assistant professors Dmitry Bedrov and Oleg Borodin for their teaching, guidance, patience, and help in completing this work. I am very thankful to them for their vital role in developing my perspective on the research. I also would like to thank Professor Thomas E. Cheatham and Professor Feng Liu for their time, valuable comments, and corrections on my work.

Special thanks to the Department of Materials Science and Engineering of the University of Utah, especially to Professor Anil V. Virkar, Professor Grant D. Smith, and Professor Feng Liu for their great lectures and challenging exams.

Acknowledgments are expressed for the financial support from the National Science Foundation through grants CBET-0708368 and MRSEC (University of Colorado) DME-0213918.

1. INTRODUCTION

Water is a good dispersive medium for broad spectra of compounds including rare gases, polymers, and metals.[1] Good solvation properties of water can be attributed to its polar nature as having a permanent dipole moment. A mixture of water with inorganic or organic elements is often referred to as an aqueous solution. Aqueous solutions can be comprised of many unlike compounds that are solvated, or hydrated, forming binary, ternary, and higher order multicomponent systems. These aqueous solutions usually show a complex phase behavior as a function of temperature and concentration. This complex behavior has been investigated for many years and it is still a subject for experimental, theoretical, and computer simulation studies. Understanding of molecular interactions, molecular forces, and energies associated with solvation or hydration of solutes is of fundamental and practical importance. Molecular interactions reveal many solvation phenomena including hydrophobic hydration,[2] self-assembly,[3,4] helix-coil conformational transition,[5,6] and "close loop" phase behavior.[7,8] Some of the compounds involved in such phenomenological behavior are alkanes, alkyls, surfactants, lipids, nucleic acids, peptides, proteins, polysaccharides, and a wide class of amphiphilic block copolymers including polyethers.[1] These aqueous solutions are usually characterized in terms of solvation or hydration structures, thermodynamic and dynamic solution properties, and kinetic mechanisms of the solvation and molecular self-association.[4]

The present work is primarily focused on the studies of polyether/water solutions by means of nonbonded intermolecular interactions. It involves three consecutive steps: (a) literature review of previous experimental, theoretical, and computer simulation studies; (b) force field development and parameterization of nonbonded PEO/water intermolecular interactions based on *ab initio* calculations; and (c) molecular dynamics simulations and characterization of PEO/water and PPO/water aqueous solution's phase behavior.

1.1. Poly (ethylene oxide) and poly (propylene oxide) nonionic polymers

Poly (ethylene oxide) or PEO is a nonionic polyether also known as poly (ethylene glycol) or PEG. Repeat unit of poly (ethylene oxide) is ethylene oxide, as shown in Figure 1. PEO can exist with various terminal groups including methyl ($-CH_3$), hydroxyl (-OH) and a combination of the two. One of the most important characteristics of PEO is an ability to dissolve in water for a wide range of molecular weights and temperatures forming homogeneous aqueous solutions. It is biocompatible, nontoxic, and nonreactive, which makes it attractive for a wide variety of practical applications ranging from biomedical to viscosity modification.[9-11]

Poly (propylene oxide) or PPO is a nonionic polyether also known as poly (propylene glycol) or PPG. Repeat unit of poly (propylene oxide) is propylene oxide, as also indicated in Figure 1. Poly (propylene oxide) is a structurally similar compound to PEO having and additional methyl group on a central carbon of a repeat unit.

PPO can exist with various terminal groups including that indicated for PEO. Despite structural similarity with PEO backbone, PPO exhibits a strong temperature

Figure 1. Chemical structures of 1,2-dimethoxyethane (a), 1,2-dimethoxypropane (b), poly (ethylene oxide) (c), and poly (propylene oxide) (d) compounds, where n is the number of repeat units.

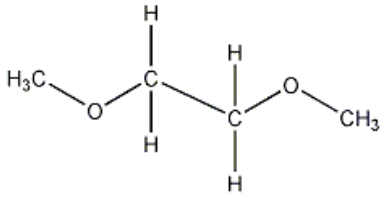

(a)

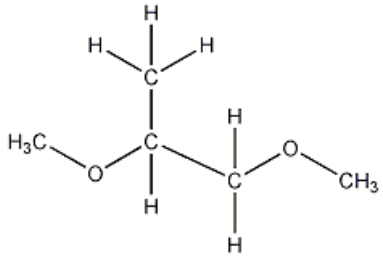

(b)

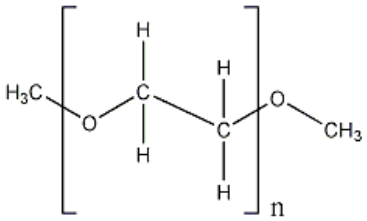

(c)

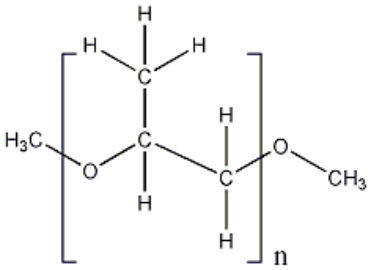

(d)

dependence in water becoming insoluble for low molecular weights at moderate and elevated temperatures. A wide range of practical applications can also be attributed to the unique interactions of PEO and PPO with water when single chains of PEO and PPO are combined to form PEO-PPO diblock or PEO-PPO-PEO triblock copolymers.[12,13]

These diblock and triblock copolymers exhibit a self-associating phenomenon when placed in water. Many of these amphiphilic block copolymers utilize PEO as a soluble block and PPO as an insoluble block for various architectures.[9-11] The well known PEO-PPO-PEO triblock architectures as produced by BASF are referred to as Pluronics®.[14] At low concentrations and temperatures, Pluronics® typically exist as fully solubilized, isolated chains, or unimers. Transition from the unimer to micelle state occurs with increasing concentration or temperature when critical micelle concentration (CMC) or critical micelle temperature (CMT) is reached.[15-24] As a result, spherical micelles are formed with external PEO coronas and central PPO cores are often observed.[25,26] Other structures are achievable with particular length ratios of hydrophilic and hydrophobic blocks.[26,27] The self-assembly of PEO-PPO-PEO triblock polymers in water into micelles with increasing temperature is thought to be due to the increasing hydrophobicity of the central PPO block while PEO remains soluble as water becomes a poor solvent for PPO.[7,8,28,29] In this context, solution thermodynamics and the phase behavior of PEO and PPO in aqueous solution is quite relevant to consider.

1.2. Survey of experimental studies of PEO and PPO aqueous solutions

There was a lot of attention to thermodynamic,[30-28] dynamic,[30,35] and structural[36] properties of PEO and PPO aqueous solutions. Most of the thermodynamic and dynamic

properties were obtained for DME/water solutions. Thermodynamic properties of interest included excess volume ΔV^E, free energy of solvation ΔG_{solv}, enthalpy of solvation ΔH_{solv}, enthalpy of mixing ΔH_{mix}, and others. Dynamic properties included excess viscosity $\Delta\eta^E$ and water self-diffusion coefficient D_w. Phase behavior of PEO/water and PPO/water solutions were also a subject of extensive experimental investigations.[7,8,29-38] Experimental studies of PEO/water and PPO/water solutions as a function of temperature provided the positions of LCST and UCST temperatures for wide molecular weights. In addition, systematic investigations have been carried out to study the effect of various terminal groups, molecular weight, and concentration on solvation properties of these compounds.

Das et al. determined excess volume ΔV^E and excess viscosities $\Delta\eta^E$ for DME/water solutions at 298 K, 308 K, and 318 K.[30] It has been pointed out that the sign and magnitude of an excess volume of binary solutions give an estimate to the strength of intermolecular interactions.[30] Positive values of excess volume indicate weak, unfavorable solute/solvent intermolecular interactions while negative values indicate strong, favorable solute/solvent intermolecular interactions. Results of experimental excess volumes and excess viscosities as a function of concentration are compared for two temperatures in Figure 2 (a-b). Comparison of those results indicates no temperature dependence in excess volume and strong temperature dependence in excess viscosity of DME/water solutions.

Biros et al. performed calorimetric investigations of PEG/water solutions.[31] Effect of hydroxyl (-OH) and methyl ($-CH_3$) groups on interactions of oligomers with water was studied by measuring enthalpy of mixing. Experimental results were analyzed and

Figure 2. Excess volume ΔV^E (a) and excess viscositiy $\Delta\eta^E$ (b) are given as a function of DME concentration from experiment at 298 K and 318 K. These graphs were reproduced from Ref. [30]

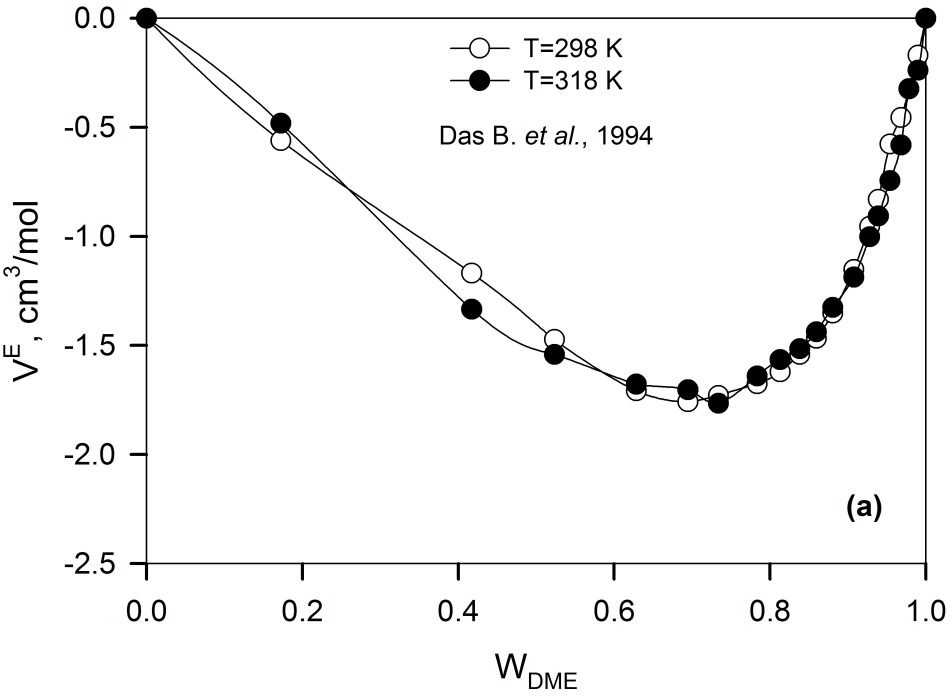
T=298 K
T=318 K
Das B. et al., 1994
(a)
V^E, cm^3/mol
W_{DME}

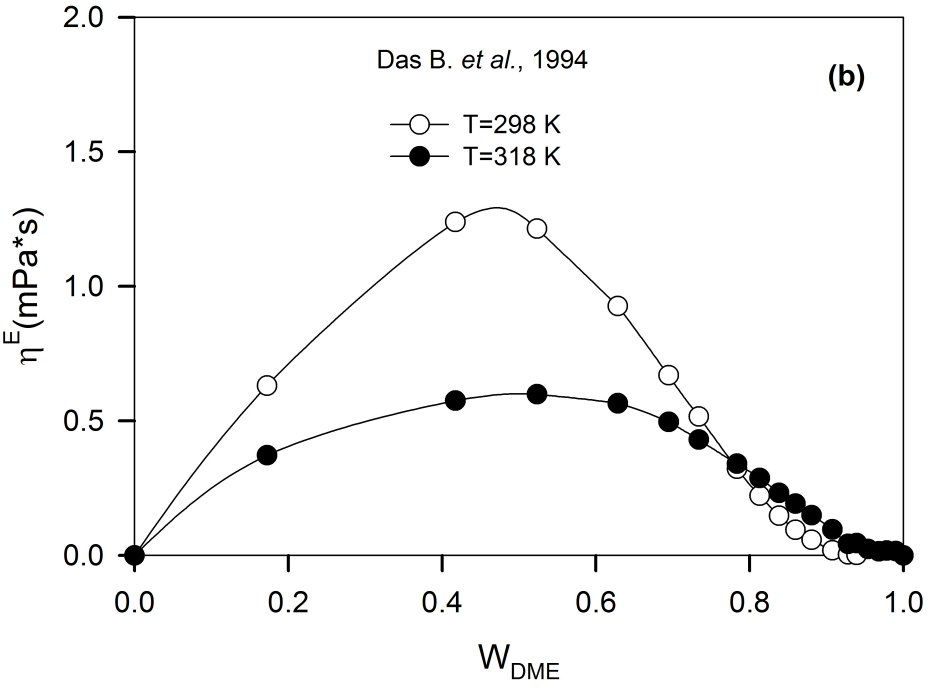
Das B. et al., 1994
(b)
T=298 K
T=318 K
η^E(mPa*s)
W_{DME}

compared for various chain lengths, end groups, and solution concentrations. It was suggested that enthalpy of mixing strongly depends on chain length, type of an end group, and concentration. The formation of hydrogen bonds was referred to as the most preferable intermolecular interactions of PEG with water. Two different solvation mechanisms were proposed for dilute and concentrated solutions.[31] Favorable intermolecular interactions between oxygen of ether and water were referred to as a solvation mechanism for dilute solutions. Chain "cooperativity" was referred to as a solvation mechanism for concentrated, polymer rich solutions.[31,32]

Dohnal et al. measured enthalpies of mixing of highly dilute aqueous solutions for a number of organic molecules at 298 K and determined limiting partial molar excess enthalpies.[33] The solvation of poly (ethers) was found to be energetically favorable as it was indicated by exothermic solvation. Linear dependence of excess enthalpies was obtained as a function of molecular weight. Increase in excess enthalpies was observed with increasing a polymer molecular weight. In particular, linear dependence of excess enthalpies was obtained for DME, diglyme, triglyme, and tetraglyme oligomers of PEO.[33]

Kustov et al. carried out calorimetric measurements of enthalpies of DME solvation in water/1-propanol and water/glycerol solvents.[34] Those measurements have been performed at 298 K for highly dilute DME concentrations. Favorable interactions of DME with water were confirmed by obtaining negative enthalpies of solvation with corresponding exothermic reactions.[34]

Experimental results by Biros et al., Dohnal et al., and Kustov et al., are summarized in Figure 3 (a-b). Enthalpies of DME solvation ΔH_{solv} and enthalpies of mixing ΔH_{mix} (c) are given as a function of DME concentration at 298 K. The area in the

Figure 3. Enthalpy of DME solvation (ΔH_{solv}) is given for the entire concentration (a) and for the dilute solutions (b). Enthalpy of mixing (ΔH_{mix}) is given for the DME aqueous solutions (c) at 298 K as obtained from experiments. These graphs were reproduced from Ref. [31,33,34]

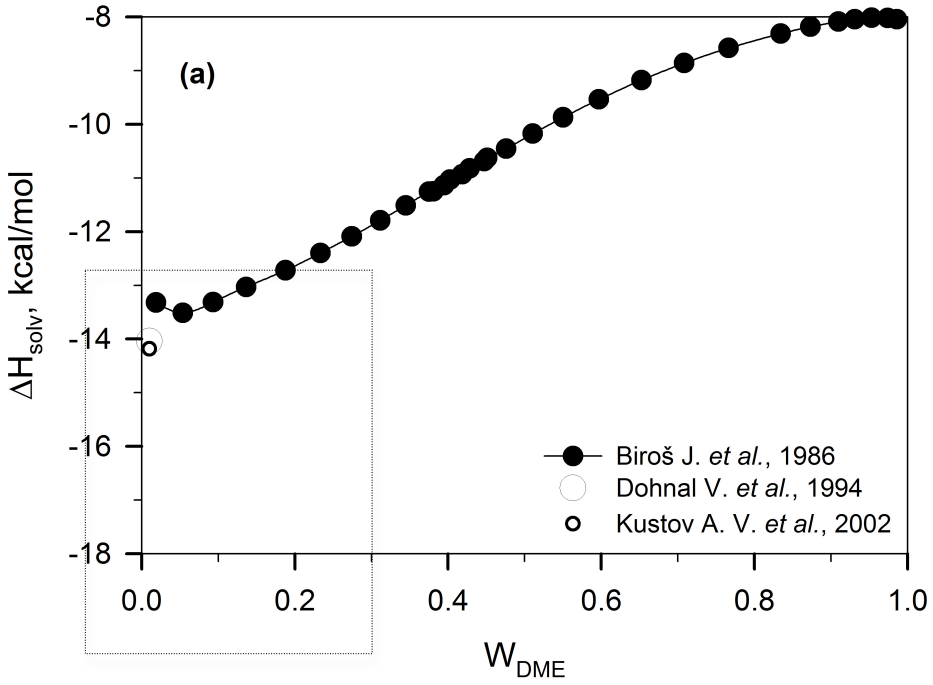
(a)
-8
-10
-12
-14
-16
-18
0.0
0.2
0.4
0.6
0.8
1.0
ΔH_solv, kcal/mol
W_DME
Biroš J. et al., 1986
Dohnal V. et al., 1994
Kustov A. V. et al., 2002

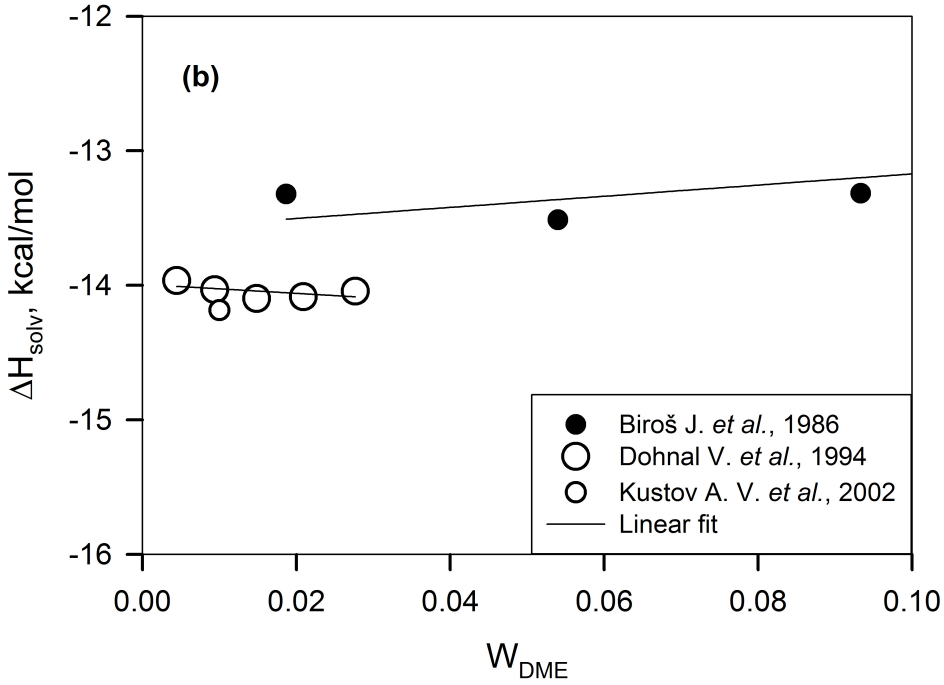
(b)
-12
-13
-14
-15
-16
0.00
0.02
0.04
0.06
0.08
0.10
ΔH_solv, kcal/mol
W_DME
Biroš J. et al., 1986
Dohnal V. et al., 1994
Kustov A. V. et al., 2002
Linear fit

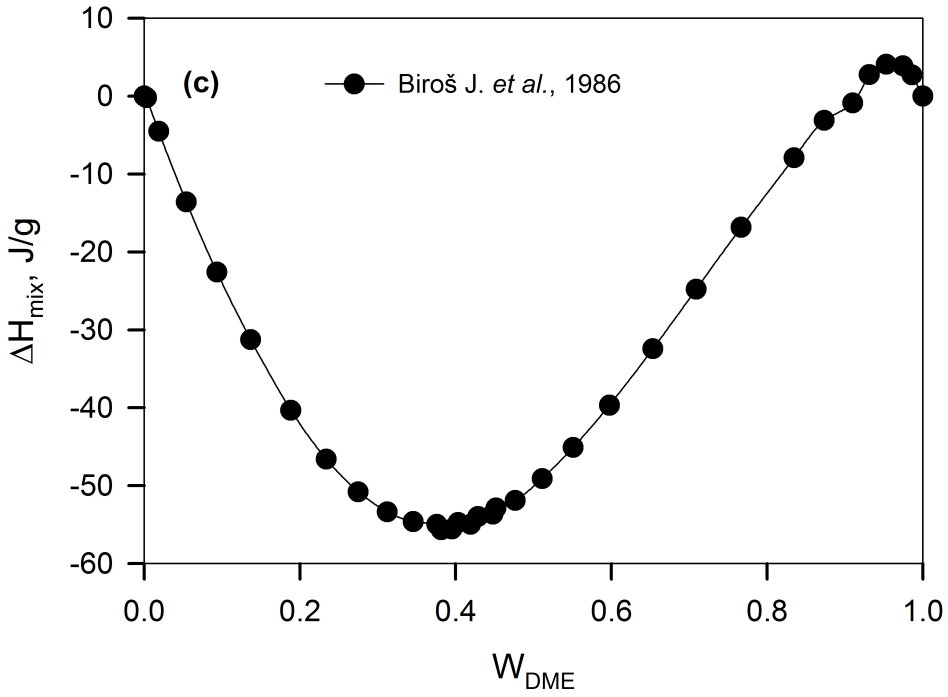

Figure 3. Continued

frame of Figure 3 (a) is zoomed in as shown in Figure 3 (b) to compare experimental results for dilute concentrations of DME.

Trouw et al. carried out QENS measurements of water self-diffusion coefficients for DME/water solutions as a function of DME concentration at 318 K.[35] Water self-diffusion coefficients D_w have been obtained by fitting scattering results to the theoretical model using Teixeira approach.[39] This theoretical approach consists of two independent test models including jump translational motion of the center of mass and rotational diffusion models.

The translational water self-diffusion coefficients are summarized in Figure 4 as obtained from QENS measurements and fitting to the jump translation model.[35] Water self-diffusion coefficients are also included as obtained for pure water at 318 K using the isotopic method[40] and pulsed magnetic field gradient NMR method[41] for comparison.

Bieze et al. studied the water structure around PEO using the neutron diffraction technique.[36] The radial distribution functions have been obtained and distribution of water around polymer protons was built based on those radial distributions.

Bae et al. performed thermo-optical measurements of cloud points for various molecular weights of PEG.[7] The solute/solvent intermolecular interactions were referred to as “oriented dependent” interactions or specific interactions also known as hydrogen bond. A standard “close loop” behavior was determined for all molecular weights studied. The positions of LCST and UCST temperatures were found to strongly depend on molecular weight of PEG. However, “closed loop” solvation behavior of PEG was found to disappear completely for molecular weights less than 48 repeat units.[7]

Malcolm et al. studied experimentally thermodynamic properties of PEG and PPG

Figure 4. Experimental results on water self-diffusion coefficients are given as a function of DME concentration at 318 K. Experimental results for the pure water are also included. This graph was reproduced from Ref. [35,40-42]

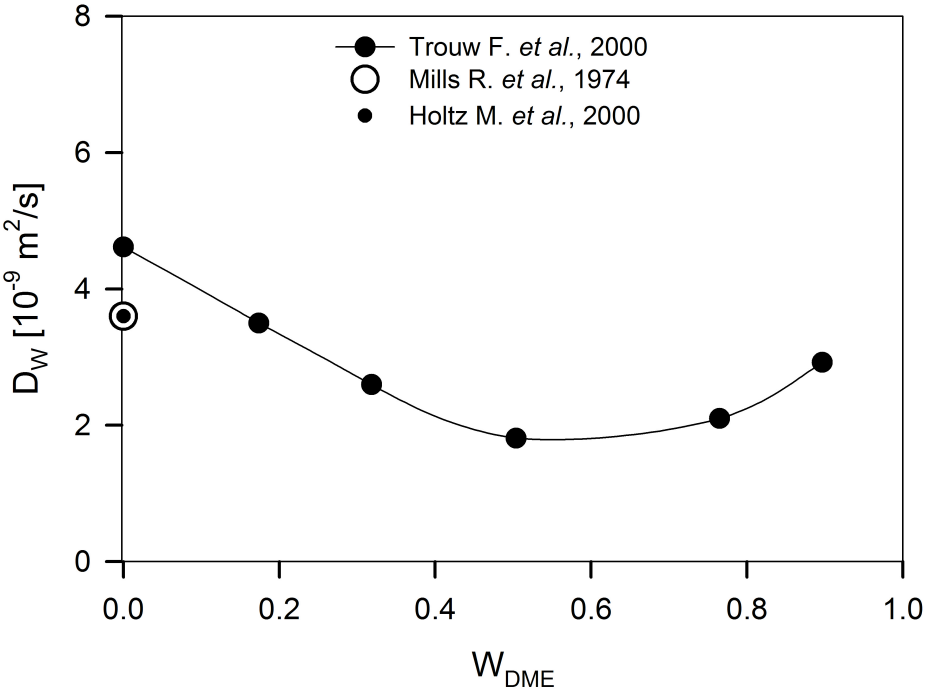
Trouw F. et al., 2000
Mills R. et al., 1974
Holtz M. et al., 2000
D_W [10^-9 m^2/s]
W_DME
0
2
4
6
8
0.0
0.2
0.4
0.6
0.8
1.0

aqueous solutions.[28] A wide variety of thermodynamic properties were reported including free energy, enthalpy, entropy of mixing, densities, and excess volumes. Various molecular weights of PEG and PPG were studied as a function of temperature. Positions of UCST and LCST were determined for all molecular weights.

Phase diagrams were constructed indicating a "closed loop" phase behavior for high molecular weights PEG. No phase separation was determined for PEG with the molecular weight less than 7 repeat units. LCST was determined to be 318 K for PPG with molecular weight of 6 repeat units Effect of the end groups was studied on solution behavior of DME and ethylene glycol monomethyl ether. Positive heat of mixing was obtained for DME with ($-CH_3$) methyl end groups in dilute concentrations. Negative heats of mixing were obtained for monomethyl ether with the presence of both methyl ($-CH_3$) and hydroxyl (-OH) end groups at all concentrations.[28]

Saeki et al. determined experimentally LCST and UCST for various molecular weight of PEG in water.[8] The temperature-weight fraction phase diagrams were constructed and positions of critical solution temperatures were obtained. It was found that PEG exhibits a "close loop" phase behavior in water as a function of molecular weight, concentration, and temperature. The phenomenon of the "close loop" behavior of PEG in water was referred to the presence of specific solute/solvent intermolecular interactions.[8] It was also suggested that the solvation structure of PEG/water breaks down upon temperature increase near the critical point. Pressure dependence on positions of LCST and UCST temperatures has also been investigated. It has been shown that critical solution temperatures are insensitive to the pressure up to 50 atm.[8] The results for PEG phase behavior are summarized in Figure 5.

Figure 5. Phase diagram of PEO aqueous solutions is given for various molecular weights and concentrations obtained from experiments. This graph was reproduced from Ref. [8]

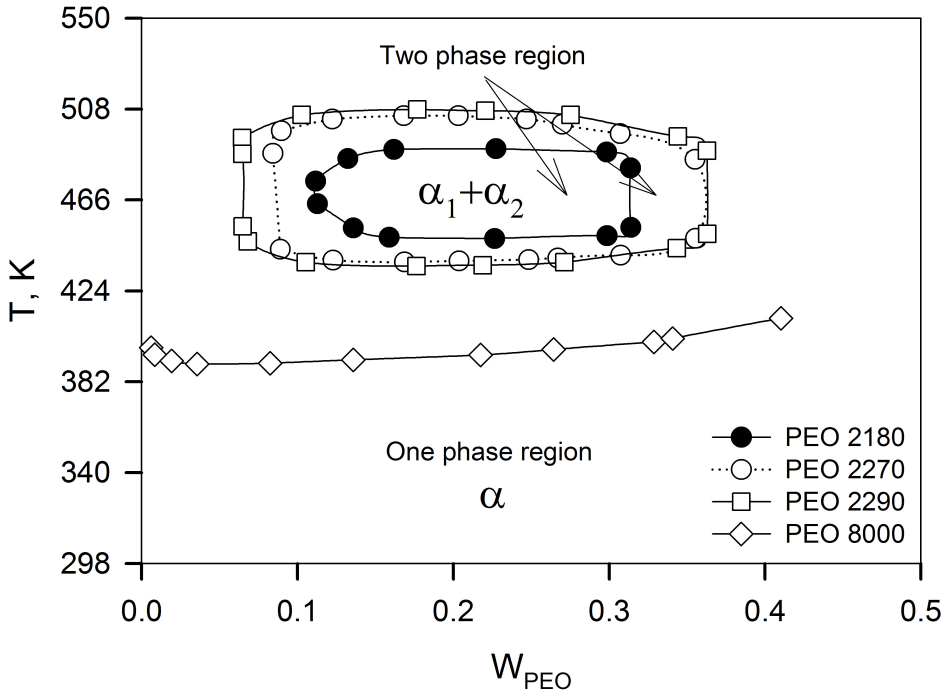
550
508
466
424
382
340
298
T, K
0.0
0.1
0.2
0.3
0.4
0.5
W_PEO
Two phase region
α1+α2
One phase region
α
PEO 2180
PEO 2270
PEO 2290
PEO 8000

Bilimova et al. investigated phase equilibrium of PPG aqueous solutions for a wide range of molecular weights and various types of end groups.[29] A few conclusions were made based on experimental results. The concentration of hydroxyl end (-OH) groups mainly dictated phase behavior of PPG aqueous solutions. Linear dependency of the critical temperature positions was observed as a function of concentration of hydroxyl end groups. Replacement of hydroxyl groups by acetyl end groups, for low molecular weights PPG, shifted the position of LCST to lower temperatures indicating decrease in solubility. A good agreement with other experiments was obtained on the position of lower critical solution temperature for 6 repeat unit PPG.

Crowther et al. performed rheological and densitometric studies of PPO/water solutions over a wide temperature range.[37] Negative excess specific volumes were determined for all temperatures indicating favorable PPO/water interactions. A phase diagram was constructed for 6 repeat unit PPO as a function of concentration and temperature. Studies of PPO phase behavior revealed a developed minimum of LCST at 0.3-weight fraction of PPO indicating dominance of hydrophobic effect at that concentration. LCST was determined to be above 328 K.[37]

Medved et al. investigated the effect of terminal end groups on phase behavior of PEG and PPG aqueous solutions for various molecular weights.[38] Effect of several groups was studied including hydroxyl (-OH) end group. Again, the position of LCST was systematically lowered as hydroxyl end group was replaced with acetoxy or phenyl urethane terminal groups. A number of thermodynamics properties were also determined including free energy of mixing.[38] Excess free energy of mixing was determined to be negative for all concentrations of PEG aqueous solutions and found to have a “wave”

shape for those systems. At low concentration, up to 0.3 weight fraction of PPG, excess free energy of mixing is found to be positive in contrast to PEG solvation. It was also found that excess volume for PPG is more negative than for PEG due to the difference in molecular volumes.[38]

Stephenson et al. measured the solubility for a number of compounds in a wide temperature range.[43] It was found that DMP is consoluble with water in the temperature range from 273 to 363 K.

Phase behavior of PPG aqueous solutions as a function of concentration and temperature are summarized in Figure 6. A good agreement in the position of LCST was established as obtained from different experiments performed by Malcolm et al., Bilimova et al., and Crowther et al.

1.3. Survey of theoretical studies of PEO/water and PPO/water solutions

Phase behavior of PEO/water and PPO/water solutions has been a subject of extensive theoretical investigations.[37,44-46] A few theoretical models were proposed to describe interactions between polymer and water including the polar and nonpolar conformation model of PEO,[47] PEO/water hydrogen bond model,[48] and competitive PEO/water and water/water hydrogen bond model.[49]

Semiquantitative agreement has been established with experiments for PEO/water and PPO/water temperature-concentration phase diagrams implementing conformational model. Better agreement with experiment has been achieved implementing the hydrogen bond model. Significant improvement has been reached in describing phase diagrams using the competitive PEO/water and water/water hydrogen bond model.

Figure 6. Phase diagrams of PPO aqueous solutions are given as obtained from experiments. This graph was reproduced from Ref. [28,29,37]

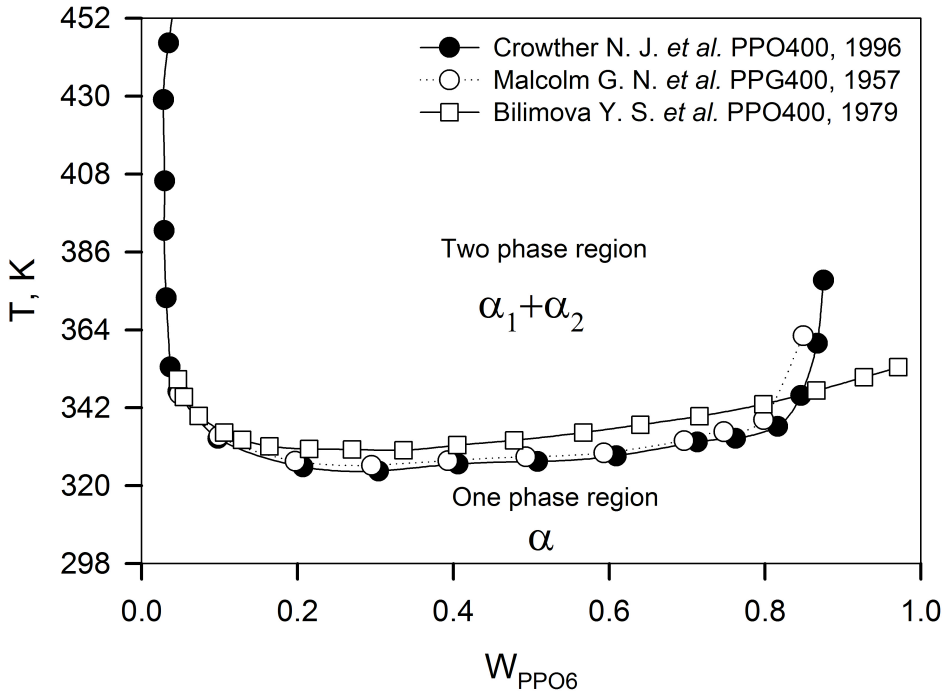
452
430
408
386
364
342
320
298
T, K
0.0
0.2
0.4
0.6
0.8
1.0
W_PPO6
Crowther N. J. et al. PPO400, 1996
Malcolm G. N. et al. PPG400, 1957
Bilimova Y. S. et al. PPO400, 1979
Two phase region
α1+α2
One phase region
α

These theoretical investigations and the performance of solvation models are discussed below.

Karlström et al. implemented the conformational solvation thermodynamic model to describe phase behavior of PEO/water solutions.[47] A polymer chain was represented by two distinct segments. One segment was defined as polar and corresponded to the *gauche* conformation of PEO repeat unit and another was defined as nonpolar and corresponded to the *trans* conformation. A polar segment has favorable interactions with water while a nonpolar segment has unfavorable interactions. These segments were related to the low and high temperature states, respectively. Free energy of mixing was calculated using Flory-Huggins theory.[50] The expressions for the energy ΔU_{mix} and entropy ΔS_{mix} were defined in terms of the probability P of finding a segment in low or high temperature states with corresponding energy interaction parameters ε_{ij}. Five interaction energy parameters were taken into account to describe the thermodynamic state of a system including interaction parameters for low and high temperature states, PEO/water interaction energy, and their cross terms. Free energy of mixing was determined by minimizing the total free energy of a system with respect to the probability of a segment state *i*. Poor description of PEO phase behavior was obtained in comparison with experimental data due to model simplicity. However, predicted LCST for low molecular weights PEO was in a good agreement with experiment.[47]

Matsuyama et al. introduced a solvation model that employed hydrogen bonding between repeat unit of PEO and water molecule to predict phase behavior of PEO/water solutions.[48] Quality of the solvent was characterized by a fraction of hydrogen-bonded PEO/water pairs to the free solvent molecules. Free energy of a system was calculated as

a contribution due to the free energy of quasireference state and the free energy of mixing. Quasireference state was calculated as a sum of chemical potentials of the free solvent molecules and PEO/water clusters. Free energy of mixing was calculated using standard Flory-Huggins approach.[50] Five parameters were taken into account to describe the thermodynamic state of a system such as functionality of PEO, number of statistical segments in PEO chain, PEO/water hydrogen bond entropy parameter, hydrogen bond energy parameter, and PEO/water interaction parameter. Hydrogen bond entropy and energy parameters were adjustable parameters. Positions of LCST and UCST temperatures were calculated for a number of molecular weights by minimizing free energy of a system. In addition, an average number of solvent molecules that are hydrogen-bonded to PEO was calculated as a function of temperature. It was shown that the average number of hydrogen-bonded solvent molecules is decreasing when a system is approaching LCST temperature. Semiquantitative agreement with experiment has been established in describing phase behavior of PEO/water solutions for a wide range of PEO molecular weights.

Dormidontova et al. studied behavior of PEO/water solutions introducing a new solvation PEO/water model that incorporated a competitive formation of PEO/water and water/water hydrogen bonds. Free energy of a system was represented by a sum of three independent terms as free energy of a reference state, interaction free energy, and association free energy. Free energy of a reference state corresponded to the energy of noninteracting polymers. Interaction free energy corresponded to the energy due to nonbonded PEO/water interactions that do not involve a formation of hydrogen bonds. And, association free energy corresponded to the energy due to PEO/water and

water/water hydrogen bonding. The first two terms are denoted as standard Flory-Huggins free energy of mixing.[50] The last term is defined in terms of a partition function that accounts for PEO/water and water/water hydrogen bonds where energetic values associated with bonds formation are based on available experimental data. Good agreement has been established with experiment in predicting LCST and UCST temperatures as a function of PEO molecular weight and concentration. In addition, an average number of hydrogen bonds between PEO/water and water/water molecules have been predicted as a function of PEO concentration and temperature. Results were compared with available experimental and theoretical data. Better agreement with experiment in predicting of a number of PEO/water hydrogen bonds has been reached implementing the competitive hydrogen bond model than the hydrogen bond model introduced by Matsuyama et al.[48] The latter has resulted in incorrect quantitative predictions of number of hydrogen bonds as a function of concentration and temperature.[49]

Dormidontova et al. studied the influence of hydroxyl (-OH) and methyl ($-CH_3$) end groups on phase behavior of PEO/water solutions.[46] The previous competitive hydrogen bond solvation model was generalized in a way to account for PEO/water, water/water, water/PEO, and PEO/PEO hydrogen bonds. Free energy of a system was also a sum of three independent energy terms. However, two additional parameters were added to the association free energy term to account for water/PEO and PEO/PEO hydrogen bonds. A significant effect of end groups was obtained on solvation properties of PEO. The hydroxyl end groups provide additional hydrogen bonds at high temperatures or high PEO concentrations that increase the overall solubility. The

presence of the methyl end group increases the volume occupied by a chain that decreases the solubility. These solvation effects were more pronounced for short polymer chains. Improved agreement with experiments has been established in positions of LCST and UCST temperatures for low molecular weight PEO implementing the generalized solvation model. Based on the results for high molecular weight PEO, phase behavior for low molecular weight PEO has been predicted to study the solvation effects of methyl and hydroxyl end groups. These predictions are summarized in Figure 7. Experimental data are also given along with calculations. It can be seen that the solubility of ($-CH_3$)/($-CH_3$) terminated chains is significantly lower than for the ($-CH_3$)/(-OH) and (-OH)/(-OH) terminated chain.

1.4. Survey of simulation studies of PEO/water and PPO/water solutions

A number of *ab initio* calculations have been performed to study the electronic structures of PEO and PPO model compounds. Nonpolarizable force fields were developed based upon *ab initio* calculations and stochastic dynamics (SD) and molecular dynamics (MD) simulations were performed for the gas and liquid states, respectively.[51-57] The conformations,[58-62] structure,[63] dynamics,[58] hydrogen bonding,[64-66] water dynamics,[67,68] and thermodynamics properties[42,69-71] of PEO/water and PPO/water solutions have been studied employing Monte Carlo (MC) and molecular dynamics (MD) simulations.

Jaffe et al. performed *ab initio* electronic structure calculations of isolated DME at various levels of theory.[51] Conformational energies of DME were determined relative to the energy of *ttt* conformer. It was shown that *ttt, tgt,* and $tg^{\pm}g^{\mp}$ are low energy

Figure 7. Phase diagram of PEO aqueous solutions is given as predicted by theoretical studies and obtained from the experiment. This graph was reproduced from Ref. [49]

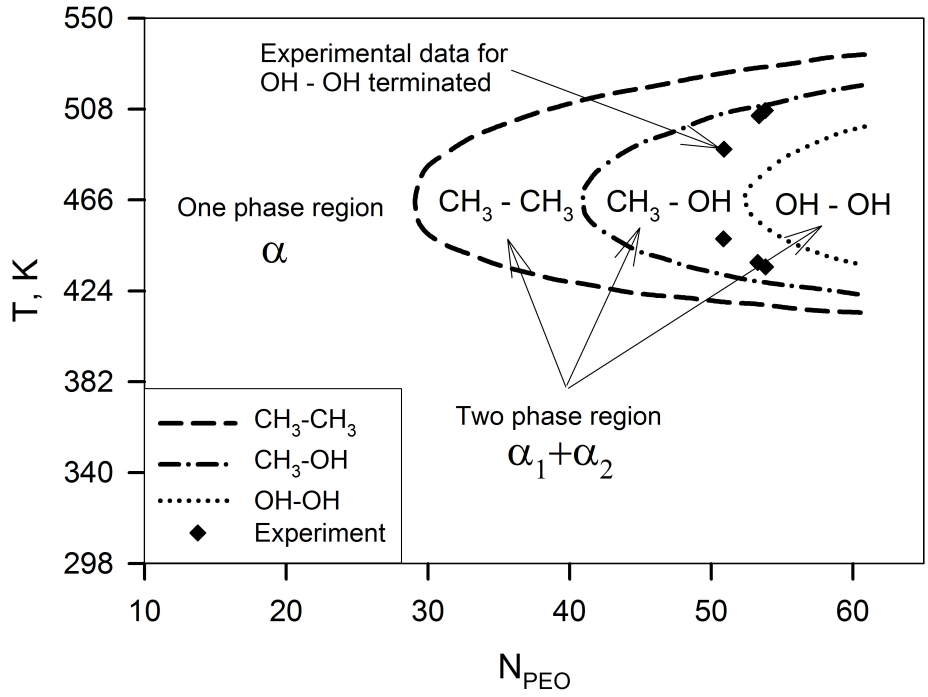
550
508
466
424
382
340
298
T, K
10
20
30
40
50
60
N_PEO
Experimental data for
OH - OH terminated
One phase region
α
CH3 - CH3
CH3 - OH
OH - OH
Two phase region
α1+α2
CH3-CH3
CH3-OH
OH-OH
Experiment

conformers in the gas phase of DME at 273 K.

Smith et al. performed *ab initio* electronic structure calculations of isolated DMP.[52] Conformational energies of DMP were also determined relative to the energy of *ttt* conformer. It was shown that *ttt*, *ggt*, and *gtt* are low energy conformers in the gas phase of DMP.

Smith et al. parameterized the nonpolarizable force field for PEO and PPO based upon *ab initio* electronic structure calculations of DME and DMP oligomers.[53,57] Stochastic and molecular dynamics simulations were performed to study population, structure, thermodynamics, and dynamics properties of those compounds. Conformational populations in the gas phase were obtained from stochastic dynamics simulations. The force field developed has been shown to reproduce conformational populations of DME in a reasonable agreement with experimental electron diffraction analysis and other works.[53,54] The force field developed for PPO well predicted the gas phase populations of the DMP, which was also in a good agreement with experiment.[57]

Smith et al. performed molecular dynamics simulation study of conformational populations for DME and DMP in water.[61] A lower population of *tgt* conformers in aqueous solution is obtained for DMP in comparison with DME. However, a high population of other hydrophilic conformations such as $t\bar{g}t$ and $g\bar{g}g$ compensated for the low population of *tgt* conformation. The most populous hydrophilic conformation of DMP was $t\bar{g}t$. Overall population of hydrophilic conformers was higher for DME than for DMP due to more energetically favorable interactions of ether with water.

Smith et al. performed molecular dynamics simulation studies of hydrogen bonding in PEO/water solutions.[66] These studies suggested that a number of PEO/water

and water/water hydrogen bonds is increasing upon dilution up to 0.5-weight fraction of PEO. Further dilution resulted in a number of hydrogen bonds to be almost invariant. Good agreement in number of hydrogen bonds was attained with theoretical predictions as a function of composition.[49] Water clustering has been determined at high concentrations 0.9-weight fraction of PEO. A decrease in a number of PEO/water and water/water hydrogen bonds was seen upon temperature increase. This trend was valid for low and high concentrations of PEO in water.

Smith et al. carried out molecular dynamics simulations to study the influence of the PEO/water and water/water hydrogen-bonding on conformations, hydration thermodynamics, and structure of PEO and DME as a function of composition.[64] Similar results were obtained for dilute regimes of DME aqueous solutions. A number of hydrophilic *tgt* and *tgg* conformations was increasing towards dilute regimes of PEO and DME aqueous solutions, while a population of hydrophobic *ttt*, *ttg*, *and* tg^+g^- conformations was decreasing. Local conformations of DME upon hydration are found to be similar to PEO. The hydration structures of PEO and DME were analyzed using pair distribution functions. Dependence of the solvation structures on the solution composition was found to be similar for DME and PEO. The number of hydrogen bonded water molecules was increasing for higher concentrations of PEO and DME indicating similar concentration dependence on solution composition.[64]

Smith et al. investigated the influence of the basis sets and level of theory on ether/water complexation energy.[42] Complexation energy was calculated for DME/water and dimethyl ether/water complexes along various paths. Geometry optimization of those complexes was performed at B3LYP level of theory an aug-cc-pvDz basis set.

Complexation energies were calculated at Møller-Plesset (MP2) and Hartree Fock (HF) levels of theory and various basis sets as aug-cc-pvXz where X=2,3,4. It was found that implementing HF level of theory is insensitive to the basis set while MP2 level gives significant dependence on the size of a basis set. Based on those studies, a revised force field was obtained to describe nonbonded interactions of DME with water following by molecular dynamics simulations. A number of thermodynamic properties for DME/water solutions were calculated from simulations such as free energy ΔG_{solv} and enthalpy ΔH_{solv} of DME solvation.

However, an accurate description of the potential energy for an ensemble of atoms is necessary to reproduce thermodynamic, dynamic, structural, and other properties of interests regardless of employed simulation methods or techniques. Distortion of the potential energy is usually described by analytical functions with a set of predefined parameters often referred to as a force field (FF). The force field is a vital element for molecular simulation as it carries the necessary energetic and geometric information for intra- and interatomic interactions. Predictive capabilities of molecular simulations mostly rely on the accuracy of implemented force field.

2. DEVELOPMENT OF THE PEO/WATER POLARIZABLE FORCE FIELD

In order to utilize high-quality polarizable potentials in simulations of PEO/water solutions, it is necessary to develop high-quality polarizable potentials for the water/water, polymer/polymer, and polymer/water interactions. It is also important to get a correct balance of those interactions for accurate predictions of solution properties.

Polarizable water potential SWM4-DP[72] was found to be the most adequate to represent a solvent for PEO/water solutions. However, the Drude polarization mechanism of SWM4-DP was replaced with the atomic point polarizable dipole mechanism (AD) resulting in the SWM4-AD polarizable potential. Validation of the SWM4-AD potential was performed by a series of MD simulations of single-phase water as a function of temperature. A number of thermodynamic properties were compared with other non-polarizable and polarizable water potentials and experiments.

The ether model with two-extended charges was chosen as the most accurate in the description of electrostatic potential around PEO. Validation of this model is performed by a series of molecular dynamics simulations of pure DME in liquid and gas phases. Enthalpy of vaporization for DME was obtained using the new ether model and compared with nonpolarizable force field and available experimental data.

Nonbonded force field parameters were developed for PEO/water interactions

based upon high level *ab initio* calculations and validated by a series of MD simulations of DME/water and PEO/water solutions over a wide temperature range. Structural thermodynamic, and dynamic properties from simulations were compared with available experimental data and with simulations using our previous TIP4P-based nonpolarizable force field.[42]

2.1. Methodology of the force field development

In order to develop an accurate potential for the atomistic MD simulations of PEO aqueous solutions, a number of steps have been performed: (a) an appropriate polarizable water model has been selected and validated by comparing thermodynamic properties with experiment; (b) an appropriate ether model has been chosen to get an accurate description of the electrostatic potential around PEO; (c) quantum chemistry studies have been carried out for a model PEO compound and electrostatic interactions have been re-parameterized; and (d) quantum chemistry study of interactions of the model PEO compound with water have been performed and ether/water interactions have been parameterized based upon these studies. APPLE&P[73-74] (Atomistic Polarizable Potential for Liquid Electrolytes and Polymers) with Lucretius[75] modeling software package and fitting tool kit have been used for the force field development and validation. Development of transferable polarizable potential for intermolecular interactions represents a big challenge in particular for binary aqueous systems. Most of the force fields utilize combining rules or perform empirical adjustments to get accurate thermodynamic properties.

In order to develop an accurate potential for atomistic MD simulations of

nonionic polymer aqueous solutions, it is necessary to select an appropriate polarizable water model first. In previous work, atomistic molecular dynamics simulations have been utilized to gain insight into the behavior of PEO in aqueous solutions as described in Section 1.4. While these studies have provided valuable insight into PEO/water solutions, including the temperature dependence of solution properties, they suffer from the shortcomings of the TIP4P[76] water potential, which was employed in these simulations. Specifically, it is well known that the TIP4P potential, while reproducing density and self-diffusion coefficient of pure water at and near room temperature with reasonable accuracy, does a poor job in reproducing these and other properties at high temperatures. As discussed in the following section, the temperature dependence of thermodynamic and transport properties of water can be much better reproduced utilizing water models that include atomic dipole polarizability (AD).

2.2. Water polarizable model

The COS/B2,[77] COS/G2,[78] TIP4P/FQ,[79,80] POL5/TZ,[81] and SWM4-DP,[72] models were considered as candidate polarizable water models. Results are also shown for the nonpolarizable TIP4P[76] model for comparison. Model simplicity and accuracy in reproducing thermodynamic, dynamic, and dielectric properties were the main criteria for the selection. Specifically, the liquid density ρ, enthalpy of vaporization ΔH_{vap}, and self-diffusion coefficient D_w, were considered as a function of temperature (see Figure 8 (a-d)). All thermodynamic properties for water were obtained from available literature [72,77-85] except for the SWM4-DP model.

Since it appears that the liquid state properties of water as a function of

Figure 8. Water densities (a), enthalpies of vaporization (b), and water self-diffusion coefficients (c) are summarized as a function of temperature for the various models. Average dipole moment and water permittivity (d) are given at 298 K as obtained from simulations and experiments. Dashed line indicates experimental value for water permittivity.

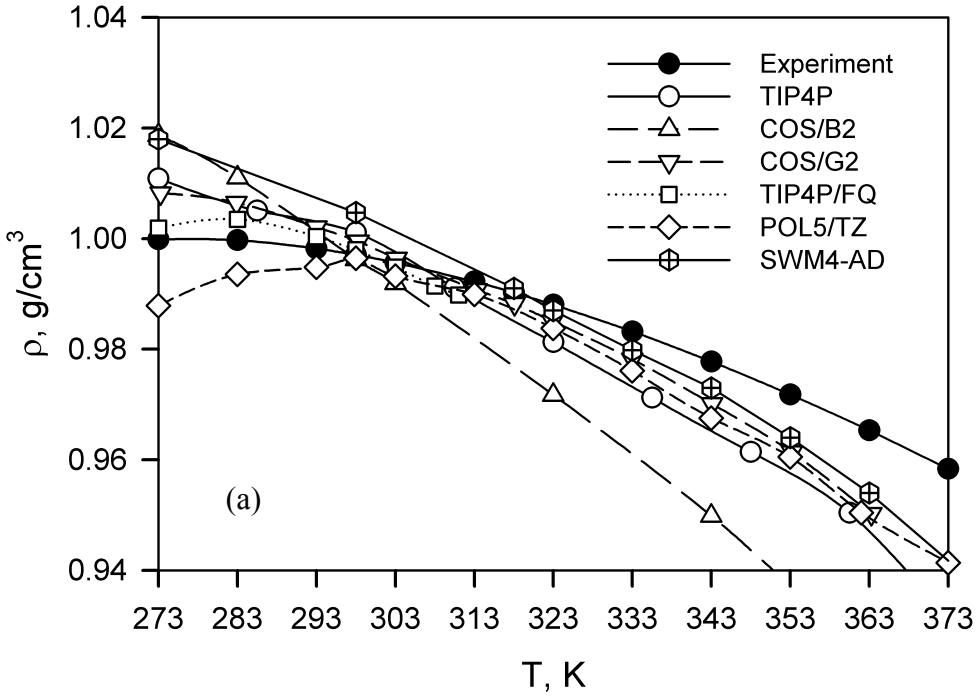
1.04
1.02
1.00
0.98
0.96
0.94
ρ, g/cm3
273
283
293
303
313
323
333
343
353
363
373
T, K
(a)
Experiment
TIP4P
COS/B2
COS/G2
TIP4P/FQ
POL5/TZ
SWM4-AD

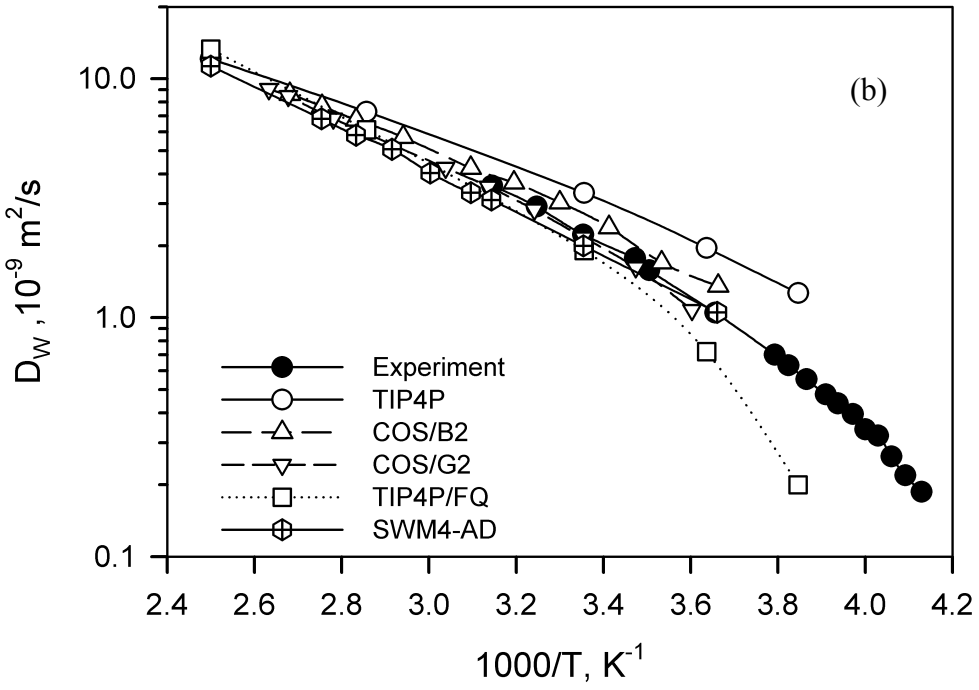
10.0
1.0
0.1
DW ,10-9 m2/s
2.4
2.6
2.8
3.0
3.2
3.4
3.6
3.8
4.0
4.2
1000/T, K-1
(b)
Experiment
TIP4P
COS/B2
COS/G2
TIP4P/FQ
SWM4-AD

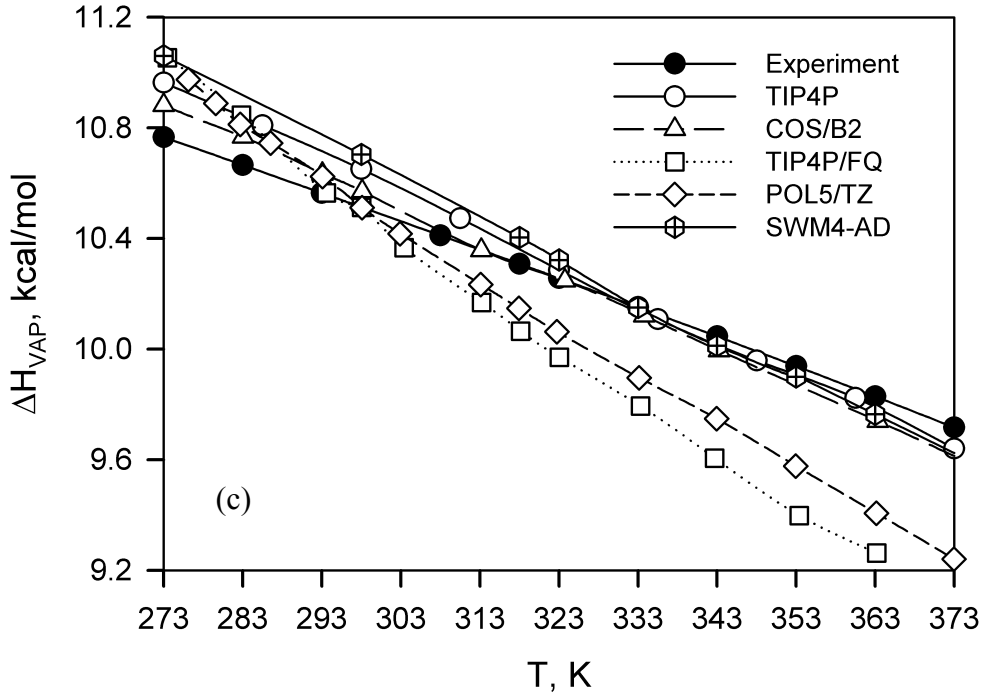

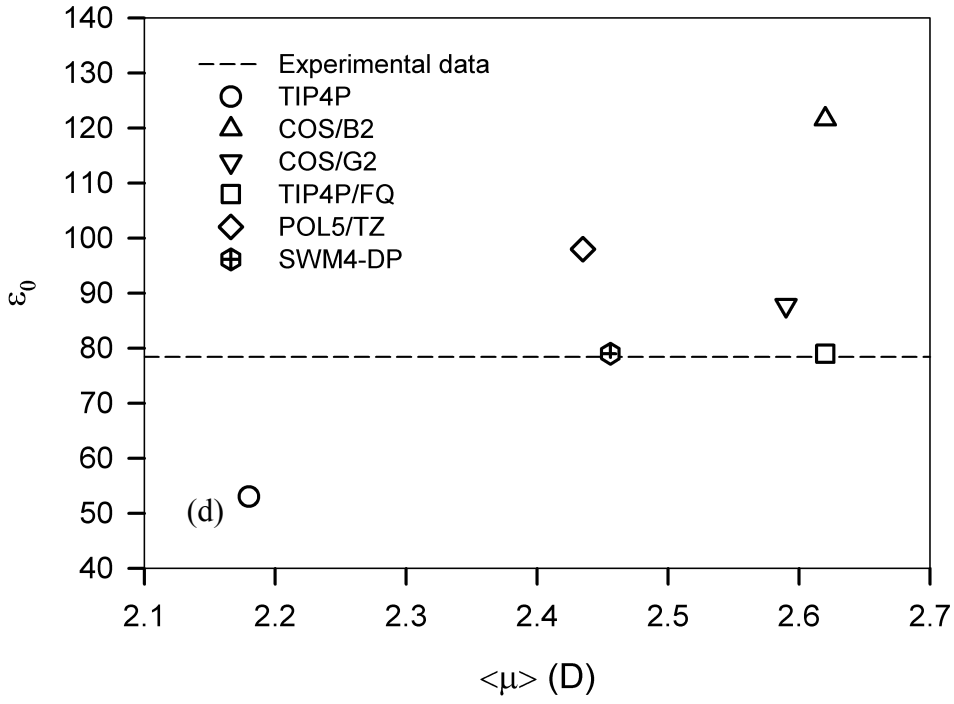

Figure 8. Continued

temperature have not been reported for the SWM4-DP model, the properties of interest were determined by performing a series of MD simulations implementing this water model with modification of the polarization mechanism as described in the next section. The modified water model is referred to as the SWM4-AD model, where AD stands for the atomic point polarizable dipole. The simulations were performed on an ensemble of 500 molecules utilizing a version of the MD simulation package Lucretius that includes isotropic atom dipole polarizability. Initially, equilibration for 5 ns was performed until steady state equilibrium properties were established followed by sampling trajectories of 20 ns. Isobaric-isothermal (NPT) ensemble simulations were performed at 1 atmosphere and 298-363 K. All bond lengths were constrained during the simulation using the Shake algorithm.[86] The Ewald summation method[87] with $\alpha = 0.232$ and $k = 6$ parameters was used to treat long-range electrostatic interactions. A multiple time step reversible propagator algorithm[88] was implemented to solve the equations of motion with a time step of 0.5 fs for valence interactions (bonds, bends, and torsions), 2 fs for nonbonded interactions within cutoff radius of R_{cutoff} = 6.0 Å, and 4 fs for nonbonded and electrostatic interactions within the range of 6.0 and 10.5 Å and the reciprocal part of the electrostatic interactions.

In addition to MD simulations, Brownian dynamics[89] simulations of 500 water molecules were performed to calculate enthalpy of vaporization ΔH_{vap} where the enthalpy of vaporization indicates a strength of water/water intermolecular interactions. The assumption was made that water behaves as an ideal gas at the pressure of 1 atm for calculations. Most of the water potentials do a reasonable job in reproducing experimental data at 298 K as the potentials are typically adjusted to reproduce density at

room temperature.

Among the tested models, the best agreement with experiment in water densities is observed for the SWM4-AD model. The TIP4P, SWM4-AD, and COS/B2 models all reproduce experimental data for the enthalpy of vaporization reasonably well above room temperature. Enthalpy of vaporization for the TIP4P[76] water model at 298 K is ΔH_{vap}=10.62 kcal/mol and for SWM4-AD is ΔH_{vap}=10.70 kcal/mol as obtained from the literature and simulations. Experimental value for the enthalpy of vaporization is ΔH_{vap}=10.52 kcal/mol.

Therefore, these models give a reasonable estimation of the strength of intermolecular water/water interactions as well as temperature dependence for the enthalpy of vaporization. All polarizable potentials were found to reproduce the water self-diffusion coefficient reasonably well, within 3% deviation, while the nonpolarizable TIP4P exhibits too fast water dynamics over the entire temperature range.[83] The SWM4-AD water model is selected based upon these results and the fact that the SWM4-DP water model yields a dielectric constant[72,82] and surface tension[84] in good agreement with experiment at room temperature as indicated in the Appendix.

2.2.1. Modification of the water polarizable model

The SWM4-DP polarizable water model consists of four interaction sites and Drude polarizability. The latter involves a massless charge on a spring attached to the oxygen of water. In the SWM4-AD model, Drude polarizability was replaced with an induced point dipole model. The water geometry in the SWM4-AD model was adopted unchanged from the SWM4-DP model, with an O-H bond length of 0.9572 Å and an H-

O-H angle of 104.52 °. The fourth (massless) site was attached to the oxygen of water by rigid bond at the distance of 0.238 Å along the H-O-H bisector. An isotropic atomic polarizability of 1.043 $Å^3$ was assigned to the oxygen atom. The value for the atomic polarization was taken as it was developed for the original model. It should be noted that all models studied underestimate atomic polarizability to reproduce a bulk like properties. Partial atomic charges were assigned to the massless particle (-1.1074 e) and hydrogen atoms (+0.5537 e) in accordance with the original SWM4-DP model. No partial charge was allocated on the oxygen atom of water. Lennard-Jones (12-6) repulsion and dispersion parameters were taken without any adjustments ($\varepsilon_{O\text{-}O}$ = 0.20568 kcal/mol and $\sigma_{O\text{-}O}$ = 3.18030 Å). Excellent agreement, less than 0.5% deviation, was found using the SWM4-AD model with published values using the SWM4-DP model for the liquid density, enthalpy of vaporization, and self-diffusion coefficient at 298 K.

2.3. Ether polarizable model

In order to get an accurate description of PEO/water interactions, the ether model should be considered next. Three different ether models are shown in Figure 9 that were implemented in nonpolarizable and polarizable force fields. An additional set of extended charges was necessary to improve the accuracy of electrostatic potential around the molecule and to define the directionality of intermolecular PEO/water interactions. Charge density distribution around the oxygen atom of ether is nonspherical and anisotropic due to the electron hybridization effects. The delocalization of a negative charge on oxygen is often referred to as electron lone pairs (Lp). Positions of the lone pairs are defined within a tetrahedral structure formed by sp^3 hybrid orbitals, where

Figure 9. Three ether models are illustrated with no-extended charge (a), one-extended charge (b), and two-extended charges (c). Hydrogens are omitted for clarity. Chemical structures were visualized using jmol open source software.

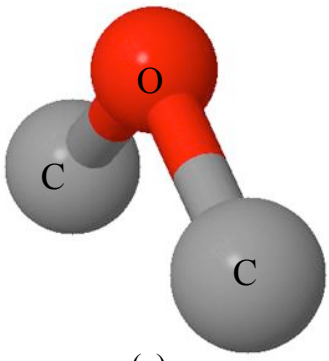

(a)

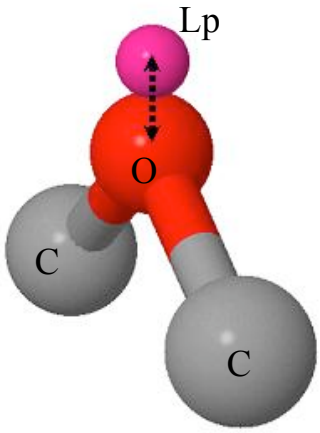

(b)

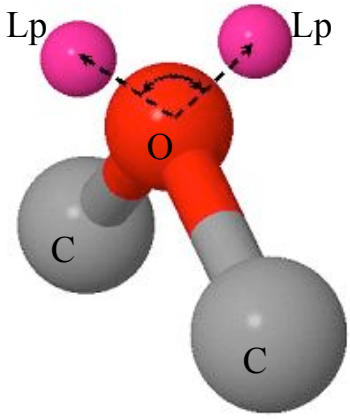

(c)

charge density is offset from the center of the oxygen atom.

Therefore, by placing an additional set of the extended charges on oxygen of ether will likely result in more accurate charge distribution around the ether moiety and, as a consequence, in more accurate description of electrostatic potential around PEO.

Three ether models were considered for the development of the polarizable force field and the two-extended charge model has been chosen as the most appropriate for the description of electrostatic potential and intermolecular interactions with water. The selection procedure involved a few consecutive steps: (a) the electrostatic potentials of PEO oligomers are obtained using *ab initio* calculations as described in Section 2.3.1; (b) fitting partial atomic charges to the electrostatic potentials is performed using predefined ether parameters as described in Section 2.3.2; (c) the most appropriate ether model is selected based on reproducible accuracy of electrostatic potential and intermolecular interactions of DME with water; and (d) adjustments of ether parameters are carried out to improve the description of intermolecular interactions of DME with water as described in Section 2.3.3.

2.3.1. Quantum chemistry calculations

DME has essentially the same local conformations as PEO in aqueous solution and similar dependence on solution composition, which makes this molecule a good model compound for developing of PEO/water potentials.[66,69,90] The electrostatic potential of PEO molecule is also obtained based on electrostatic potentials of its oligomers.

DME and diglyme are the two oligomers of PEO that were used for calculation of

the electrostatic potentials. The second oligomer was used for the purpose of providing a charge distribution on the oxygen atom that connects two repeat units of PEO. The Gaussian03 software package[91] was employed for all quantum chemistry calculations. The B3LYP[92-94] density functional,[95] in combination with the aug-cc-pvDz basis set[96] was utilized for geometry optimization of the oligomers. The B3LYP/aug-cc-pvDz level of theory was found to provide a more accurate description of molecular geometry than the HF level of theory implementing the same basis set.[42] Less deviation from the experiment of the DME backbone angles was obtained using B3LYP level of theory. Geometry optimization of isolated DME molecule was performed for hydrophobic *ttt* and *ggt* and hydrophilic *tgt* conformations that are listed in Figure 10. The dipole moments of corresponding conformers are also given as obtained from *ab initio* calculations. The geometry of the diglyme molecule was optimized for the hydrophobic *ttt* – *ttt* conformation only. Calculation of electrostatic potential on a grid of 80000 evenly distributed points was performed for each molecule in corresponding conformation at MP2 level of theory and aug-cc-pvDz basis set. The MP2/aug-cc-pvDz level of theory was found to provide with the most accurate description of relative conformational energy, electrostatic potential, and dipole moments over any other levels studied.[73] Electrostatic potentials for each molecular conformation were obtained and further included in the fitting of partial atomic charges to take into account the most important molecular conformations of PEO oligomers.

Figure 10. Hydrophilic and hydrophobic conformations are given for DME and diglyme. Atomic labels: C_m-methoxy carbon, C-methylene carbon, and O-oxygen of ether.

ttt (μ= 0.0 D)

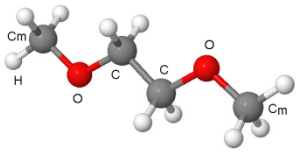

(a)

tgt (μ= 1.37 D)

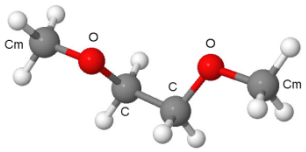

(c)

ggt (μ= 2.39 D)

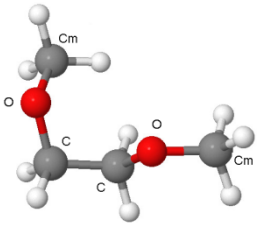

(b)

ttt-ttt (μ= 0.0 D)

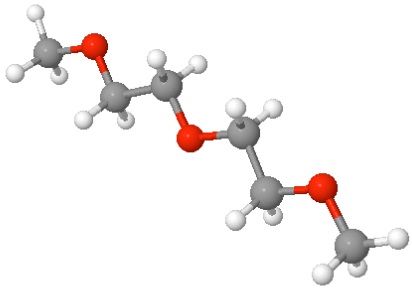

(d)

2.3.2. Parameterization of partial atomic charges

The charge fitting approach is based on a bond increment scheme that allows calculating of partial atomic charges q_i as a result from summation of all charge increments while maintaining a balance of the molecular charge distribution.[97]

$$q = \sum_{i}^{n-Bonds} \delta_{ij} \tag{1}$$

where δ_{ij} is a bond increment. The partial atomic charges were fitted to the electrostatic potentials ϕ_i^{QC} and dipole moments $\vec{\mu}_i^{QC}$ obtained from quantum chemistry calculations by least-square minimization of the objective function χ^2 including hydrophilic and hydrophobic conformers that are listed in Figure 10.

$$\chi^2\left(\vec{\delta}\right) = \sum_{i=1}^{N}\left(\sum_{j=1}^{n}\frac{\omega^{\phi}}{n}\left(\phi_i^{QC} - \phi_i^{FF}\vec{\delta}\right)^2 + \omega^{\vec{\mu}}\left(\vec{\mu}_i^{QC} - \vec{\mu}_i^{FF}\vec{\delta}\right)^2\right) \tag{2}$$

where N is a number of molecules; n is the number of grid points; ϕ_i^{QC} and ϕ_i^{FF} are the electrostatic potentials obtained form *ab initio* and force field, respectively. $\vec{\mu}_i^{QC}$ and $\vec{\mu}_i^{FF}$ are the dipole moments of a molecule from *ab initio* calculations and the force field; ω^j is the relative weight; and $\vec{\delta}$ is a charge increment. The accuracy of the fit is justified by comparing the electrostatic potentials and dipole moments obtained from *ab initio* calculations and the force fields.

Thole scaling parameter of 0.4 was used to damp induced dipole-induced dipole interactions. The reduction scale factor for the charge-dipole interactions was set to 0.8. Maximum distance included in the fit was 4.0 Å. This distance was defined within the first hydration shell but was greater than the van der Waals radius of atoms. No charge-bond constrains were imposed while fitting to the electrostatic potential; however, different weights for the geometries were used. More weight was given to the hydrophilic *tgt* conformer and less to the hydrophobic *ttt* and *tgg* conformers. Weights for the electrostatic grids were equal to unity, weight for the molecular dipole was 0.1, and weight for the molecular polarizability was 0.05. However, molecular polarizabilities were taken from existing APPLE&P force field for ethers[74] and were used to obtain partial atomic charges as defined by the force field fitting methodology.

Fitting of partial atomic charges was performed employing three ether models to study the influence of the extended charges on reproducible accuracy of electrostatic potentials and dipole moments. The no-extended charge model was used for the fitting followed by one-extended charge and two-extended charge models.

The no-extended charge model in Figure 9 (a) implemented in NPFF[42] yielded a large deviation from the electrostatic potentials and dipole moments of oligomers. The value of the objective function was χ^2=1.7. The electrostatic potential energy map of *ab initio* calculations and polarizable force field can be found in chapter 2 of the molecular simulation methods for predicting polymer properties.[98]

The one-extended charge model was considered next. This ether model was introduced in polarizable force field developed by Borodin et al.[74] A single extended charge (or one Lp) was placed on the oxygen of ether at the distance of 0.5 Å along a

bisect of C-O-C angle away from oxygen (see Figure 9 (b)). The presence of an extended charge resulted in smaller deviations from the electrostatic potential and dipole moments than the previous ether model. The effective magnitude obtained for the extended charge was q_{Lp}=-0.2126 e. The value of the objective function was χ^2=0.9. It was also found that the ether/water liquid state structure was significantly affected by the ether model geometry and the extended charge magnitude. The first and second hydration shells around the DME molecule were well structured and shifted to the shorter ether/water distances.

The ether model, shown in Figure 9 (c), with two-extended charges (or two lone pairs Lp) was investigated next. The electrostatic potential ϕ_i^{FF} was calculated as a function of an Lp-O-Lp angle and a O-Lp separation distance from the oxygen of ether and energy map was built for the square value of the objective function χ^2 (see Figure 11). The smallest deviation from electrostatic potential ϕ_i^{QC} was obtained for the Lp-O-Lp angle of 96°, Lp-O separation distance of 0.7 Å, and a single charge magnitude of q_{Lp} = -0.2200 e. The two-extended charge model was also implemented in CHARMM[99] force field. However, the reported parameters of the ether model are quite different. The optimal Lp-O-Lp angle was 104° and the Lp-O separation distance was 0.35 Å. The effective charge magnitude for a single lone pair was a half of the oxygen atom q_{Lp}=-0.1100 e. These parameters resulted in a greater deviation from the electrostatic potential ϕ_i^{QC} as indicated in the energy map of the objective function. The ether model geometry implemented in the CHARMM[99] polarizable force field has also significantly influenced the DME/water liquid structure. The first and second hydration shells were shifted to the shorter O_E-O_W distances with a well-developed water structure around DME.

Figure 11. Energy map is given for the square value of the objective function χ^2. Energies are in kcal/mol.

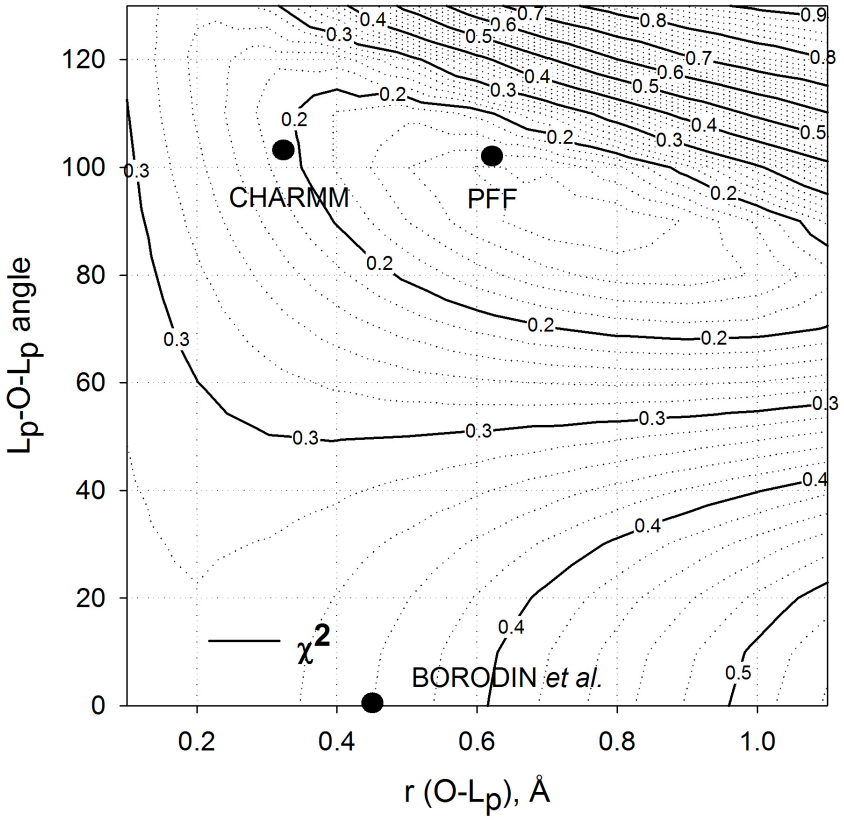
CHARMM
PFF
BORODIN *et al.*
χ^2
L_p-O-L_p angle
r (O-L_p), Å
0
20
40
60
80
100
120
0.2
0.4
0.6
0.8
1.0

2.3.3. Empirical adjustment of ether parameters

The two-extended charge model with the Lp-O-Lp angle of 96° and the Lp-O distance of 0.7 Å has been chosen for the ether as the most accurate in the description of electrostatic potential. However, fitting of DME/water binding energies using those parameters resulted in some deviations from quantum chemistry calculations of non-bonded interactions. Therefore, empirical adjustments were performed for the ether parameters to simultaneously obtain an improved fit of DME/water binding energies.

The assignment of PEO partial atomic charges is given in Table 1. Partial atomic charges implemented in nonpolarizable force field are also included in that table for comparison. The major difference in partial charges can be seen for the oxygen atoms. Oxygen atoms of the extended charge models have positive partial charge while the nonpolarizable model and noextended charge model have negative charges.

The charges are also negative for the methylene carbons as a result of the charge disbalance on the oxygen of ether. No atomic partial charges were assigned to the oxygen atoms in CHARMM[99] ether model. The charge density is concentrated on the extended charges only. Drude anisotropic polarizability is placed on the oxygen of ether in CHARMM[99] model.

2.3.4. Many body polarizable model

The ability of a molecule to be polarized due to the fluctuations in the surrounding electric field of a system is a very important factor to be considered.[100] Nonpolarizable force fields incorporate polarization effects on average while polarizable force fields explicitly account for the molecular polarization using various polarization

Table 1. Assignment of partial atomic charges for PEO using different ether models.

Atom type	Two-extended charge model [a]	Two-extended charge model [b]	One-extended charge model [c]	No-extended charge model [d]	NPFF [e]
O (C-O-C)	0.4296	-	0.1500	-0.2340	-0.2560
O (C_m-O-C)	0.4348	-	0.1500	-0.2348	-0.2560
C_m	-0.3507	-0.0520	-0.2987	-0.2470	-0.1630
H_m	0.1169	0.0540	0.1100	0.1169	0.0970
C	-0.1100	-0.1620	-0.1887	0.0152	-0.0660
H	0.0576	0.0540	0.1100	0.0576	0.0970
Lp	-0.2200	-0.1100	-0.2126	-	-

[a,d] Current work

[b] Ref. [99]

[c] Ref. [74]

[e] Ref. [42]

mechanisms.[101]

The isotropic atomic dipole polarization mechanism was implemented in APPLE&P polarizable force field.[74] The SWM4-DP water model was also modified to incorporate the atomic dipole polarization described in Section 2.2.1. Therefore, current polarizable force field is being developed in a framework of APPLE&P force field[102] employing an isotropic atomic polarizable dipole. This polarizable model makes possible both intra- and intermolecular polarization effects. An atom of a molecule can induce a dipole on another atom separated by three covalent bonds providing the self-polarization effects. Intermolecular polarization includes charge-induced dipole, dipole-induced dipole, and induced dipole-induced dipole interactions. These interactions are also referred to as dispersion interactions and classified as Debye, Keesom, and London interactions.[103]

2.3.5. Parameterization of atomic polarizabilities

Atomic polarizabilities are usually obtained before fitting of partial charges to accurately describe molecular self-polarization effects.[98] However, this section is included for the informative purpose only in order to provide a complete description of the force field development methodology. A more rigorous description can be found in a series of publications.[73,74,97]

The fitting procedure consists of two consecutive steps. *Ab initio* calculations are performed to obtain polarization energy potential as a function of separation by placing a test charge along defined paths near the atoms of interest. Polarization energy is calculated as a difference between electrostatic potential energy of a complex (a molecule

and a test charge) and self energy of a single molecule plus electrostatic potential energy at the position of a test charge.[73]

$$\Delta U_{POL}^{QC} = U_{mol+q}^{QC} - \left[U_{mol}^{QC} + U_{q}^{QC}\right] \tag{3}$$

where U_{mol+q}^{QC} is polarization energy of a complex, U_{mol}^{QC} is a self energy of a molecule, and U_{q}^{QC} is electrostatic potential energy at the position of a test charge. Fitting the polarization energy is performed next in a similar way as fitting partial atomic charges discussed in Section 2.3.2 by minimizing the value of the objective function χ^2.

$$\chi^2(\alpha) = \sum_{i}^{N}\sum_{j}^{n} \omega\left(U_{POL}^{QC} - U_{POL}^{FF}\right)^2 \tag{4}$$

where N is the number of different paths and n is a number of grid points; ω is a weight for a path *i*, U_{POL}^{QC} polarization energy obtained from eq. 3, and U_{POL}^{FF} polarization energy of the force field.

Polarization energies for a DME molecule were obtained from *ab initio* calculations at MP2 level of theory and aug-cc-pvDz basis set.[73] Atomic polarizabilities of ether molecule were calculated by fitting polarization energy along five different paths.[73] Good agreement in polarization energy between *ab initio* calculations and the force field was attained along all paths considered. Therefore, for the development of current polarizable force field, atomic polarizabilities of the ether oxygen and methylene

carbons were taken from APLE&P polarizable force field.[73,74,97,104] No atomic dipole polarizabilities were placed on the hydrogens.

2.4. Intermolecular interactions

All valence parameters (bonds, bends, and torsional), dispersion/repulsion parameters for the ether/ether intermolecular interactions were taken from the quantum chemistry-based APPLE&P® polarizable force field that was found to provide a consistent description of density ρ, heat of vaporization ΔH_{vap}, and transport properties of a variety of polymers, including poly (ethers).[73,74,97,104] However, backbone torsional parameters were refitted to the energies obtained at the MP2/aug-cc-pvDz level of theory (see the Appendix). The polarizable water model is described above in Section 2.2, while the ether model is described in Section 2.3. In order to complete the description of PEO/water systems within the atomistic polarizable force field framework, dispersion/repulsion parameters for the intermolecular interactions between the ether and water need to be determined. This represents a big challenge to obtain the right balance between repulsion and dispersion intermolecular interactions. For this purpose, extensive *ab initio* calculations of the binding energy between DME and a single water molecule were conducted for a number of ether/water designed configurations, as shown in Figure 12. MP2/aug-cc-pvDz level calculations with basis set superposition error (BSSE)[105] were performed using the counter poise correction approach.

Figure 12. Schematic representations of the testing configurations are given for the calculation of DME/water binding energies in (a), (b), and (c) respectively. DME is in hydrophobic *ttt* (a and c) and hydrophilic *tgt* (b) conformations. Gray atoms represent carbons, white are hydrogens, and red are oxygen atoms. Dashed arrows indicate the directions along which the water molecule to be shifted. Chemical structures were visualized using jmol open source software.

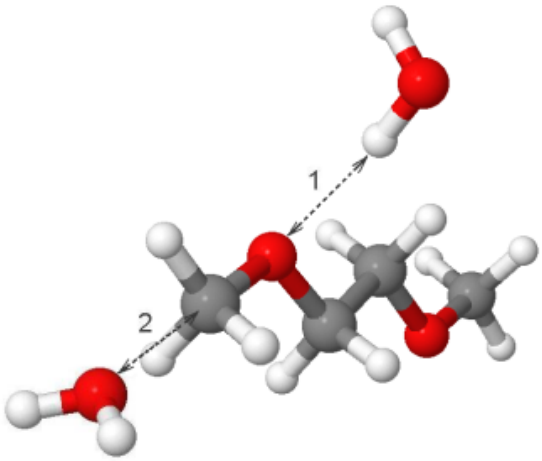

(a)

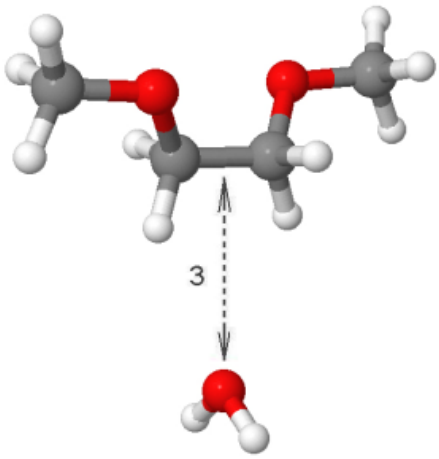

(b)

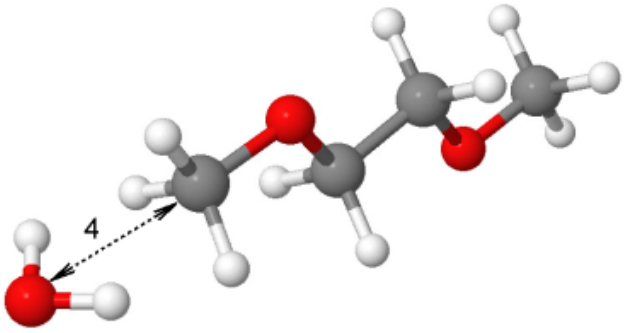

(c)

2.4.1. Development and predictions of the original nonpolarizable force field

Development of the nonpolarizable force field included studies of intermolecular interactions of DME with water along hydrophilic and hydrophobic paths.[42] No interactions of the methoxy group with water were investigated. Geometry optimization of dimers was performed at the B3LYP/aug-cc-pvDz level while calculations of total binding energies were obtained as a sum of the Hartree Fock and extrapolation energies.[42] A hydrophilic path was designed as a single water molecule is interacting with two oxygen atoms of DME in *tgt* conformation. Hydrophobic path was similar to the Path 3, as shown in Figure 12 (b). The TIP4P water model was used in fitting of intermolecular interactions. Repulsion parameters for nonbonded intermolecular interactions were determined first by fitting to the dimer binding energies obtained from *ab initio* calculations. A short-range hydrogen bond function was introduced to improve an agreement with the first principal calculations. Dispersion parameters were obtained next by performing an empirical adjustment. Total interaction energy for hydrophilic and hydrophobic paths can be found in corresponding reference.[42] A good agreement of the nonpolarizable force field with *ab initio* calculations was established for both paths. However, the hydrophilic path was not well described within the dispersion part of the pair potential; dispersion interactions were underestimated at separations distances larger than the equilibrium distance. On the contrary, the hydrophobic path was overestimated at the potential minimum and at larger separation distances.

In this work, a different approach is implemented to study intermolecular ether/water interactions. The paths are designed to differentiate binding energies of a

water molecule with particular atoms among atomic groups while the influence from other atoms is minimized if possible.

Molecular dynamics simulations of DME in water resulted in too favorable free energy and enthalpy of DME solvation, ΔG_{solv}=-6.2 kcal/mol and ΔH_{solv}=-17.1 kcal/mol. High deviation in excess volume for DME/water solutions was obtained. These studies revealed that the enthalpy of DME solvation was mostly influenced by hydrophilic interactions while DME excess volume was affected by interactions of water with methylene carbons (see Path 3 in Figure 12 (b)).

2.4.2. Ether/water quantum chemistry paths

The interactions of a water molecule with the hydrophobic *ttt* and hydrophilic *tgt* conformers of DME have been investigated along various ether/water paths designed to provide information about the interaction of water with ether oxygen atoms, methylene and methoxy groups. Quantum chemistry calculations were also performed for dimethyl ether/water in order to provide additional information on the interaction of water with ether oxygen atoms. The paths are illustrated in Figure 12 (a, b, and c). Path 1, which involves hydrogen bonding between a water hydrogen atom and an ether oxygen atom, was investigated for the DME in *ttt* conformation as well as for the dimethyl ether. In the *ttt* conformer, the ether oxygen atoms of DME are on the opposite sides of the molecule, facilitating investigation of hydrogen bonding between water and a single ether oxygen atom. Path 2, which involves interaction of water with the methyl group of the methoxy group, was also investigated for the *ttt* conformer of DME. Path 3 involves interaction of water with the “hydrophobic” side of DME, i.e., the methylene groups as opposed to the

ether oxygen atoms. Path 4 involves interactions of water hydrogens with methoxy hydrogens. For all paths, the local optimized geometry was obtained at the B3LYP/aug-cc-pvDz level. Subsequently, the energy of the ether/water complex was determined at the MP2/aug-cc-pvDz level with fixed water and ether geometries, with the distance between the water oxygen being systematically increased or decreased along the ether oxygen/water oxygen vector (Path 1), the carbon/water oxygen vector (Paths 2 and 4), and the vector between the midpoint of the carbon-carbon bond and the water oxygen (Path 3). Binding energies are reported as the difference between the BSSE[105] (counterpoise method) corrected ether/water complex energy and that of the geometry optimized ether and water at infinite separation.

2.4.3. Ether/ether repulsion/dispersion parameters

Ether/ether repulsion/dispersion parameters were determined by fitting parameters to dimer energies to reproduce liquid state density ρ and heat of vaporization ΔH_{vap} for various compounds including alkanes and DME within an APPLE&P force field framework.[74] Geometry optimization for the dimers was performed at the B3LYP/aug-cc-pvDz level of theory and energy calculation at the MP2/aug-cc-pvDz level. Repulsion/dispersion parameters for sp^2 carbon and hydrogen atoms were taken as determined for n-alkanes and for the oxygen atom as obtained for dimethoxyethane.[74]

Nonbonded intermolecular interactions are described by Buckingham potential employing Waldman-Hagler (WH) combining rule.[106] Waldman-Hagler combining rule was found to provide the best description of thermodynamic properties for PEO/PEO intermolecular interactions.[74] Therefore, repulsion A and B parameters were calculated as

indicated by equations 5 and 6 and dispersion parameter C was calculated using geometric rule, eq. 7.

$$A_{ij} = \sqrt{A_{ii}A_{jj}}\,\frac{B_{ij}^{6}}{B_{ij}^{3}B_{ij}^{3}} \tag{5}$$

$$B_{ij} = \left(\frac{2}{B_{ii}^{-6} + B_{jj}^{-6}}\right)^{\frac{1}{6}} \tag{6}$$

$$C_{ij} = \sqrt{C_{ii}C_{jj}} \tag{7}$$

These combining rules were designed to be used for Buckingham potential only and were successfully implemented in simulations of ionic liquids and electrolytes.[74,97,104]

2.4.4. Water/water repulsion/dispersion parameters

Water/water repulsion/dispersion parameters were determined based on water dimer intermolecular interactions and oxygen-oxygen equilibrium distance as to accurately reproduce water density ρ, and enthalpy of vaporization ΔH_{vap}. Therefore, repulsion/dispersion parameters are implemented as developed for the SWM4-DP water model.[72] It should be noted that water nonbonded interactions are described by Lennard-Jones[107,108] potential and not by Buckingham[109] intermolecular potential.

2.4.5. Ether/water repulsion/dispersion parameters

There are three consecutive steps in development of nonbonded ether/water force field parameters. First, two sets of nonbonded parameters have been developed to study the effect of short- and long-range O_E-H_W intermolecular attraction on the performance of the force fields. Second, O_E-H_W repulsion and dispersion parameters are empirically adjusted for both sets to get the best agreement in free energy of solvation from the experiment using thermodynamic perturbation method,[110] as described in Chapter 4. Third, O_E-H_W repulsion and dispersion parameters are empirically adjusted to get the free energy of DME solvation by 1 kcal/mol lower than experimental results to study energetic effect on liquid properties of PEO aqueous solutions. These parameters, combined with the two-extended charge polarizable ether model (with other parameters obtained from APPLE&P® force field) and the SWM4-AD polarizable model for water, are further referred to as the polarizable force fields PFF-X, where X represents the version of the developed nonbonded parameters (1-6).

2.4.6. Functional form of the pair potentials

Intermolecular interactions between ether and water atoms were described using the Buckingham (exp-6) potential for all pairs:

$$U^{Exp-6}\left(r_{ij}\right) = A_{ij}\exp\left(-B_{ij}r_{ij}\right) - \frac{C_{ij}}{r_{ij}^6} + D\left(\frac{12}{B_{ij}r_{ij}}\right)^{12} \tag{8}$$

where i=O_w or H_w and j=C, H, O, and C_m. A_{ij} and C_{ij} are the repulsion and dispersion parameters, respectively. Atom labels are shown in Figure 10. The term, $D\left(\frac{12}{B_{\alpha\beta}r_{ij}}\right)^{12}$ with D = 5 · 10^{-5} kcal/mol for all pair interactions, is essentially zero at typical nonbonded atomic separations, but becomes dominant at r_{ij} < 1 Å, ensuring that $U^{RD}(\mathbf{r})$ is repulsive at distances much smaller than the size of an atom.

2.4.7. Dispersion interactions

Dispersion (C_{ij}) parameters for i=O_w; j=C, H, O_E, and C_m were determined using the Waldman-Hagler (WH) combining rule[106] and hence were not adjustable parameters. Dispersion parameters for i=H_w; j=C, H, and C_m were set to zero. Dispersion parameter C_{ij} of the i=H_w; j=O_E atomic pair is set to zero in PFF-1 force field and not an adjustable parameter while the dispersion parameter in PFF-2 is not set to zero and treated as adjustable.

2.4.8. Repulsion interactions

A major contribution to the dimer binding energies comes from the electrostatic interactions such as polarization and Coulomb interactions.[103] Fitting of the repulsion parameters to the total dimer binding energies for all paths simultaneously did not provide with a good quality fit. Difference in interaction energies for the hydrophilic path 1, Figure 12(a), and hydrophobic paths 2, 3, and 4 Figures 12(b-c), resulted in overweighting of binding energies near and at the equilibrium minimum position for the Path 1 where electrostatic interactions are predominant while a significant

underestimation of short-range repulsion and long-range dispersion interactions was obtained for paths 2, 3, and 4. To make weighting of binding energies comparable for all three paths, a decision was made to fit energies due to 'nonelectrostatic' intermolecular interactions only, which is further referred to as van der Waals interactions. Van der Waals energies ΔU^{vdW} are obtained as a difference of the total energy from *ab initio* calculations ΔU_{TOTAL}^{QC} and electrostatic energy of the force field ΔU_{EL}^{FF}.

$$\Delta U^{vdW}\left(r_{ij}\right) = \Delta U_{TOTAL}^{QC}\left(r_{ij}\right) - \Delta U_{EL}^{FF}\left(r_{ij}\right) \tag{9}$$

where $\Delta U_{EL}^{FF}\left(r_{ij}\right) = \Delta U_{CB}^{FF}\left(r_{ij}\right) + \Delta U_{POL}^{FF}\left(r_{ij}\right)$ is a sum of the energies coming from interactions of partial charges q_i and induced dipoles $\vec{\mu}$, k_b is the Boltzmann constant, and T is the temperature.

2.4.9. PFF-1

The first set of parameters, PFF-1, was determined by simultaneously fitting only A_{ij} repulsion parameters for ether/water pair of atoms. Intermolecular interactions between ether atoms and water are described by Buckingham potential (exp-6) functions with the exception of O_E-H_W intermolecular interaction, which was represented by a short-range "hydrogen bond" function, indicating no presence of a dispersion parameter C_{ij}, as specified by the following equation

$$U^{O_E-H_W}\left(r_{ij}\right) = -A_{ij}^{O_E-H_W}\exp\left(-B^{O_E-H_W}r_{ij}\right) \tag{10}$$

It should be noted that an additional term D is zero for this functional form of the pair potential.

2.4.10. PFF-2

The second set of parameters, PFF-2, was determined by simultaneously fitting A_{ij} repulsion parameters and a single C_{ij} dispersion parameter of the "hydrogen bond" function, where all intermolecular interactions were described by Buckingham potential including O_E-H_W interactions, which is defined as long-range due to the presence of the dispersion C_{ij} term. An additional term D is applied for the exp-6 pair potential as discussed in Section 2.4.6.

2.4.11. Fitting procedure

Both sets of parameters were fit to the van der Waals binding energies by optimization of the objective function

$$\chi^2 = \sum_{path(i)} \sum_{geometry(j)} \omega_{ij} \left(U_{B,ij}^{FF} - U_{B,ij}^{QC} \right) \tag{11}$$

where $U_{B,ij}^{FF}$ is the binding energy for geometry i of path j predicted by the force field, while $U_{B,ij}^{QC}$ is the same quantity from quantum chemistry calculations.

Each point was weighted in the fit using the Boltzmann weighting factor ω_{ij}

$$\omega_{ij} = \exp\left[-\frac{U_{B,ij}^{QC} - U_{B,ij}^{EL}}{k_b T} \right] \tag{12}$$

where T = 298 K and $U_{B,ij}^{EL}$ is the electrostatic (polarization and Coulomb) contribution to the DME/water binding energy for each ether/water pair geometry as determined from already established atomic polarizabilities and partial atomic charges.

In order to determine the molecular mechanics energy along each path, a molecular mechanics geometry optimization was first performed, and the path was determined by systematically changing the ether/water separation for the fixed ether and water geometries, analogous to the procedure used for determining the quantum chemistry paths. A comparison of molecular mechanics ether/water binding energies with the best-fit PFF-1 and PFF-2 ether/water parameters with quantum chemistry binding energies are shown in Figure 13 (a-c). Excellent agreement, less than 1% deviation, of binding energies with quantum chemistry data was obtained for all paths.

Ether/water binding energies for Paths 1, 2, and 3 for NPFF[42] with the TIP4P[76] water model are also shown in Figure 13 (a-c) for comparison. It can be seen that PFF-1 and PFF-2 provide an improved description of ether/water interactions over the NPFF force field. Specifically, the NPFF resulted in underestimation of binding energies for the "hydrophilic" path 1 at separations larger than the equilibrium distance. Figures 13 (b) and (c) further illustrate that the NPFF force field overestimates binding energies of water with methoxy carbon (Path 2) and methylene carbons (Path 3).

This strong attractive interaction replaces the "hydrogen bonding" function in nonpolarizable potential where C_{ij} for the O_E-H_W interaction was set to zero and attraction was represented with a negative value of A_{ij} in the exponential term of eq. 10 for this interaction. It was found that allowing a large dispersion interaction gives a much better description of DME/water for distances beyond the minimum energy configuration for

Figure 13. DME/water total ΔU_{QC}^{Total} (open circles) and van der Waals ΔU^{vdW} (open diamonds) energies are given as obtained from *ab initio* calculations. Lines indicate a reproduction accuracy of PFF-1 and PFF-2 force fields.

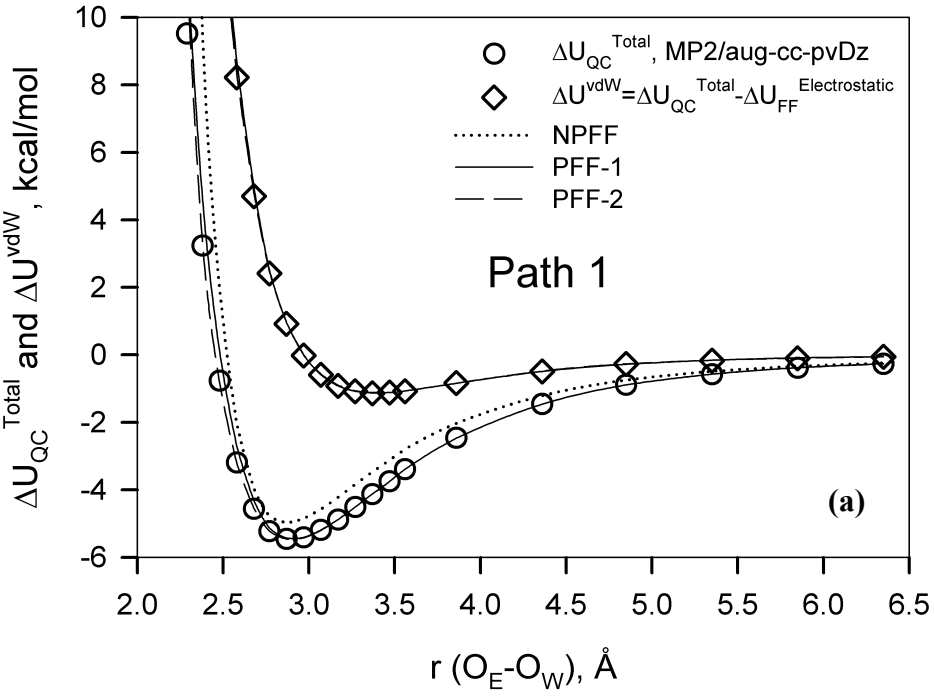
ΔU_QC^Total, MP2/aug-cc-pvDz
ΔU^vdW=ΔU_QC^Total-ΔU_FF^Electrostatic
NPFF
PFF-1
PFF-2
Path 1
(a)
ΔU_QC^Total and ΔU^vdW, kcal/mol
r (O_E-O_W), Å

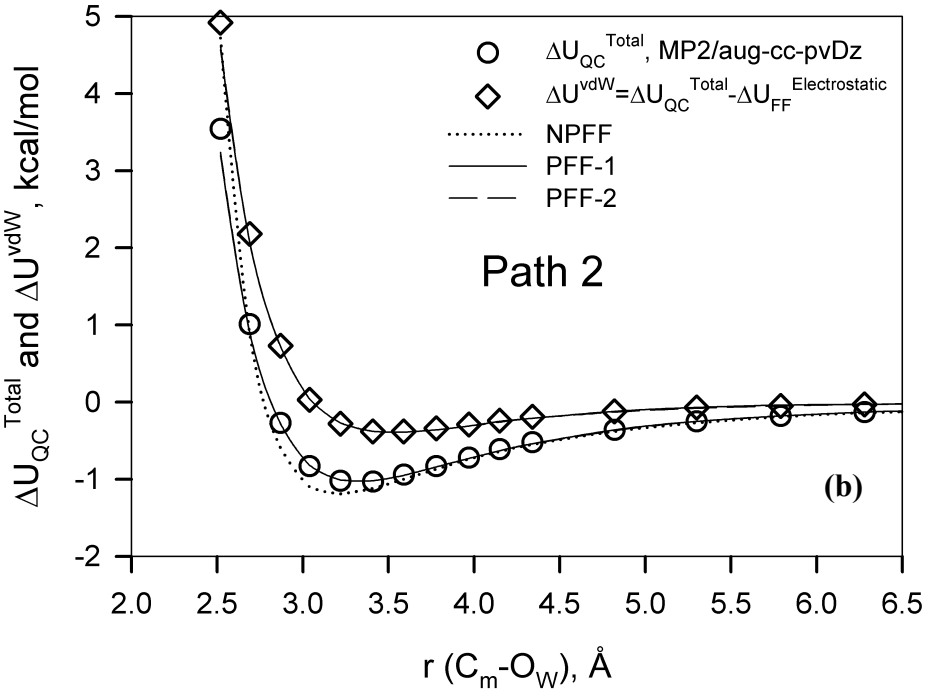
ΔU_QC^Total, MP2/aug-cc-pvDz
ΔU^vdW=ΔU_QC^Total-ΔU_FF^Electrostatic
NPFF
PFF-1
PFF-2
Path 2
(b)
ΔU_QC^Total and ΔU^vdW, kcal/mol
r (C_m-O_W), Å

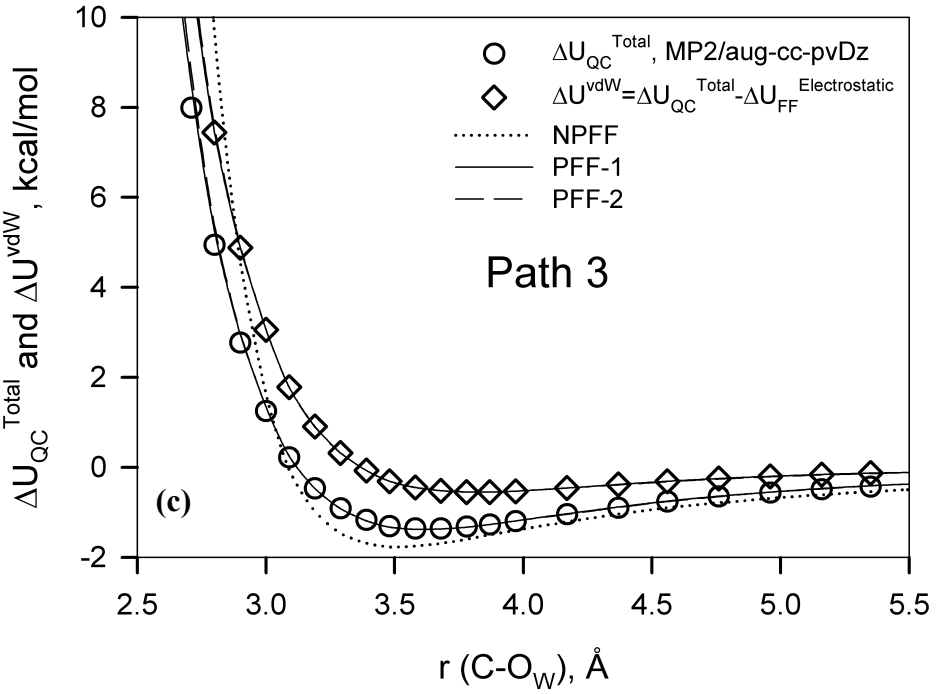

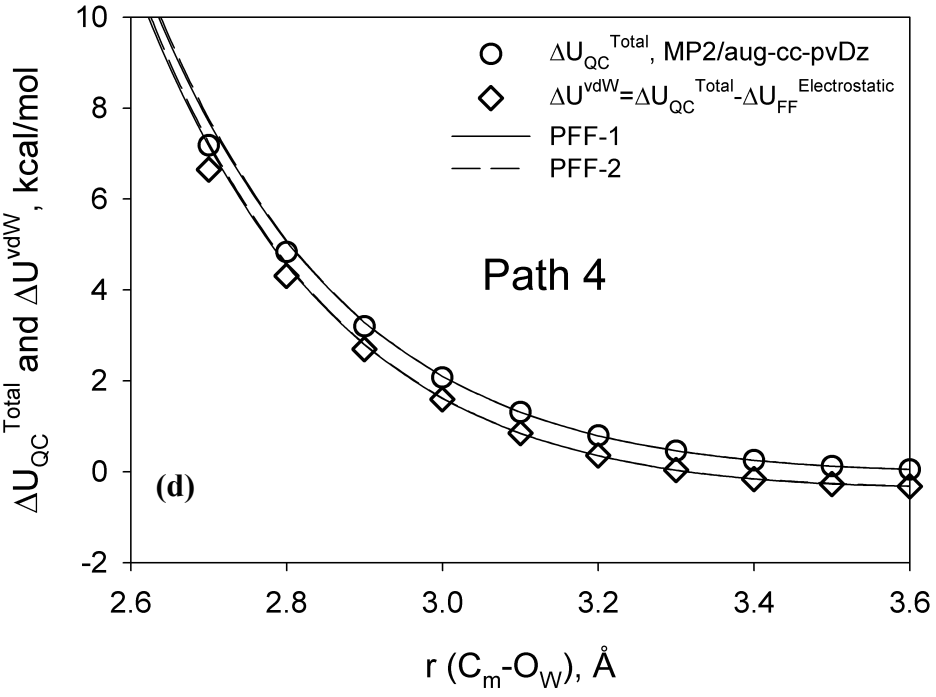

Figure 13. Continued

the Path 1 than the negative A_{ij} approach because of the longer-range nature of the dispersion interaction compared to the exponential term. However, the dispersion energy contribution is quantitatively similar for both functions at the distances longer than 2.5 Å. Contribution from these interactions eventually becomes negligible at the distances of 5.0 Å. It is unclear why a strongly attractive O_E-H_W nonbonded interaction is necessary to accurately describe Path 1, i.e., why binding along this path is not well described by Coulomb, polarization, and nonbonded interactions between O_E-H_W and the ether atoms This could be due to some covalent character of the O_E-H_W or inadequacies in the description of Coulomb/polarization interactions upon close approach of these atoms. The fitted force field parameters are shown in Table 2.

Molecular mechanics for the ether/water dimer is performed next to find minimum equilibrium interaction distances and energies obtained implementing two sets of nonbonded force field parameters. Binding energy is calculated as a difference of interaction energy of complex and individual energies of molecules. The equilibrium ether/water separation and minima energies (Path 1) predicted by nonpolarizable and polarizable force fields are compared with *ab initio* data and the CHARMM[99] polarizable force field in Table 3. It can be seen that there is a little difference in the optimal oxygen-hydrogen separation distance and ether/water binding energy for both force fields. Interaction energies are overestimated as predicted by PFF-1 and PFF-2 and underestimated as predicted by the NPFF force field. However, optimal separation distance is shorter for the CHARMM[99] polarizable force field using the original SWM4-DP water model. Interaction energy is significantly underestimated almost by1 kcal/mol.

Table 2. Nonbonded repulsion and dispersion parameters for ether/water interactions

	PFF-1		PFF-2		PFF-1/2
Ether/water pair	A_{ij}, kcal/mol	B_{ij}, Å^{-1}	A_{ij}, kcal/mol	B_{ij}, Å^{-1}	C_{ij}, kcal/mol Å^6
C_m-O_w	14500.76	3.28913	24893.76	3.32675	690.76
C_m-H_w	35764.40	4.85465	45764.40	4.83499	0.00
O-O_w	341418.22	3.94109	787505.34	4.17895	451.12
O-H_w[a]	-21.60[b] (PFF-1) -20.00[c] (PFF-3) -16.50[d] (PFF-5)	1.38137	1841.85[d]	3.12997	355.75 (PFF-2) 330.00 (PFF-4) 310.00 (PFF-6)
C-Ow	29589.70	3.55272	79674.89	3.58426	665.24
C-Hw	34242.45	4.73729	43297.32	4.81314	0.00
H-O_w	11934.82	3.67285	5445.07	3.50718	138.67
H-H_w	2361.00	3.98266	2506.97	4.08434	0.00

[a] "Hydrogen bond" adjustable function;

[b, c, d] PFF-1/3/5 does not have a dispersion parameter

Table 3. Ether/water equilibrium distances and interaction energies in gas phase for quantum chemistry and molecular mechanics calculations

$R_{(O\text{-}Hw)}$, Å (see Figure **12 a**)				Binding energy, kcal/mol			
QC[a]	NPFF[b]	PFF-[X][c]	CHARMM[d]	QC[a]	NPFF[b]	PFF-[X][c]	CHARMM[d]
1,2-dimethoxyethane (*ttt* conformer)							
1.92	1.91	**1.90 [1]**	1.81	-5.46	-5.25	**-5.74 [1]**	-4.65
2.03[f]		**1.88 [2]**				**-5.74 [2]**	

[a] Quantum chemistry at the MP2/aug-cc-pvDz level (this work)

[b] Nonpolarizable force field of Ref. [42], reproduced values from that work

[c] Polarizable force field, this work

[d] Polarizable force field of Ref. [99], values taken from that work

[f] Optimized geometries at SCF/D95** level, values are taken from previous work [42]

3. VALIDATION OF THE PEO/WATER POLARIZABLE FORCE FIELD

Molecular dynamics simulations of PEO/water solutions were performed in order to (a) validate the PFF-X by comparison of thermodynamic, transport, and dynamic properties obtained from MD simulations with available experimental data; (b) compare predictions of the developed PFF-X with the NPFF[42] and CHARMM[99,111] polarizable force fields; and (c) conduct initial studies of the phase behavior of PEO/water solutions as a function of temperature. It should be noted that obtaining an accurate representation of PEO/water solutions as a function of temperature was primary motivation for the development of the PFF-X force fields.

3.1. Simulation methodology

Molecular dynamics simulations of 1,2-dimethoxyethane (DME, 93 Da) and 12 repeat unit PEO (PEO12, with CH3 terminal groups, 530 Da) in aqueous solution have been performed in the composition range (ether weight fraction) w_p=0.01-0.93. Aqueous solutions were comprised of 1-72 solute molecules and 1200-100 water molecules depending upon the composition. The polarizable version of the Lucretius© simulation package[75] was used to carry out MD simulations using a cubic simulation cell with periodic boundary conditions. The standard Shake algorithm[86] was employed to constrain

the bond lengths and water geometry. Charge-charge long-range electrostatic interactions were computed employing Ewald summation.[87] The reaction field scheme[87] was implemented to handle long-range induced dipole-induced dipole calculations. A cutoff radius was 10.5 Å for nonbonded interactions. A reversible multiple time step propagator algorithm[88] was implemented to solve the equations of motion with the parameters as specified in Section 2.2 of the force field development. Simulations were performed in the temperature interval from 298 K to 550 K. The pressure was increased by 20 atm at 450 K and 550 K to keep the systems in the liquid state. All systems were initially equilibrated at isothermal-isobaric ensemble until satisfactory steady state properties (such as density of the solutions) were reached. Sampling trajectories were generated in the NPT over 20 ns.

3.2. Thermodynamic properties

Poly (ethylene oxide) aqueous solutions are usually characterized by solvation thermodynamics of their oligomers including solvation structure, free energy, enthalpy, and entropy of solvation.[28,34,38] Other properties include enthalpy of mixing,[28,33,31,44] heat capacity,[32] density,[112] excess volume and excess viscosities,[30,37] intrinsic viscosities,[113] and more.[20] Therefore, solvation thermodynamics of DME in water is considered first, followed by transport and dynamic properties of aqueous solutions.

3.2.1. DME solvation structures

The local structure of water around DME is obtained using pair correlation function. The pair correlation function gives a probability of finding the pairs of atoms at

a separation distance r_{ij} as indicated by eq. 13.

$$\rho g\left(r_{ij}\right) = \frac{1}{N}\left\langle \sum_{i}^{N}\sum_{j\neq i}^{N}\delta\left[r - r_{ij}\right]\right\rangle \tag{13}$$

where N is the number of atoms, ρ=N/V is the liquid density, r_{ij} is a vector between centers of atoms i and j, and <> is the time average.

Structural analysis has been performed for the composition of 0.17 weight fraction of DME in water at 298 K. The most preferred DME/water interactions are donor-acceptor type interactions also known as a hydrogen bond. Therefore, a structure of O_E-H_W pair is considered as the most adequate for DME/water solutions. Radial distributions for O_E and H_w pairs are illustrated in Figure 14. The hydration structures are found to be very similar for all considered force fields as indicated by three peak distributions. Positions of the peaks are nearly invariant.

The first maximum corresponds to the probability of finding water molecules that are hydrogen bonded to DME. The third maximum corresponds to the probability of finding water in the second hydration shell.

The structures are more developed using polarizable potential as indicated by well-defined narrow peaks of the distributions while distribution peaks are broad for the nonpolarizable force field. These structural differences can be referred to the enhanced directionality of O_E-H_W interactions that is achieved by implementing two-charge ether model in polarizable force fields. The first peak of DME aqueous solution is also shifted to the shorter distances as obtained for PFF-1 and PFF-2 force fields. Position of the first

Figure14. O_E-H_W intermolecular radial distribution functions are given for DME/water solutions as obtained from MD simulations at 298 K.

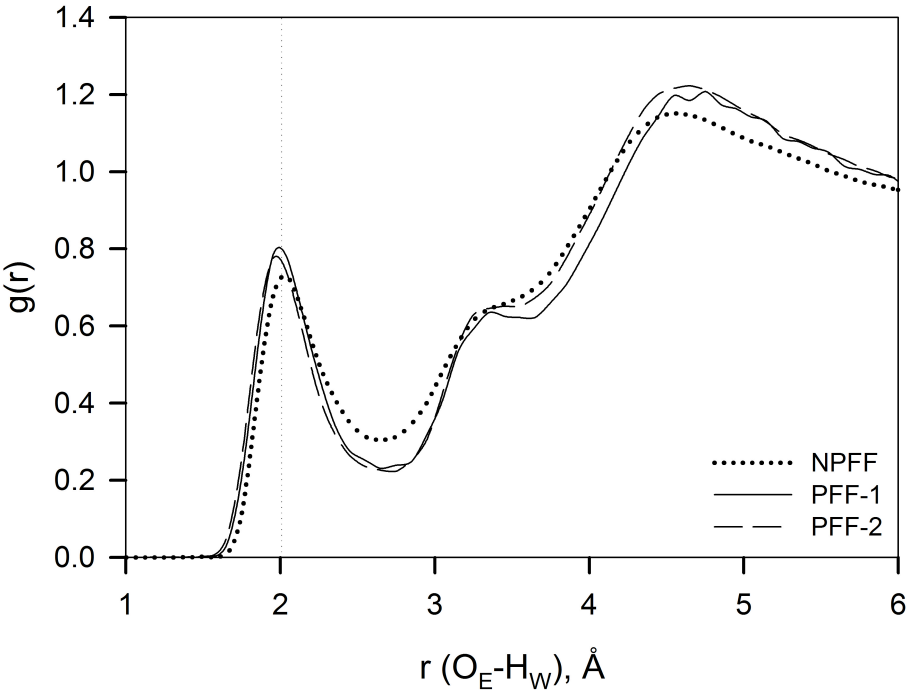
1.4
1.2
1.0
0.8
0.6
0.4
0.2
0.0
g(r)
1
2
3
4
5
6
r (O_E-H_W), Å
NPFF
PFF-1
PFF-2

peak is at 2.01 Å for NPFF.

Pair distributions show no difference in positions of the second peaks and some deviation in the third peak. The probability of finding a water molecule in the second hydration shell is systematically less using nonpolarizable potential. Systematically lower probability of finding a water molecule in the first hydration shell of DME is obtained for PFF-2. At the same time, the probability of finding a water molecule around DME in the second hydration shell is higher.

Solvation structures of O_E-O_W were also studied (not shown in Figure 14) and compared with water solvation structure. It was concluded that solvation structure of DME/water, implementing *ab initio* polarizable potentials, can not be fitted into hydrogen bond network as it was suggested by Kjellander and Florin.[114] A similar conclusion was observed in previous studies of solvation structures for PEO/water solutions using nonpolarizable force field where the solvent was represented by the TIP4P water model.[64] This information was also confirmed from experiment using neutron diffraction.[36]

3.2.2. Free energy of DME solvation in water

Free energy of solvation should be determined to differentiate the predominant effect involved in solvation process of DME. Solvation of a solute can be entropically driven or can be a result of strong intermolecular interactions. Previous studies of solvation thermodynamics have shown energetically favorable (strong DME/water interactions) and entropically unfavorable solvation of DME in water.[61] There are few available methods to compute free energy of solvation such as potential of mean

constrained force (POMF), the self-consistent histogram method (SHM), free energy perturbation (FEP), or thermodynamic integration (TI) methods.[110] In previous works, the self-consistent histogram method has been employed to calculate the free energy of solvation scaling linearly the repulsion/dispersion and electrostatic parameters between ether and water intermolecular interactions.[61,64] This method is difficult to implement to the nonadditive force fields due to nonlinear many body polarization effects. Therefore, a new method has been developed to estimate free energy of solvation ΔG_{solv}, as described in the Appendix, which is further referred to as the interface transit method (IT).

A film of water comprised of 500 molecules was created in the center of an orthorhombic cell with dimensions of 24.6 Å x 24.6 Å x 84.6 Å in the x, y, and z directions, respectively. DME molecule was initially placed in the center of the vacuum. The water film is periodic in the x- and y- directions and has a thickness of approximately 29 Å in the z-direction.

The Ewald summation method[87] with α=0.232 and k_{limit} in x, y, z =6, 6, 11 was used to treat long-range electrostatic interactions. Otherwise, the simulation methodology and parameters were identical to those employed in the bulk solution simulations described in Section 2.2 except that a single time step algorithm with a time step of 1 fs was employed instead of the multiple time step algorithm. In order to adequately thermalize the single gas-phase molecule, the solute was subjected to additional Brownian force[89] with a friction coefficient of γ=0.002 fs^{-1}. The average constrained force for a given Δz, $\langle F(\Delta z)\rangle$, was determined from 4 ns trajectories and 57 (Δz) windows ranging from 0 (in the middle of the film) to 30 Å (middle of the vacuum

phase). The instantaneous force, F(Δz), has been calculated every time step t_i as a function of coordinate.

A mean constraint force, <F(Δz)>, is obtained as a sum of all instantaneous forces from the entire simulation run.

$$\langle F(\Delta z)\rangle = \sum_{i}^{N} \frac{1}{N}\left(F_i(\Delta z)\right) \tag{14}$$

where N is the number of simulation steps and Δz is the distance between center of masses of DME and water film.

Mean constraint force profiles are given in Figure 15 for PFF-1 and PFF-2 force fields. The force in the center of the vacuum equals to zero $<F(\Delta z_{max})>=0$. An attractive force is found to be predominant as DME approaches water/vacuum interface. It was found that a minimum of the potential is located next to the water/vacuum interface indicating a surface of the bulk water as a preferable location for the molecule.

The free energy of transfer of DME from vacuum phase to the liquid phase (center of the film) is given as

$$\Delta G_{solv} = -\int_{\max}^{0} \langle F(\Delta z)\rangle d(\Delta z) \tag{15}$$

Here Δz=max corresponds to the center of the vacuum region. The direct equating of the free energy of transfer with the Gibbs free energy of solvation ΔG_{solv} is a consequence of the reference states used in defining ΔG_{solv}.[115,116] Even though the IT method simulations

Figure 15. Mean constraint force <F> profiles are given for PFF-1 and PFF-2 as a function of position relatively to the center-of-mass of water film. Dotted line is indicating a position of artificial boundaries.

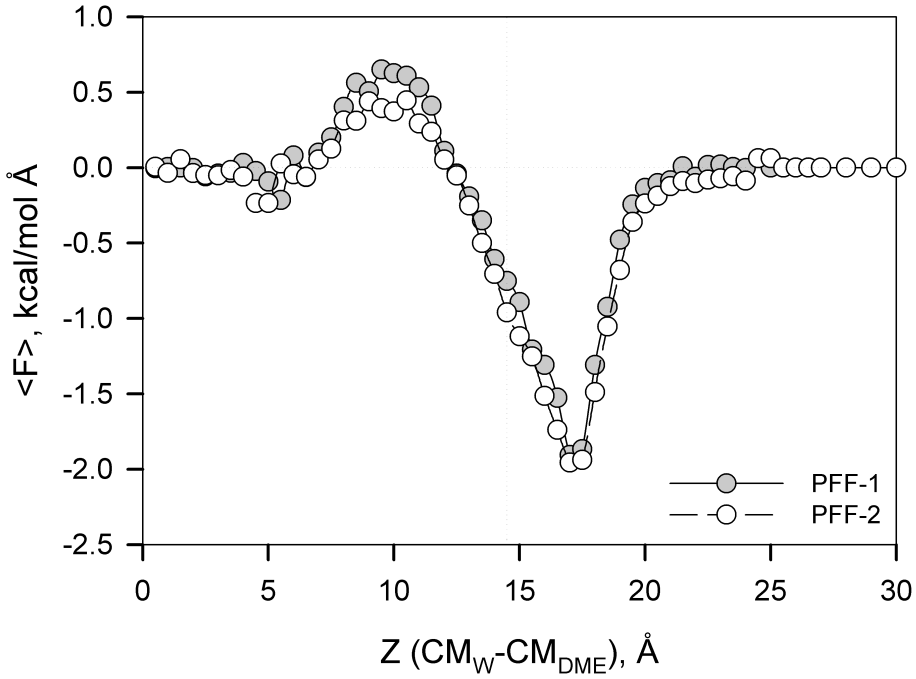
1.0
0.5
0.0
-0.5
-1.0
-1.5
-2.0
-2.5
<F>, kcal/mol Å
0
5
10
15
20
25
30
Z (CM$_W$-CM$_{DME}$), Å
PFF-1
PFF-2

are carried out in the NVE ensemble, the film is able to adjust dimensions upon insertion of the solute so as to maintain negligible normal stress in the z-direction. Consequently, the free energy change determined from integration of the potential of the mean force (eq. 15) is the Gibbs free energy and not the Helmholtz free energy.

Validation of the IT method was carried out first by testing the method to determine ΔG_{solv} for the TIP4P water model. The IT method yielded a value of ΔG_{solv} =-5.9±0.6 kcal/mol that is in excellent agreement with Monte Carlo simulation results of ΔG_{solv} =-6.1±0.3 kcal/mol, and experimental data of ΔG_{solv} =-6.3 kcal/mol.[117] The uncertainty of the free energy calculations is also estimated as described in a series of publications.[118,119] Implementing the IT method for the first set of parameters PFF-1 and PFF-2 resulted in the free energy of solvation of ΔG_{solv} =-5.7 kcal/mol and ΔG_{solv} =-6.6 kcal/mol, respectively, within an error bar of ± 0.6 kcal/mol. Free energy of solvation was found to be ΔG_{solv} =-6.2 kcal/mol using nonpolarizable force field.[42] There are two versions of the CHARMM force fields[99,111] with different polarizability scaling factors. One version, where polarizability scaling factor is 0.7, resulted in underestimation of the free energy of solvation by 1 kcal/mol or ΔG_{solv} =-3.8±0.59 kcal/mol.[99] Another version of the CHARMM force field (polarizability scaling factor is 0.85) showed overestimation of free energy by 0.8 kcal/mol or ΔG_{solv} =-5.61±0.54 kcal/mol.[111]

3.2.3. Enthalpy of DME vaporization

Enthalpy of vaporization is usually used as a reference in parameterization of the force fields to describe the strength of intermolecular interactions, cohesion energy. Water/water intermolecular interactions were characterized by calculating enthalpies of

vaporization for SWM4-DP[72] and TIP4P[76] water models as discussed in Section 2.2. In order to give an estimate of the strength of ether/ether intermolecular interactions, the enthalpy of vaporization is calculated for DME. Polarizable and nonpolarizable force fields are employed for calculations and results are compared with experimental data. The enthalpy of vaporization corresponds to the amount of energy needed to transfer DME molecule from the liquid phase to the gas phase at constant pressure as indicated by eq. 16

$$\Delta H_{vap} = \left[E^{g}_{DME}(P,T) - E^{l}_{DME}(P,T) \right] + RT \tag{16}$$

where the subscript l or g indicates liquid or gas phase, E is the internal energy at temperature T, P is the pressure, and R is the universal gas constant. The assumption is made that DME at 298 K and 1 atm behaves as an ideal gas. The internal energy of the gas phase DME molecule was determined from Brownian dynamics[89] simulations of 125 DME molecules performed at 298 K. The internal energy of the liquid phase DME was determined from MD simulations of 125 DME molecules.

Implementing polarizable force field resulted in ΔH_{vap} = 8.53 kcal/mol that is in a good agreement with experimental value of ΔH_{vap} = 8.70 kcal/mol.[120] However, enthalpy of vaporization using NPFF is 10.04 kcal/mol as it was obtained from calculations. Therefore, nonpolarizable force field significantly overestimates the strength of ether/ether intermolecular interactions by more than 1 kcal/mol in comparison with polarizable potential.

3.2.4. Enthalpy of DME solvation in water

One of the most important characteristics of DME/water solutions is enthalpic contribution to the solvation as an indicator of the formation of hydrogen bonds with water. The enthalpy of solvation of DME in water corresponds to the energy transfer of solute molecules from the gas phase to the solution at constant pressure.[115,116] The enthalpy of DME solvation in water was determined at 298 K and 1 atm as

$$\Delta H_{solv} = E^{l}_{H_2O+DME}(P,T) - \left[(w)E^{l}_{H_2O}(P,T) + (1-w)E^{g}_{DME}(P,T)\right] \quad (17)$$

where the subscript l or g indicates liquid or gas phase, E is the internal energy, P is the pressure, T is the temperature, and w is the weight fraction of H_2O. The internal energy of the gas phase of DME molecules was determined in a similar manner as for the enthalpy of DME vaporization. It should be also noted that the enthalpy of solvation ΔH_{solv} minus RT term would approach enthalpy of vaporization ΔH_{vap} by absolute value as water concentration is approaching zero.

Enthalpies of DME solvation are compared with experimental data using both sets of nonbonded parameters and with the values obtained using NPFF in Figure 16. It is clear from the Figure 16 (a) that both force fields developed are overestimating enthalpies of solvation at all concentrations except high concentrations where the ether/ether interactions are predominant. Enthalpies of solvation are also overestimated implementing NPFF. The area in the frame corresponds to the enthalpies of solvation obtained from MD simulations for 0.01, 0.08, and 0.17 weight fractions of DME. Those

Figure 16. Enthalpies ΔH_{solv} of DME solvation in water are compared as obtained from MD simulations and experiment at 298 K. Lines in figure (b) represent linear fits. Experimental data were taken from Ref. [33,34,31]

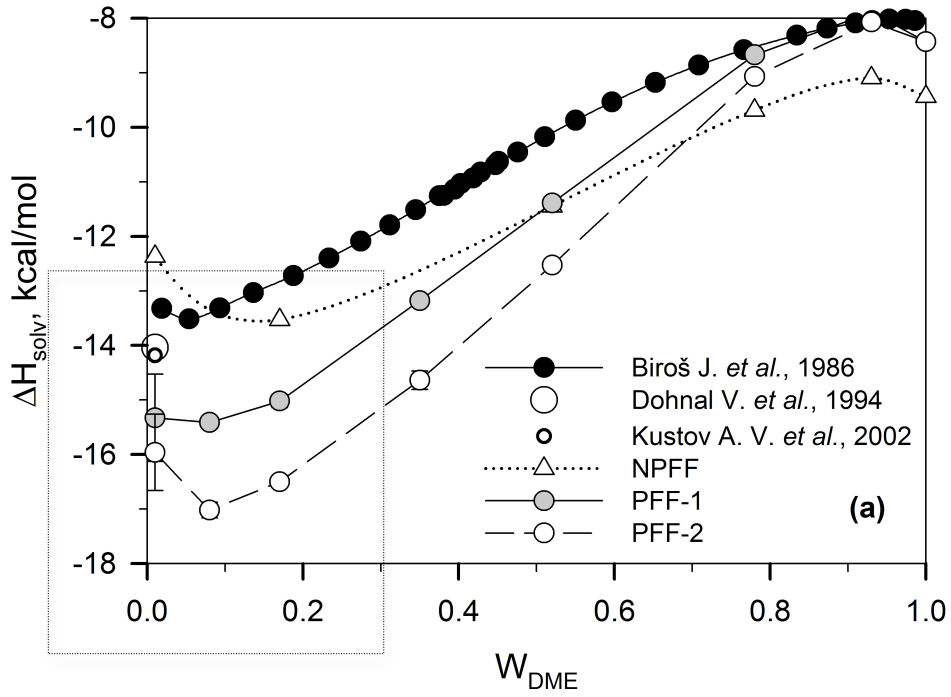
-8
-10
-12
-14
-16
-18
0.0
0.2
0.4
0.6
0.8
1.0
ΔH_solv, kcal/mol
W_DME
Biroš J. et al., 1986
Dohnal V. et al., 1994
Kustov A. V. et al., 2002
NPFF
PFF-1
PFF-2
(a)

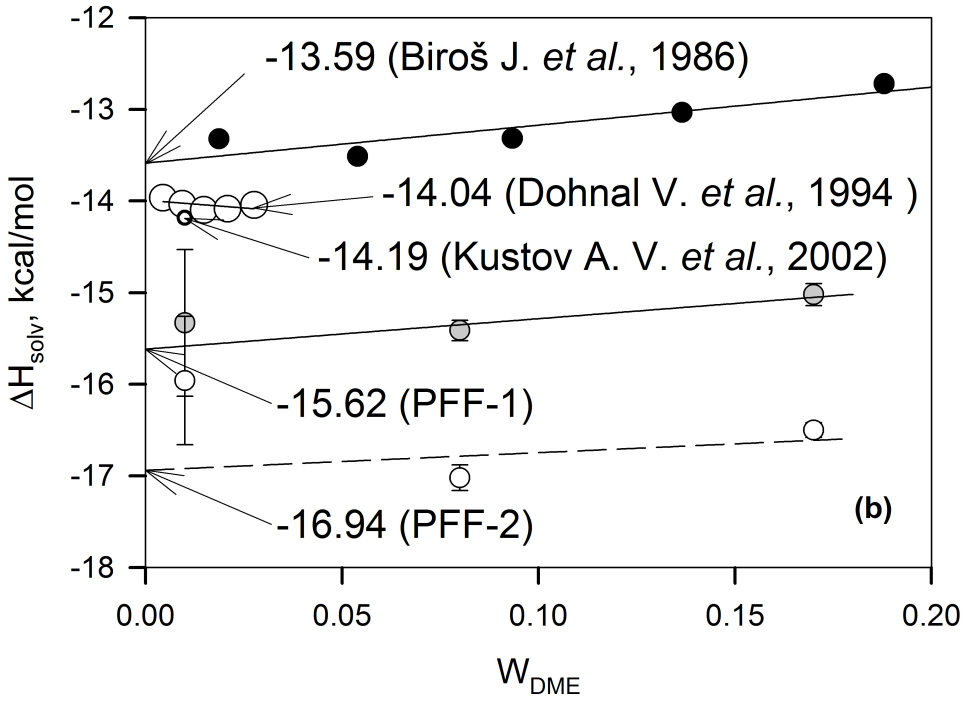
-12
-13
-14
-15
-16
-17
-18
0.00
0.05
0.10
0.15
0.20
ΔH_solv, kcal/mol
W_DME
-13.59 (Biroš J. et al., 1986)
-14.04 (Dohnal V. et al., 1994)
-14.19 (Kustov A. V. et al., 2002)
-15.62 (PFF-1)
-16.94 (PFF-2)
(b)

concentrations are compared with the experimental data for dilute aqueous solutions, Figure 16 (b). Each value is given with the corresponding error bars calculated from MD simulations for 20 ns runs.

As it can be seen, the error bars are higher for lower concentrations of DME while the error bars obtained from the experiments are within 0.01 kcal/mol for all concentrations. Linear fits of those values are performed for each force field and experimental data where the weight for each value of the enthalpy in the fit are taken as inversely proportional to the absolute values of the error bars from MD simulations, $w_f=|\text{error bar}|^{-1}$.

In Figure 16 (b), lines specify the fitting trends and the intercepts of those lines with the y-axis are extrapolated values for the enthalpies of DME solvation. Those values are taken as final for comparison. It can be seen that in dilute regime, the enthalpy of solvation also depends on composition. Enthalpy of DME solvation is getting more favorable with decreasing of DME concentration. Similar composition tendency was observed for the oxygen and nitrogen contained hydrophilic compounds including diethylene glycol.[33] However, no composition dependence of the enthalpy was observed for DME and other compounds in dilute regime as it was obtained from experiment.[33]

Three values for the enthalpies are obtained from the fitting of experimental data as ΔH_{solv}=-14.19 kcal/mol, ΔH_{solv}=-14.04 kcal/mol, and ΔH_{solv}=-13.59 kcal/mol. Despite a small uncertainty reported for the experimental measurements the values obtained from three independent sources vary within 0.6 kcal/mol. Implementing both polarizable force fields, PFF-1 and PFF-2, have resulted in ΔH^{∞}_{solv} =-15.62 kcal/mol and ΔH^{∞}_{solv} =-16.94 kcal/mol, respectively.

As it was expected, enthalpy of solvation is more favorable implementing PFF-2 force field by almost ~3 kcal/mol in comparison with PFF-1 that overestimated by ~2 kcal/mol. This difference can be attributed to the presence of a dispersion parameter on the "hydrogen bond" function of PFF-2 force field that accounts for the long-range intermolecular interactions.

Enthalpies of solvation obtained for NPFF are ΔH_{solv}=-12.37 kcal/mol and ΔH_{solv}=-13.53 kcal/mol for 0.01 and 0.17 DME weight fraction, respectively. The final value for the enthalpy of solvation implementing NPFF is taken as an average of two resulting in ΔH_{solv}=-12.95 kcal/mol. This value underestimates ether/water intermolecular interactions for dilute solutions. However, enthalpy of DME solvation is significantly overestimated at higher concentrations. It should be noticed that enthalpy of solvation obtained from MD simulations is different from data reported in previous publication (ΔH_{solv}=-17.1 kcal/mol).[42]

Previous *ab initio* studies have revealed that hydrophobic ether/water interactions, interactions of water with methylene segment of DME backbone, mostly influenced excess free energy and enthalpy of solvation.[42] PFF-1 and PFF-2 force fields have a perfect agreement in describing interaction energies of water with methylene segment of DME. However, excess enthalpy of DME solvation is still significantly overestimated implementing both polarizable force fields. As a consequence, the assumption is made that intermolecular interactions of water with hydrophobic as well as hydrophilic segments of DME dictate excess thermodynamic properties of DME aqueous solutions. This assumption is further investigated in polarizable force fields by performing

empirical adjustments to the interaction parameters of the "hydrogen bond" functions that result in reduction of DME/water favorable interactions.

3.2.5. Enthalpy of DME/water mixing

The enthalpy of mixing was calculated as a function of DME concentration. The enthalpy of mixing DME with water corresponds to the energy transfer of solute molecules from the liquid phase to the solution at constant pressure at 298 K and 1 atm as

$$\Delta H_{mix} = E^{l}_{H2O+DME}(P,T) - \left[(w)E^{l}_{H_2O}(P,T) + (1-w)E^{l}_{DME}(P,T)\right] \quad (18)$$

where the subscript l indicates liquid phase, E is the total energy, P is the pressure, T is the temperature, and w is the weight fraction of H_2O.

The enthalpies of mixing are compared with experimental data in Figure 17. The results are also compared with values obtained for the NPFF force field. It can be noticed that NPFF gives the best description of the experimental enthalpy of mixing. These unexpected results arise more likely due to the errors in the description of ether/water and ether/ether intermolecular interactions. Interaction energies of ether/water and ether/ether are overestimated by the NPFF, while water/water interactions are well-described as indicated by the enthalpy of TIP4P vaporization as ΔH_{vap}=10.51 kcal/mol. Therefore, a good agreement reached in energies of mixing implementing NPFF might be a result of an error cancelation in ether/water and ether/ether interactions.

Qualitatively similar results are obtained implementing PFF-1 and PFF-2 force fields. As can be seen from Figure 17, PFF-1 is less hydrophilic than PFF-2 but still

Figure 17. Enthalpies of mixing ΔH_{mix} are compared as a function of solution concentration at 298 K for DME/water solutions. Experimental data were taken from Ref. [31]

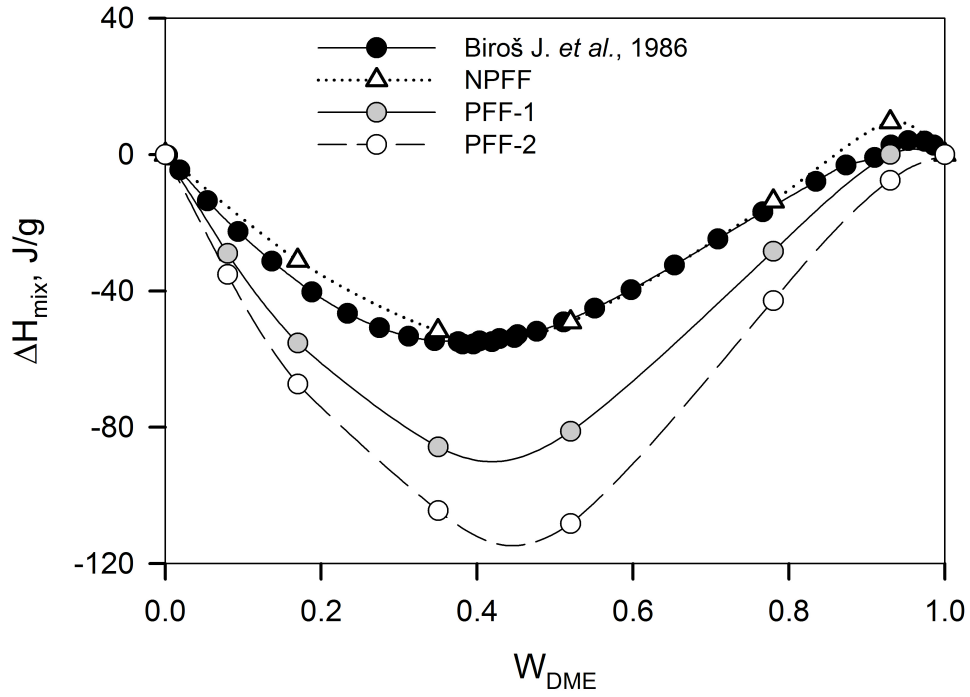
40
0
-40
-80
-120
0.0
0.2
0.4
0.6
0.8
1.0
ΔH_mix, J/g
W_DME
Biroš J. et al., 1986
NPFF
PFF-1
PFF-2

significantly overestimates the enthalpy of mixing. These results are well correlated with free energy of DME solvation where PFF-1 force field predicts almost ~1 kcal/mol less favorable energy than PFF-2 and, therefore, gives a better description of the enthalpy of mixing. Again, those deviations in the free energy and enthalpy of mixing can be referred to the presence of a dispersion parameter on "hydrogen bond" function that results in more favorable ether/water interactions due to the presence of a long-range character. Qualitatively similar results in the enthalpy of mixing was obtained for higher molecular weight PEO with various terminal groups including ($-CH_3$) and (-OH) terminal groups.[28,33]

3.2.6. Excess volume of DME/water solutions

Excess volume is often considered as a result of solvation (mixing) process for two or more compounds. It can be negative or positive depending upon several solvation effects as discussed in introduction Section 1.2.[30] Positive excess volume usually indicates weak, unfavorable solute/solvent intermolecular interactions while negative excess volume is an indicator of strong favorable interactions. Here, the strength of DME/water intermolecular interactions is studied by calculating the excess volume as a function of DME concentration. The excess molar volume ΔV^E of ether/water solutions is determined as indicated by the eq. 19

$$\Delta V^E = V_{mixture} - \left(x_{solvent} V_{solvent} + x_{solute} V_{solute}\right) \tag{19}$$

where $V_{mixture} = \frac{x_{solvent}M_{solvent} + x_{solute}M_{solute}}{\rho_{mixture}}$ is the molar volume of the mixture, $V_i = \frac{x_i M_i}{\rho_i}$ is the molar of the pure components (solvent and solute), M_i is the molecular weights of the pure components, x_i is the mole fraction of solvent or solute in the mixture, and ρ is the density.

Experimental data for the excess volume are available for three temperatures as indicated in Section 1.2. Comparison of DME/water excess volume at 298 K and 318 K revealed no substantial difference between the two (Figure 2 (a)). Therefore, comparison of the results from MD simulation and experiments is given at 318 K in Figure 18.

Qualitative agreement with experiment has been reached in excess volume using both polarizable force fields. Implementing PFF-1 resulted in underestimation of the excess volume while implementing PFF-2 resulted in large negative deviations indicating strong binding of DME with water. Again, this can be attributed to having a large dispersion parameter on the "hydrogen bond" function that accounts for long-range intermolecular interactions. Both force fields predict minimum between 0.6-0.8 weight fractions of DME. Similar quality agreement for the excess volume is obtained at 298 K. In contrast, implementing NPFF resulted in the minimum shifted to the less concentrated solutions. The minimum can be found at 0.52 weight fraction of DME. Development of nonpolarizable force field has shown that a quality fit for the hydrophobic Path 3 (see Figure 12 (b)), was influencing the overall excess volume and it was insensitive to the hydrophilic path.[42] Intermolecular interactions of water with methylene segment of DME mainly dictated the performance of the force field on the excess volume along with other excess thermodynamic properties.[42] Substantial deviation is found from experiment in excess volume for the entire concentration range for both polarizable force fields. Again,

Figure 18. Excess volumes ΔV^E are compared as a function of solution concentration at 318 K for DME/water solutions. Experimental data were taken from Ref. [30]

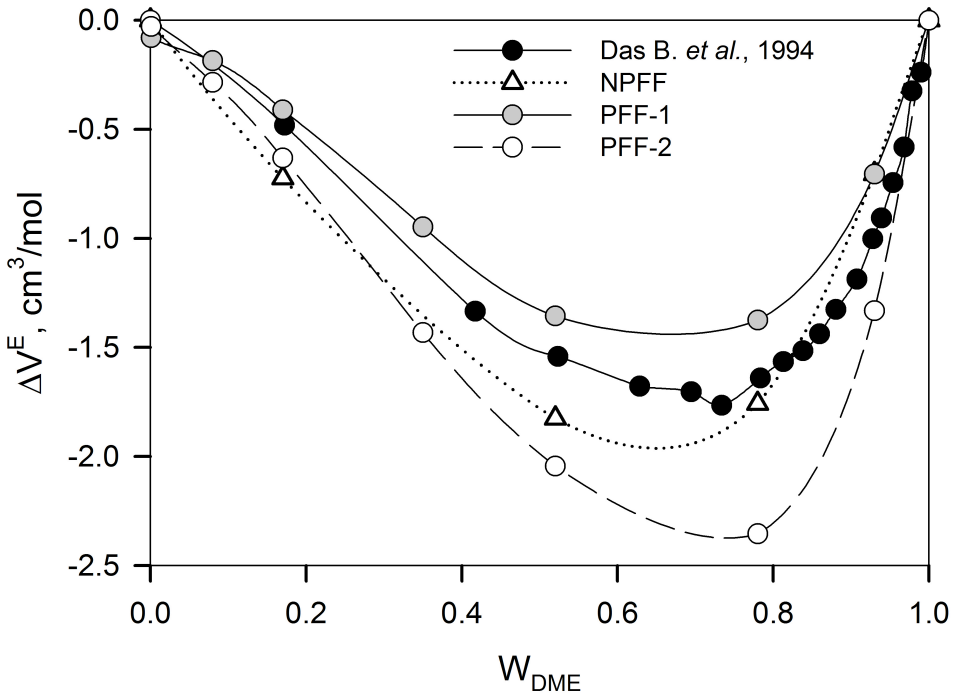
Das B. et al., 1994
NPFF
PFF-1
PFF-2
0.0
-0.5
-1.0
-1.5
-2.0
-2.5
0.0
0.2
0.4
0.6
0.8
1.0
ΔV^E, cm^3/mol
W_DME

influence of intermolecular interactions of water with hydrophilic and hydrophobic segments of DME may account for such deviations.

3.3. Transport and dynamic properties

3.3.1. Water self-diffusion coefficient of DME/water solutions

The self-diffusion of water is an important factor to be considered when dealing with solvation or interfacial properties of aqueous solutions. Mobility of water molecules near a solute is affected by hydrogen bonding or by hydrophobic hydration. It is also well known that water dynamics at the interface is much different from that of bulk water including protein/water, polymer/water, and other interfaces.[35] Here, the influence of solute concentration on water dynamics is studied by obtaining the self-diffusion coefficient of water for DME/water solutions. The self-diffusion coefficient of water was determined using Einstein relation[87] as

$$D_W = \lim_{t\to\infty} \frac{\left\langle \left(r(t) - r(0)\right)^2 \right\rangle}{6t} \tag{20}$$

where r(t) is the center of mass position of a molecule at time t, $\langle\ \rangle$ indicates an ensemble average, and $\left\langle \left(r(t) - r(0)\right)^2 \right\rangle$ corresponds to the mean square displacement of a molecule's center of mass.

The results obtained from MD simulations are compared with experiment in Figure 19. The self-diffusion coefficients of water in DME/water solutions were obtained from experiment by measuring its translational water diffusion constants using the QENS

Figure 19. Self-diffusion coefficients D_w are compared as a function of solution concentration at 318 K for DME/water solutions. Experimental data were taken from Ref. [30,40,41]

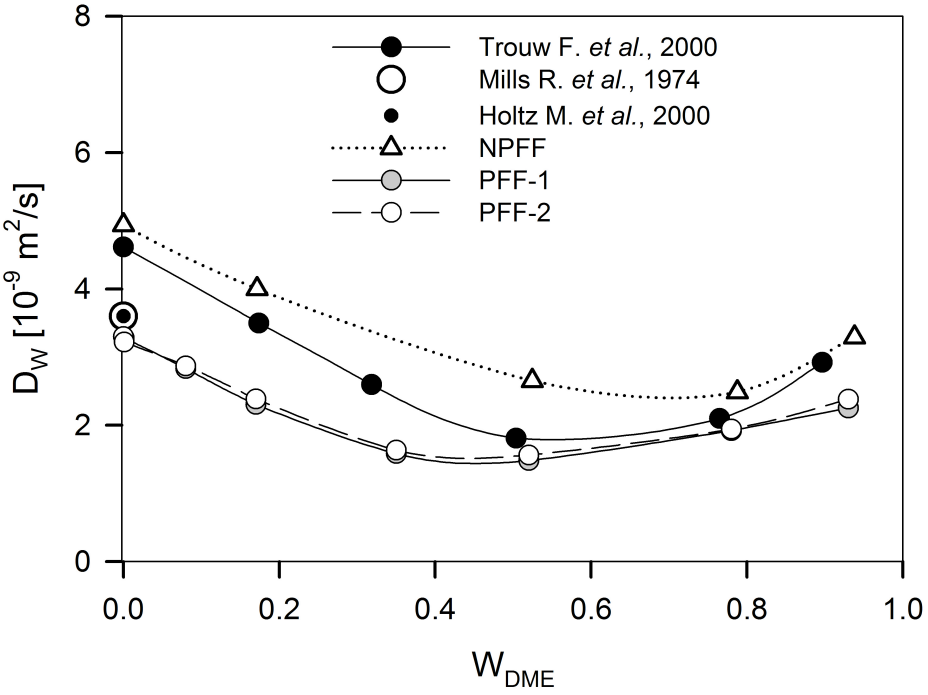
Trouw F. et al., 2000
Mills R. et al., 1974
Holtz M. et al., 2000
NPFF
PFF-1
PFF-2
D_W [10^-9 m^2/s]
W_DME
0
2
4
6
8
0.0
0.2
0.4
0.6
0.8
1.0

(quasi-elastic neutron scattering) technique as indicated in Section 1.2 (see Figure 4).[35] The performance of this model was tested on pure water from 253-293 K.[39] However, the diffusion coefficient for the pure water reported by Trouw et al.[35] is $D_W = 4.6 \times 10^{-9}$ m^2 s^{-1}. Water self-diffusion coefficient obtained using the isotopic method[40] is $D_W = 3.6 \times 10^{-9}$ m^2 s^{-1} and the pulsed magnetic field gradient NMR method[41] is $D_W = 3.6 \times 10^{-9}$ m^2 s^{-1}. The difference between Trout et al.[35] and other experimental data is ~30 %.

Therefore, reported experimental values for the self-diffusion coefficient of water as a function of DME concentration could be overestimated due to some discrepancies in the fitting model or due to statistical inaccuracy, perhaps for low DME concentrations only. As a consequence, two values for the diffusion coefficients of pure water are given in Figure 19. It can be seen that diffusion coefficient of SWM4-DP is in a good agreement with experimental data determined by isotopic and NMR methods. Analysis of DME/water solutions has shown a qualitative agreement of PFF-1 and PFF-2 with experimental data determined by Trouw et al.[35]

The minimum of water self-diffusion is located between 0.35 and 0.55-weight fraction of DME, which is also in an agreement with experiment. A significant reduction of water self-diffusion is obtained within all concentration ranges for both polarizable force fields. These results are consistent with the general trend of polarizable water models to have lower diffusion coefficient over nonpolarizable ones due to explicit polarization.[85] Agreement with experimental data can be further improved by taking into account a deviation obtained for the pure water self-diffusion coefficient. However, additional experimental studies are necessary to establish a quantitative agreement with simulation results. Implementing NPFF has greatly overestimated the water self-diffusion

at all considered concentrations. The developed minimum is also shifted to the higher concentrations, 0.78-weight fraction of DME.

3.3.2. Excess viscosity of DME/water solutions

The viscosity of DME/water solutions, pure water and pure DME were determined using Einstein relation[87] accounting for diagonal and nondiagonal elements as thoroughly described in a number of publications.[97,121,122]

$$\eta = \lim_{t\to\infty} \frac{V}{20k_bTt} \left\langle \sum \left(L_{\alpha\beta}(t) - L_{\alpha\beta}(0) \right)^2 \right\rangle \tag{21}$$

where $L_{\alpha\beta}(t) = \int_0^r P_{\alpha\beta}(t')d(t')$, $P_{\alpha\beta}$ is the symmeterized stress tensor, αβ are the components of the stress tensor, k_b is the Boltzmann constant, T is the temperature, V is the volume of the simulation box, and $\langle\ \rangle$ indicates an ensemble average.

$P_{\alpha\beta}$ is the stress sensor defined as $P_{\alpha\beta} = \frac{\sigma_{\alpha\beta} + \sigma_{\beta\alpha}}{2} - \frac{\delta_{\alpha\beta}}{3} tr(\sigma)$ where $\sigma_{\alpha\beta}$ is a stress tensor $\delta_{\alpha\beta} = 1$ for $\alpha = \beta, \delta_{\alpha\beta} = 0$ for $\alpha \neq \beta$.

And excess viscosity is given by the following relationship

$$\Delta\eta^E = \eta_{mixture} - \left(x_{solvent}\eta_{solvent} + x_{solute}\eta_{solute} \right) \tag{22}$$

where $\Delta\eta^E$ is the excess viscosity, $\eta_{mixture}$ is the viscosity of the binary solution, and η_i is the viscosity of the pure component (solvent or solute), and x_i is the molar fraction of solvent or solute in the mixture.

Experimental results indicate a systematic increase in excess viscosity up to 0.52 weight fraction of DME where a maximum is reached. Further reduction in excess viscosity is obtained for higher DME concentrations (see Figure 2 (b)).

The excess viscosities predicted using PFF-1 and PFF-2 as a function of solution composition are compared with experiment in Figure 20. Predictions in excess viscosities using NPFF are also given for comparison. Good agreement in excess viscosities is established for dilute and concentrated regimes of DME/water solutions. However, significant deviation has been obtained for concentrations between 0.2-0.6 weight fractions of DME. Excess viscosity is systematically overestimated within that concentration range. The position of the maximum is shifted to the less concentrated solutions, ~0.4 DME weight fraction. Again, higher deviation from experiment is obtained implementing PFF-2 force field. These results indicate stronger intermolecular interactions between DME and water for PFF-2 in comparison with PFF-1 force field.

Figure 20. Excess viscosities $\Delta\eta^E$ are compared as a function of solution concentration at 318 K for DME/water solutions. Experimental data were taken from Ref. [30]

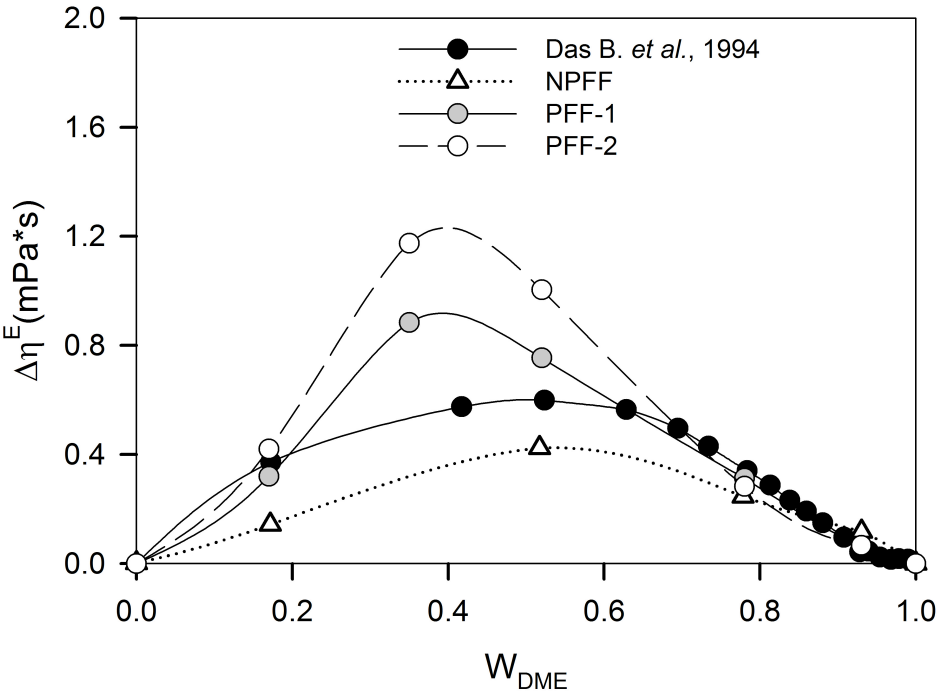
2.0
1.6
1.2
0.8
0.4
0.0
0.0
0.2
0.4
0.6
0.8
1.0
$\Delta\eta^E$(mPa*s)
W_{DME}
Das B. et al., 1994
NPFF
PFF-1
PFF-2

4. EMPIRICAL ADJUSTMENTS OF THE PEO/WATER FORCE FIELD

One of the goals of this work is to gain a better understanding of the correlation between ΔG_{solv} of DME in water predicted by a force field and other solvation thermodynamic and dynamic properties including enthalpy, entropy, excess volume, water self-diffusion coefficient, and excess viscosity. A correlation between ΔG_{solv} of DME solvation and predicted phase behavior of PEO in aqueous solution is also investigated. For this purpose, four additional forces fields are introduced that are variations of PFF-1 and PFF-2. These force fields will be more "hydrophobic" than PFF-1 and PFF-2 and will have correspondingly smaller ΔG_{solv} of DME in water as indicated in Section 4.1.

4.1. Thermodynamic perturbation method

PFF-1 and PFF-2 force fields resulted in significant deviations from experimental data, as discussed in Chapter 3. However, these polarizable force fields were developed based on pure *ab initio* calculations of binding energies of DME with water as discussed in Section 2.4. Validation of those force fields resulted in the overestimation of the free energy and enthalpy of DME solvation in comparison with the experiment and NPFF. Other properties were also overestimated including excess volume and excess viscosity.

Comparison of ΔG_{solv} for PFF-1 and PFF-2 with experiment (Table 3) reveals that these quantum chemistry-based potentials yield ether/water interactions that are too favorable. To improve an agreement with experiment of thermodynamic and, perhaps, other properties of interest, empirical adjustments are performed for both force fields. Two sets of the force fields are obtained and further referred to as PFF-3 and PFF-4, which would provide the experimental value for the free energy of DME solvation in water by making empirical adjustments to the repulsion and dispersion parameters of O_E-H_W function only. Other dispersion parameters were left unchanged, as they have been determined using experimental data of atomic polarizabilities and were validated over a number of compounds.[73,97,102] All other nonbonded parameters were also kept unchanged. Repulsion parameter $A_{O\text{-}Hw}$ of PFF-1 was adjusted to get the force field PFF-3 and dispersion parameter $C_{O\text{-}Hw}$ of PFF-2 was adjusted to get the force field PFF-4. In addition to that, two extra sets of the force fields are obtained, further referred to as PFF-5 and PFF-6, which would provide the less favorable value for the free energy of DME solvation than experiment. Therefore, adjusting repulsion parameter $A_{O\text{-}Hw}$ on the "hydrogen bond" function of PFF-1 will result in PFF-3 and PFF-5 force fields and adjusting dispersion parameter $C_{O\text{-}Hw}$ on hydrogen bond function of PFF-2 will result in PFF-4 and PFF-6 force fields, respectively.

Thermodynamic perturbation method[110] was employed to obtain free energy of solvation using trajectories of PFF-1 and PFF-2 force fields as a reference. Those trajectories were obtained from the free energy calculations employing IT method as discussed in Section 3.2.2. Two systems were chosen where the DME molecule was placed in a simulation box and the value of average constrained force was equal to zero

(<F>≈0). Every empirical adjustment was followed by calculation of the energy difference ΔG until experimental value of ΔG_{solv} =-4.8 kcal/mol was reached.[123] All the calculations were made as indicated by the following equation

$$\Delta G_{0\to X} = G_X - G_0 = -k_b T \ln\left\langle \exp\left(-\frac{E_X - E_0}{k_b T}\right)\right\rangle_n \tag{23}$$

where $\left\langle \exp\left(-\frac{E_X - E_0}{k_b T}\right)\right\rangle$ is an averaging of the ensemble for the reference systems PFF-1 or PFF-2; X indicates the version of the force field; k_b stands for the Boltzmann constant; and T is the temperature.

Repulsion parameter $A_{O\text{-}Hw}$=-20.00 kcal/mol is obtained with corresponding free energy of DME solvation ΔG_{solv} =-4.9 ± 0.6 kcal/mol that would be referred to as PFF-3 force field. A significant reduction of the dispersion parameter $C_{O\text{-}Hw}$ was necessary to reach experimental value for the free energy of DME solvation resulting in $C_{O\text{-}Hw}$=330 kcal/mol Å^6 that would correspond to the PFF-4 force field. For the purpose of studying the effect of ΔG_{solv} on phase behavior of PEO as a function of temperature, two additional forces fields are obtained, PFF-5 and PFF-6, which are variations of PFF-1/3 and PFF-2/4. Empirical adjustment is performed in a similar way as for PFF-3 and PFF-4 force fields resulting in repulsion parameter of $A_{O\text{-}Hw}$=-16.50 kcal/mol for PFF-5 and dispersion parameter of $C_{O\text{-}Hw}$=310 kcal/mol Å^6 for PFF-6. These force fields are more "hydrophobic" than PFF-3 and PFF-4 along Path-1 and, therefore, have correspondingly smaller ΔG_{solv} of DME in water (ΔG_{solv} =3.8 kcal/mol).

5. EFFECT OF EMPIRICAL ADJUSTMENTS ON THE BEHAVIOR OF PEO/WATER SOLUTIONS

5.1. Effect of empirical adjustments on DME/water interactions

Predictions of empirical force fields in binding energies of DME with water as a function of separation are considered along four different paths as design to develop PFF-1 and PFF-2 force fields. Those predictions are shown in Figure 21 (a-d). Predictions of NPFF are also given for comparison. It can be seen that despite empirical adjustments, both force fields well describe quantum chemistry on the hydrophilic Path 1 (see Figure 21 (a)), while an excellent agreement is obtained along other Paths 2, 3, and 4.

It was found that empirical adjustment of "hydrogen bond" does not have significant influence on hydrophobic interactions such as interactions with methylene and methoxy segments of DME. However, higher deviation from *ab initio* calculations is obtained using PFF-4 in comparison with PFF-3 force field.

Molecular mechanics for the ether/water dimer is performed next to find the effect of empirical adjustments on the equilibrium interaction distances and energies for empirical force fields. Binding energy and equilibrium ether/water separation distances are calculated in a similar way, as described in Section 2.4.1

The equilibrium ether/water separation distances and minima energies (Path 1) predicted by empirical force fields are compared with *ab initio* data and CHARMM[99] polarizable force field in Table 4. It can be seen that a systematic increase in equilibrium

Figure 21. Total binding energies ΔU_{QC}^{Total} are given for DME/water interactions as obtained from *ab initio* calculations and empirical force fields.

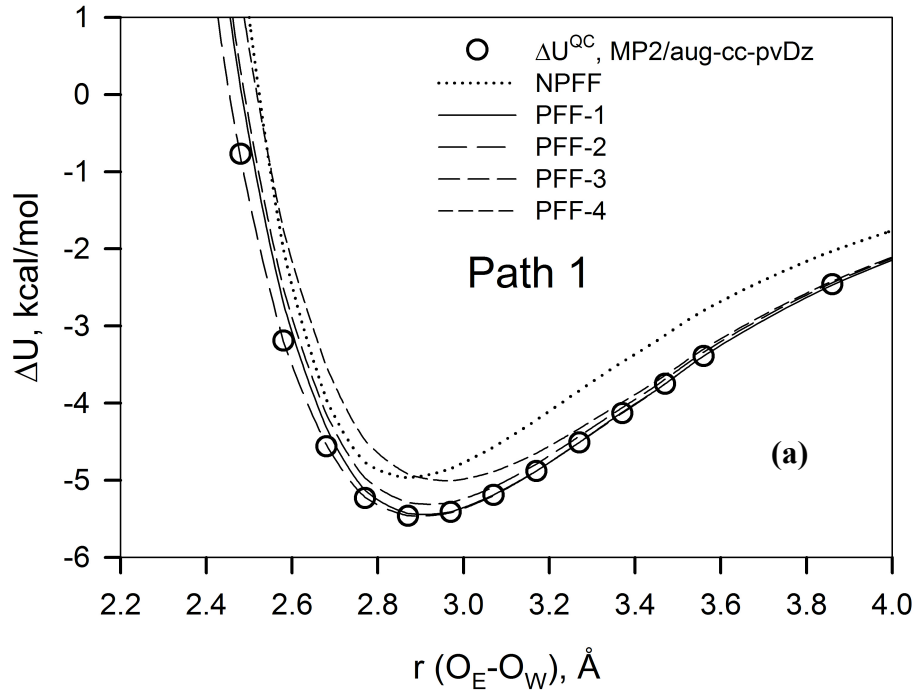
ΔU^QC, MP2/aug-cc-pvDz
NPFF
PFF-1
PFF-2
PFF-3
PFF-4
Path 1
(a)
ΔU, kcal/mol
r (O_E-O_W), Å

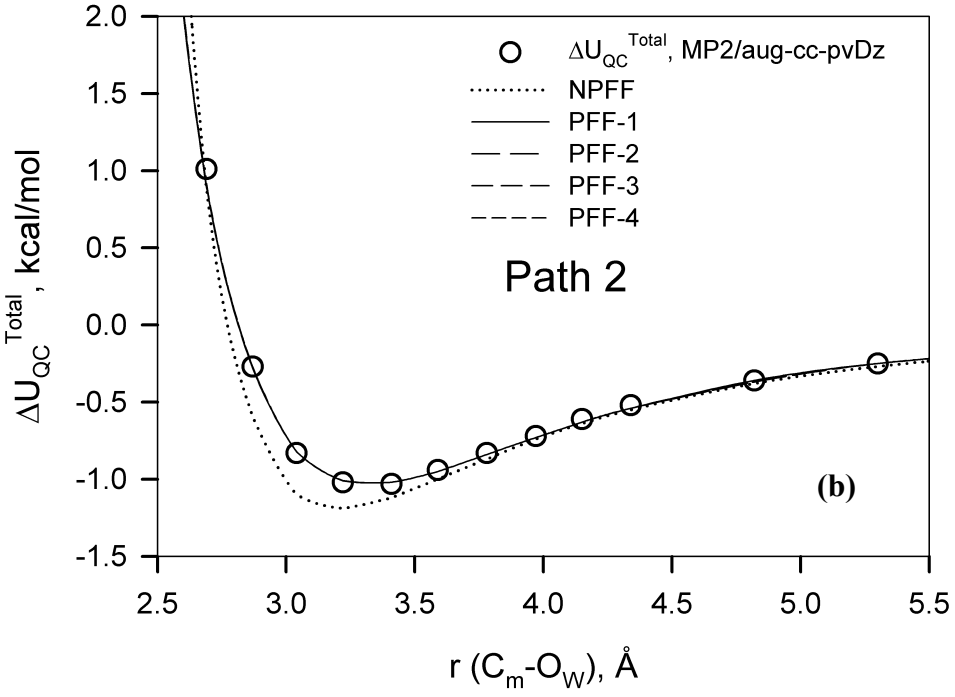
ΔU_QC^Total, MP2/aug-cc-pvDz
NPFF
PFF-1
PFF-2
PFF-3
PFF-4
Path 2
(b)
ΔU_QC^Total, kcal/mol
r (C_m-O_W), Å

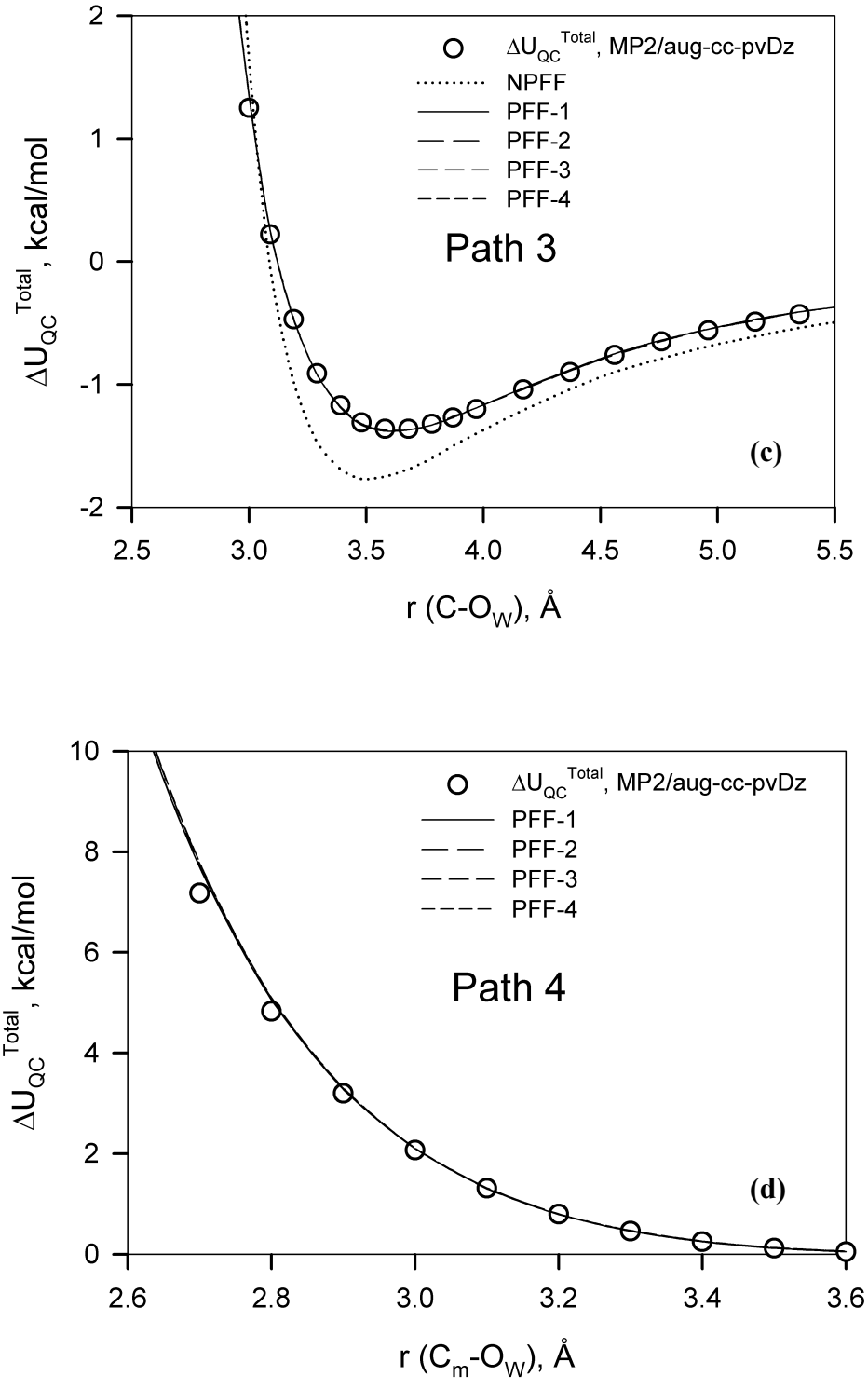

Figure 21. Continued

Table 4. Ether/water equilibrium distances and interaction energies in gas phase for quantum chemistry and molecular mechanics calculations

$R_{(O-Hw)}$, Å				Binding energy, kcal/mol			
QC[a]	NPFF[b]	PFF[c]	CHARMM[d]	QC[a]	NPFF[b]	PFF[c]	CHARMM[d]
1,2-dimethoxyethane (*ttt* conformer)							
1.92	1.91	**1.91[3]**	1.81	-5.46	-5.25	**-5.61[3]**	-4.65
		1.96[4]				**-5.21[4]**	
		1.93[5]				**-5.31[5]**	
		2.01[6]				**-4.85[6]**	

[a] Quantum chemistry at the MP2/aug-cc-pvDz level (this work)

[b] Nonpolarizable force field of Ref. [42], reproduced values from that work

[c] Polarizable force field, this work

[d] Polarizable force field of Ref. [99], values taken from that work

distances is achieved as interactions between O_E and H_W are reduced as well as interaction energies for all force fields.

The equilibrium ether/water separation distances and minima energies (Path 1) predicted by empirical force fields are compared with *ab initio* data and CHARMM[99] polarizable force field in Table 4. It can be seen that a systematic increase in equilibrium distances is achieved as interactions between O_E and H_W are reduced as well as interaction energies for all force fields. More dramatic change in equilibrium distances and energies is obtained for the force fields PFF-2/4/6 where dispersion parameter is an adjustable parameter. Interaction energies of NPFF and PFF-4 are comparable while PFF-3 gives more favorable interactions of DME with water. Interaction energy of the CHARMM[99] force field is less favorable than for the empirical force fields; however, equilibrium position is much shorter. Based on these results, it is anticipated to get significant changes in structure and solvation thermodynamics properties implementing PFF-4/6 force fields in comparison with PFF-3/5 force fields.

5.2. Effect of empirical adjustments on thermodynamic properties

Effect of empirical adjustments on solvation structure and properties of DME/water solutions is considered for the force fields PFF-3 and PFF-4 by performing a series of molecular dynamic simulations as described in Section 3.1. A comparison to the previous results is given for PFF-1 and PFF-2 force fields.

5.2.1. Effect of empirical adjustments on DME/water solvation structures

The effect of empirical adjustment on solvation structure has been studied first. Analysis of O_E-H_W pair distribution function has revealed less "hydrophobicity" of adjusted potentials in comparison with PFF-1 and PFF-2. All three peaks are well developed and positions of the second and third peaks have not been changed (see Figure 22). As it can be seen, PFF-3 and PFF-4 have fewer hydrogen bonds in the first hydration shell than PFF-1 and PFF-2 as indicated by less developed peaks of the distributions. However, a more dramatic change is observed for PFF-4 as it was anticipated based on the results of DME/water binding energy in the gas phase. The position of the first maximum has been shifted to the longer interaction distances implementing PFF-4 in comparison with PFF-1/3 and PFF-2 force fields. Probability of finding water molecule around second hydration shells remains higher for PFF-4 than for PFF-1/3 force fields.

5.2.2. Effect of empirical adjustments on enthalpy of DME solvation in water

Fitting analysis was performed for the enthalpy of solvation in analogous way as for PFF-1 and PFF-2 force fields (see Section 3.2.4). Enthalpies of solvation for PFF 3/5 and PFF 4/6 are given in Figure 23 (a and b). All plots have qualitatively similar picture. From this analysis, a better agreement in enthalpy was reached implementing PFF-3 in comparison to other force fields. Implementing PFF-4 resulted in slightly more favorable interactions of DME with water; however, this deviation is within the error bar of ±0.6 kcal/mol. Force fields PFF-5 and PFF-6 have been shown to underestimate enthalpy of DME solvation by ~0.6 kcal/mol that is in a good agreement with corresponding free energies of solvation. These results indicate that matching free energy of solvation

Figure 22. O_E-H_W intermolecular radial distribution functions are given for DME/water solutions with the composition of 0.17 weight fraction at 298 K.

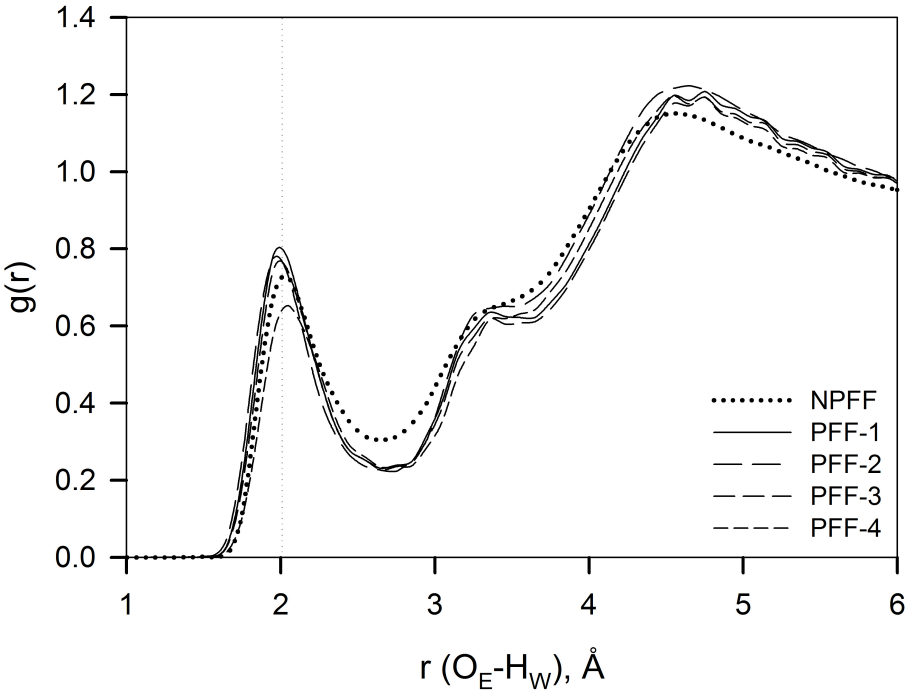
1.4
1.2
1.0
0.8
0.6
0.4
0.2
0.0
g(r)
1
2
3
4
5
6
r (O_E-H_W), Å
NPFF
PFF-1
PFF-2
PFF-3
PFF-4

Figure 23. Enthalpies of solvation ΔH_{solv} are compared as a function of solution concentration at 298 K for DME/water solutions. Lines in figure (b) represent linear fits. Experimental data were taken from Ref. [33,34,31]

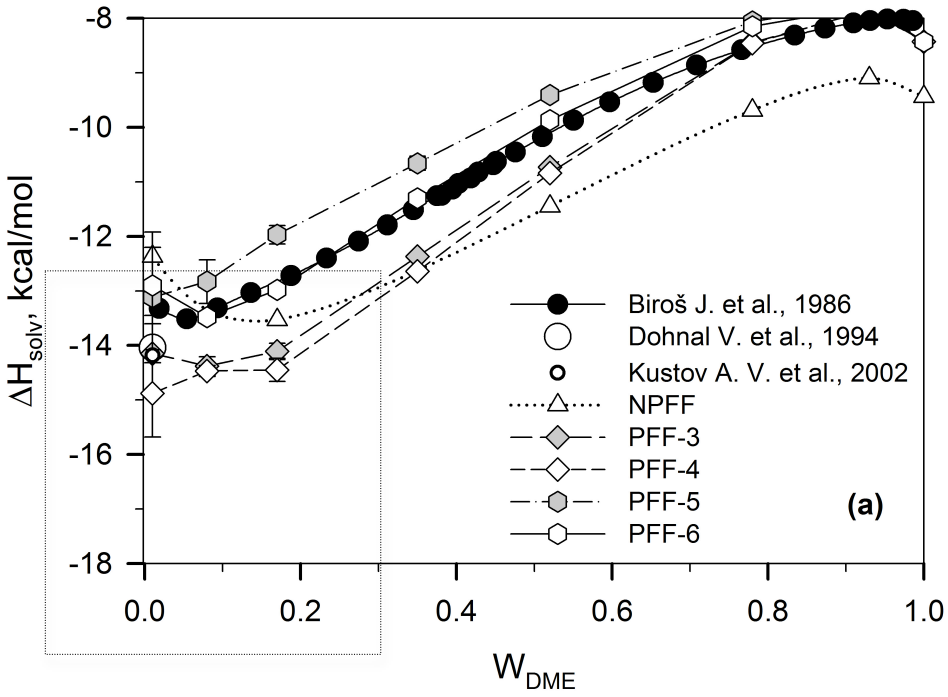
-8
-10
-12
-14
-16
-18
0.0
0.2
0.4
0.6
0.8
1.0
ΔH_solv, kcal/mol
W_DME
Biroš J. et al., 1986
Dohnal V. et al., 1994
Kustov A. V. et al., 2002
NPFF
PFF-3
PFF-4
PFF-5
PFF-6
(a)

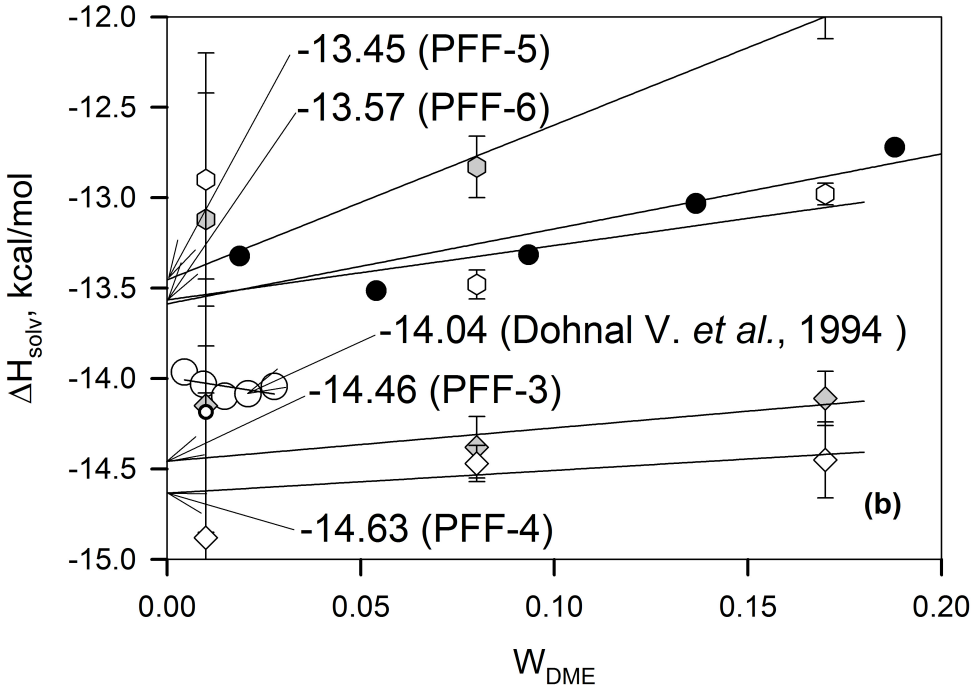
-12.0
-12.5
-13.0
-13.5
-14.0
-14.5
-15.0
0.00
0.05
0.10
0.15
0.20
ΔH_solv, kcal/mol
W_DME
-13.45 (PFF-5)
-13.57 (PFF-6)
-14.04 (Dohnal V. et al., 1994)
-14.46 (PFF-3)
-14.63 (PFF-4)
(b)

resulted in the right position for the enthalpy of DME solvation and, as a consequence, in entropy regardless of the functional form of the "hydrogen bond" potential. Based on these results, it is further expected to get similar predictions in solvation thermodynamics and dynamic properties of DME aqueous solutions for both force fields.

In Table 5, solvation thermodynamics properties are summarized for all developed force fields. Free energies of DME solvation predicted by NPFF[42,65] and CHARMM[99,111] polarizable force fields are also given for the comparison. The enthalpy of solvation is also given as obtained from the linear fitting corresponding to the infinite dilution. The entropy of solvation, calculated as $T\Delta S_{solv}=\Delta H_{solv}-\Delta G_{solv}$, is given as well. It is clear that both force fields PFF-3 and PFF-4 provide a great description of the thermodynamics of DME solvation in water compared to other potentials at 298 K.

Since those force fields utilize water potential that provides a far better description of the temperature dependence of water properties that the TIP4P potential, it is also anticipated to get a better description of ether/water solutions not only at 298 K but also at elevated temperatures.

It also should be noticed that predictions of the force fields in the gas phase does not imply direct correlation with predictions in the condensed phase as obtained for the PFF-3. Despite having a more favorable binding energy for PFF-3 in comparison with PFF-4, the enthalpy of solvation is less favorable for the first one. These results indicate the presence of local solvation effects including structural and polarization effects in the condensed phase that have a significant influence on the thermodynamics of the aqueous solutions.

Table 5. Free energy, enthalpy and entropy of solvation for DME/water solutions as obtained from molecular dynamics simulations and experiment at T=298 K

FF	ΔG_{solv} *kcal/mol*	ΔH_{solv} *kcal/mol*	$T\Delta S$ *kcal/mol*
PFF-1	-5.7	-15.6	-9.9
PFF-2	-6.6	-16.8	-10.2
PFF-3	-4.9	-14.5	-9.6
PFF-4	-4.7	-14.6	-9.9
PFF-5	-3.7	-13.5	-9.8
PFF-6	-3.8	-13.6	-9.8
NPFF[a]	-5.6	-17.1	-11.5
CHARMM[b]	-3.8[b]	-	-
CHARMM[c]	-5.6[c]	-	-
Experiment	-4.80[d]	-14.04[e]; -14.18[f]	-9.40

[a] Nonpolarizable force field of Ref. [42]. Enthalpy of solvation reported in Ref. [42] differ from those reported here by k_bT (0.6 kcal/mol) as the previously reported values did not employ the same gas-phase and solution-phase reference states as were utilized in determining the experimental values;

[b] Polarizable potential in Ref. [99], value taken from that work;

[c] Polarizable potential in Ref. [111].

[d] Ref.[124,125,];

[e] Ref.[33,34]

5.2.3. Effect of empirical adjustments on enthalpy of DME mixing with water

As can be seen from Figure 24, better agreement has been reached for the dilute and high concentrations using PFF-3 and PFF-4 force fields. It should also be noticed that both force fields reproduce quantitatively similar results. Despite a good agreement in free energies of DME solvation, the enthalpy of mixing is still being too favorable.

5.2.4. Effect of empirical adjustments on excess volume for DME/water solutions

A significant reduction is obtained for the excess volume using PFF-3 and PFF-4 force fields. Despite the fact that these force fields give similar results in free energy of solvation, quantitatively different results are obtained for the excess volume. A good agreement with experiment has been reached implementing PFF-4. Higher deviation in excess volume can be seen for PFF-3 force field that predicts less favorable ether/water interactions in comparison with PFF-1 and PFF-2/4 force fields. These results indicate that matching free energy of DME solvation does not necessarily imply a good agreement in the excess volume. It is more likely that predictions in the excess volume of the force fields relay on several intermolecular effects including energetic as well as structural effects. Analyzing radial distribution functions for interactions of oxygen, methyl, and methylene carbons of DME with water reveals a quantitative difference for PFF-3 and PFF-4 force fields.

Figure 24. Enthalpies of mixing ΔH_{mix} (a) and excess volumes ΔV^{E} (b) are given as obtained from MD simulations and experiment at 298 K and 318 K for DME/water solutions. Experimental data were taken from Ref. [30,31]

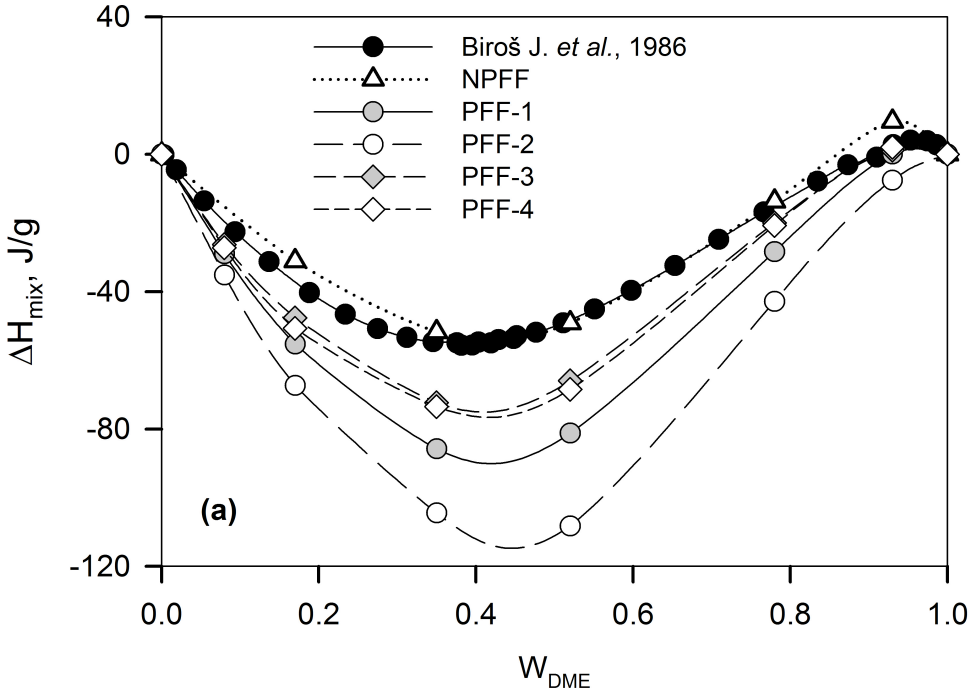
Biroš J. et al., 1986
NPFF
PFF-1
PFF-2
PFF-3
PFF-4
(a)
ΔHmix, J/g
WDME

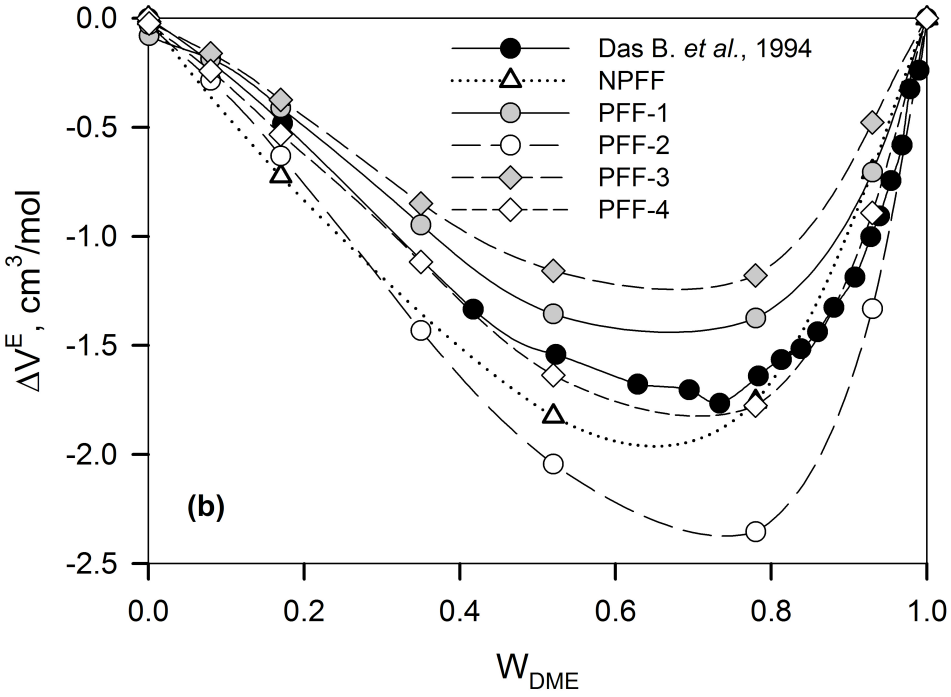
Das B. et al., 1994
NPFF
PFF-1
PFF-2
PFF-3
PFF-4
(b)
ΔVE, cm3/mol
WDME

5.3. Effect of empirical adjustments on transport and dynamic properties

5.3.1. Effect of empirical adjustment on water self-diffusion coefficient for DME/water solutions

A small increase in water self-diffusion coefficient D_W is obtained implementing PFF-3 and PFF-4 as a result of empirical adjustments (see Figure 25 (a)). When the strength of intermolecular interactions is reduced between oxygen of ether and hydrogen of water, increase in water diffusion rate is observed. The effect of reduced interactions on water diffusion rate becomes more pronounced near and at the minima corresponding to 0.35, 0.52, and 0.78 weight fractions of DME. However, no significant effects on dilute and high concentrated regimes are obtained. Higher diffusion rate is obtained implementing PFF-4 force fields due to less favorable ether/water intermolecular interactions. These results also indicate an establishment of quantitative agreement in water diffusion rate, at the minimum, upon matching free energy of DME solvation.

5.3.2. Effect on excess viscosity of DME/water solutions

Significant reduction in excess viscosity is observed implementing PFF-3 and PFF-4 force fields at all concentrations (see Figure 25 (b)). The most pronounced reduction can be seen near and at the maximum that corresponds to 0.4 weight fraction of DME. The excess viscosity is underestimated for dilute and high DME concentrations as a result of the empirical adjustments. Quantitatively similar results are obtained for both force fields upon matching free energies of DME solvation.

Figure 25. Water self-diffusion coefficients D_w (a) and excess viscosities $\Delta\eta^E$ (b) are given as obtained from MD simulations and experiment at 318 K for DME/water solutions. Experimental data were taken from Ref. [30,35]

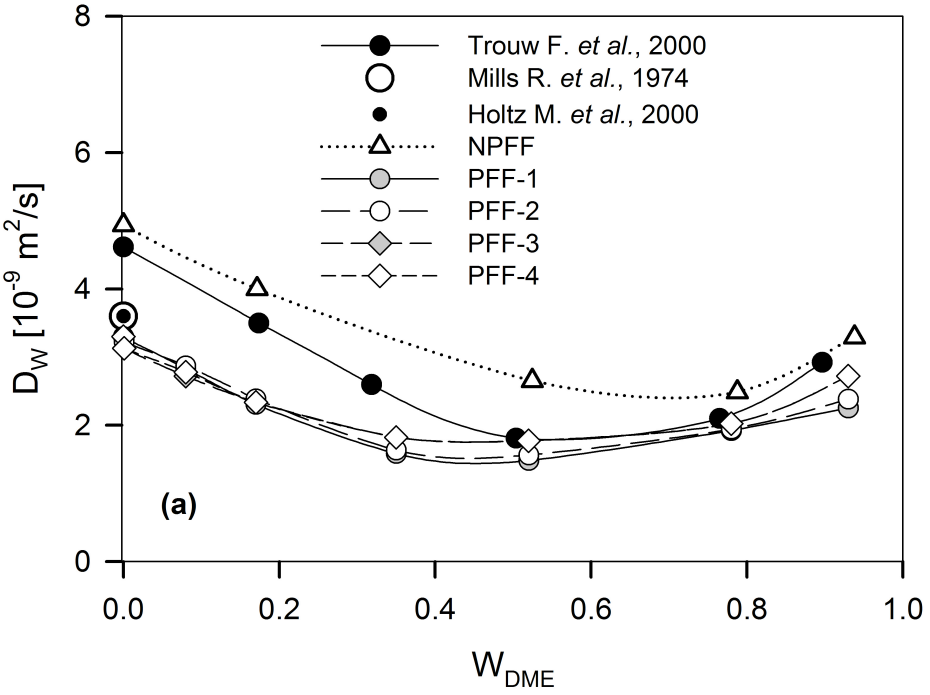
Trouw F. et al., 2000
Mills R. et al., 1974
Holtz M. et al., 2000
NPFF
PFF-1
PFF-2
PFF-3
PFF-4
(a)
D_W [10^-9 m^2/s]
W_DME
0
2
4
6
8
0.0
0.2
0.4
0.6
0.8
1.0

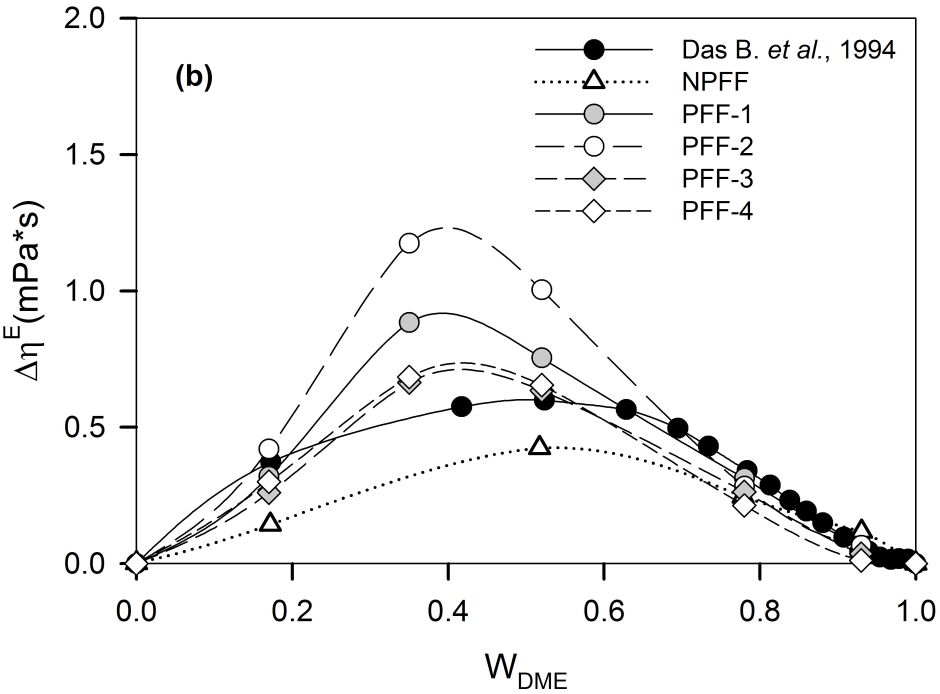
Das B. et al., 1994
NPFF
PFF-1
PFF-2
PFF-3
PFF-4
(b)
Δη^E(mPa*s)
W_DME
0.0
0.5
1.0
1.5
2.0
0.0
0.2
0.4
0.6
0.8
1.0

6. PHASE BEHAVIOR OF PEO/WATER SOLUTIONS

The survey of experimental studies of PEO aqueous solutions revealed that critical solution temperatures LCST and UCST were determined for various molecular weights and concentrations of PEO in water (see Figure 5). However, available experimental data are limited to the hydroxyl-terminated chains of PEO only, which is more hydrophilic than the methyl terminated PEO. It was also determined, by a number of investigators, that the position of critical solution temperature is lowered as hydroxyl terminal group is replaced with other groups.[28,29,38] These experimental observations are further justified by theoretical predictions of Dormidontova et al.[46] (see Figure 7). Molecular weight of PEO12 is too low to exhibit phase separation for the methyl terminated chains according to the theoretical predictions.[46] Therefore, it becomes possible to establish a correlation between predictions in free energy ΔG_{solv} of DME solvation with predictions in phase behavior of PEO/water solution as a function of temperature.

The aggregated and solvated states of PEO are characterized by structural intermolecular correlations. The average O_E-O_E coordination number was determined by counting the number of intramolecular and intermolecular contributions of given O_E. A distance is chosen to be 6.00 Å for calculations as long enough to capture the density fluctuations in the systems and short enough to define the dimension of a polymeric chain. A solution composition was chosen to be 0.35-weight fraction of PEO to get a

good statistics.

Initially, a master curve is built to define a phase transition by scaling repulsion parameter A of the "hydrogen bond" function (eq. 24) and obtaining average O_E-O_E coordination number C_n. A temperature for simulations was chosen to be 400 K to ensure a high diffusion rate of water and, at the same time, to be in a single-phase region according to PEO12 phase diagram, as indicated in Figure 7. The relationship between the extent of O_E-O_E correlation and phase behavior is illustrated in Figure 26. Here the O_E-O_E coordination number is plotted as a function of the "A" parameter. It can be seen that ether/ether coordination increases with decreasing O_E-H_w nonbonded attraction. The point of a phase transition was determined as following. First, total correlation number data are fitted to the sigmoidal distribution using eq. 24

$$y = y_0 + \frac{a}{1 + e^{-\left(\frac{x - x_0}{b}\right)}} \tag{24}$$

where y corresponds to the coordination number C_n and x to the interaction parameter A; y_0, x_0, a and b parameters were determined from the fit.

Second, a point of a phase transition is determined as an inflection point where a second derivative of the sigmoidal distribution changes a sign from negative to positive and coordination number is defined at that point. Clearly A = -15.00 kcal/mol is phase separated, A = -17.50 kcal/mol is at transition point, and A = -30.00 kcal/mol is homogeneous solution. Based on these studies, a value of C_n (O_E-O_E) ≈ 6.6 is defined as a phase transition point in the 35 weight percent PEO12/water solutions that is indicated by a dotted horizontal line in Figure 26 (a).

Figure 26. Average coordination number $<C_n>$ is given for the O_E-O_E intermolecular correlation as a function of O_E-H_W interaction parameter A. Open circles are values from MD simulations and line is a sigmoidal fit. Water density distributions are given for the three interaction parameters A.

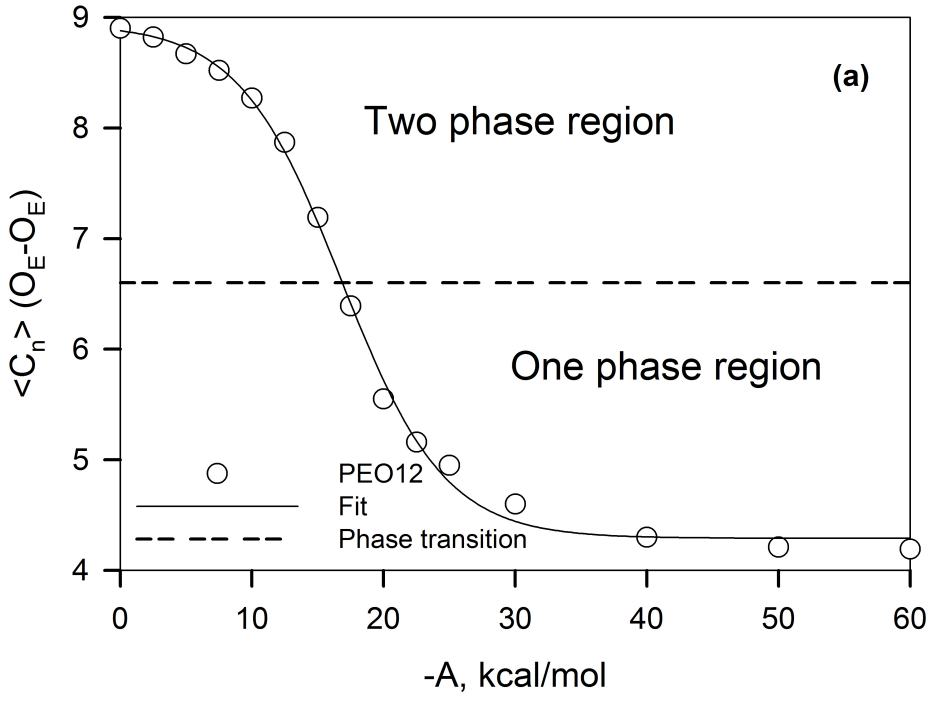
(a)
Two phase region
One phase region
PEO12
Fit
Phase transition
<C_n> (O_E-O_E)
-A, kcal/mol
9
8
7
6
5
4
0
10
20
30
40
50
60

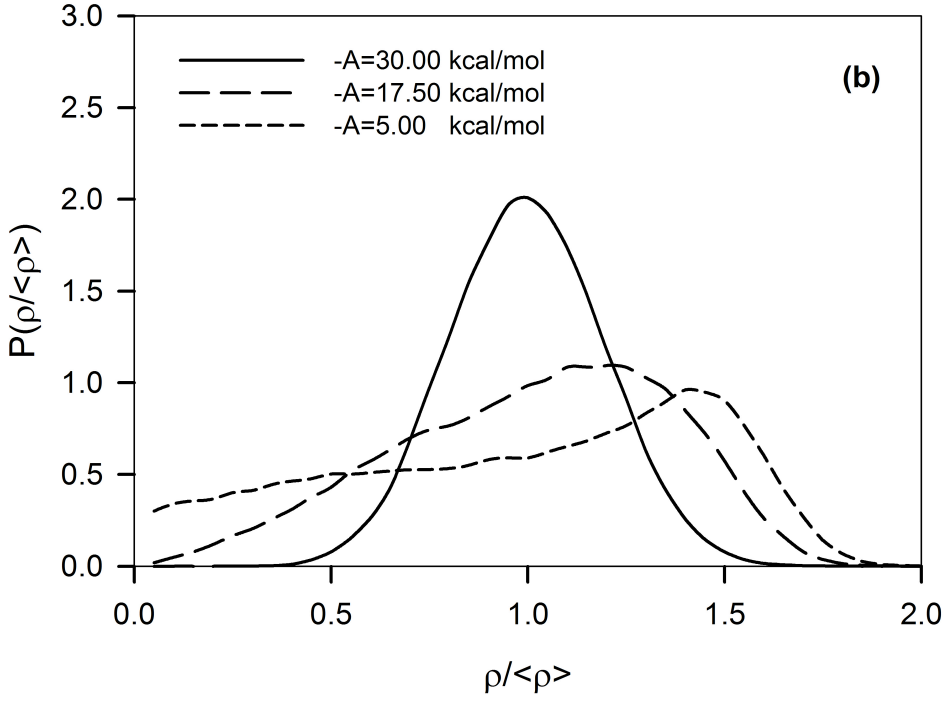
(b)
-A=30.00 kcal/mol
-A=17.50 kcal/mol
-A=5.00 kcal/mol
P(ρ/<ρ>)
ρ/<ρ>
3.0
2.5
2.0
1.5
1.0
0.5
0.0
0.0
0.5
1.0
1.5
2.0

In addition to the structural intermolecular correlation analysis of PEO12, water density distribution is characterized using a block density technique.[126] This method is described in the Appendix. The probability distribution is expected to be Gaussian-like for the homogeneous solution and non-Gaussian as solution undergoes spinodal decomposition. Water density distributions for the three interaction parameters A are shown in Figure 26 (b). It can be seen that water density distribution is Gaussian for A = -30.00 kcal/mol indicating one phase homogeneous solution due to the strong favorable interactions between O_E and H_W. Phase transition can be seen as indicated by a broad water density distribution for A = -17.50 kcal/mol. A complete phase separation is obtained for A = -5.00 kcal/mol as indicated by well-developed two peak non-Gaussian distribution as O_E and H_W intermolecular interactions were significantly reduced. Corresponding snapshots from MD simulations are given in Figure 27 (a-c).

Phase behavior of PEO12/water solutions is studied next for PFF-1/3/5, PFF-2/4/6, and NPFF force fields at various temperatures. A series of molecular dynamics simulations is performed next for systems of 0.35 weight fraction of PEO12 and temperatures 298 K, 363 K, 450 K, and 550 K.

The production runs were obtained over 20 ns for each temperature and force field and were analyzed for the ether oxygen/ether oxygen (O_E-O_E) correlation. It is reasonable to associate an increased ether/ether correlation with decreasing solvent quality, which is expected for PEO/water solutions since they exhibit LCST behavior at sufficiently high molecular weight, as discussed in Section 1.2.

Figure 27. Snapshots of PEO12/waters solutions are given as obtained from MD simulations. Hydrogen atoms are omitted for clarity. Homogeneous solution is obtained for A=-30 kcal/mol (a), A=-17.50 kcal/mol (b), phase separated system is obtained for A=-5 kcal/mol (c).

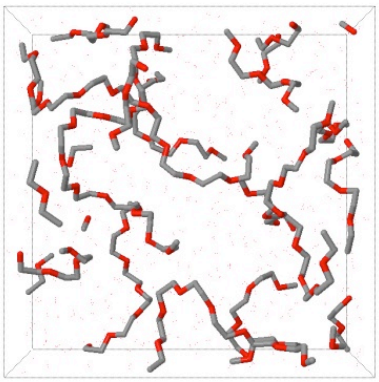

(a)

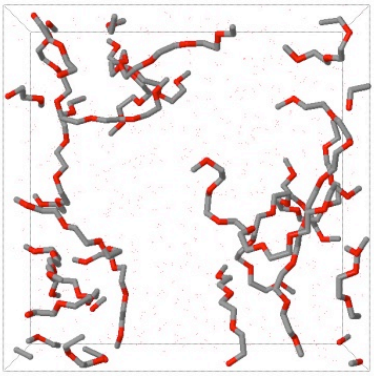

(b)

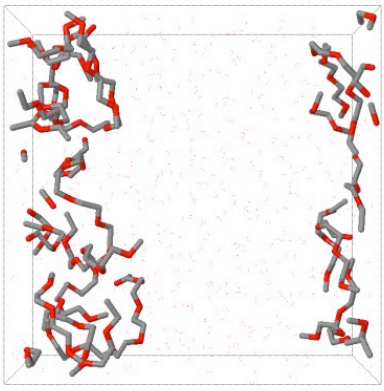

(c)

O_E-O_E correlation increases for PEO12/water solutions with increasing temperature for all the force fields investigated (see Figure 28). At even higher temperatures, the ether/ether correlation decreases, which is consistent with the USCT behavior exhibited by PEO/water solutions. Furthermore, it can be seen that the most hydrophilic force fields (PFF-1 and PFF-2), with the largest ΔG_{solv} of DME in water, show the least ether/ether correlation, while the most hydrophobic force fields with the smallest ΔG_{solv} of DME in water (PFF-5 and PFF-6) exhibit the greatest extent of the ether/ether correlation. Hence, force fields PFF-1, PFF-2, PFF-3, and PFF-4 exhibit expected phase behavior for the PEO12/water solutions while PFF-5 and PFF-6 appear to be too hydrophobic in the description of ether/water interactions, as expected. Implementing NPFF has resulted in very similar behavior of PEO12/water solutions as for PFF-4.

Figure 28. Phase diagrams for PEO12/water solutions are given as obtained from MD simulations for various force fields investigated. Dotted line indicates a phase transition as it was obtained from the phase analysis.

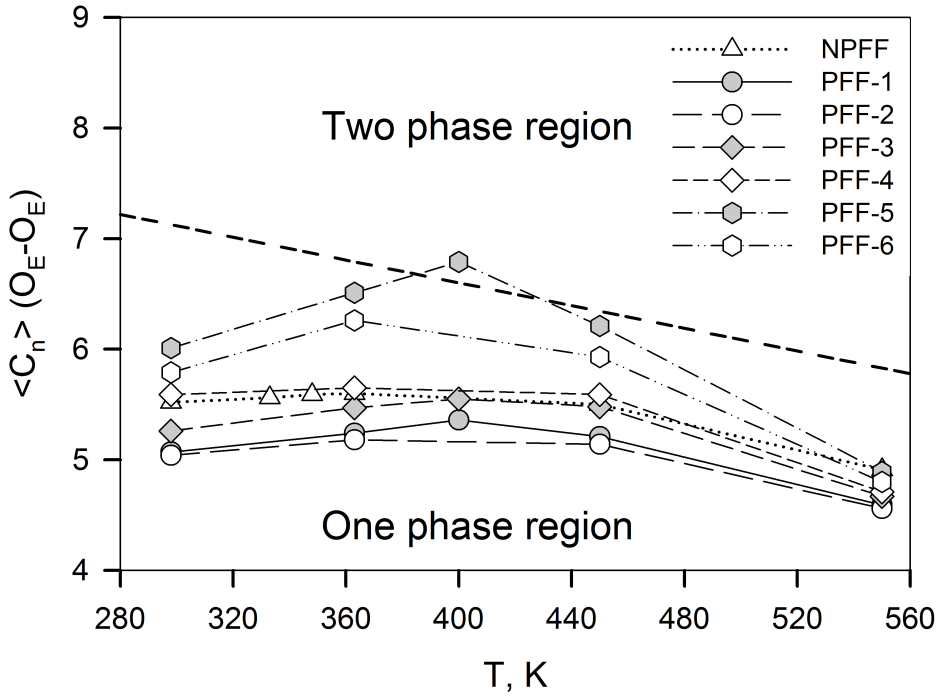
9
8
7
6
5
4
280
320
360
400
440
480
520
560
T, K
<C_n> (O_E-O_E)
Two phase region
One phase region
NPFF
PFF-1
PFF-2
PFF-3
PFF-4
PFF-5
PFF-6

7. TRANSFERRABILITY OF THE DEVELOPED FORCE FIELD PARAMETERS TO PPO/WATER SOLUTIONS

DMP has essentially the same local conformations as PPO in aqueous solution and similar dependence on solution composition; hence, this molecule is a good model compound for developing of PPO/water potentials.[57]

The polarizable water model is described above in Section 2.2, while the ether model is described in Section 2.3. In order to complete the description of PPO/water systems within the atomistic polarizable force field framework, a few steps need to be performed: (a) reparameterize partial atomic charges using a new two-charge ether model; (b) reparameterize backbone torsional parameters; (c) perform *ab initio* studies of intermolecular interactions of DMP with water; and (d) transfer nonbonded dispersion/repulsion parameters developed for DME to the chemically similar groups or atoms of DMP if possible.

7.1. Parameterization of DMP partial atomic charges

Geometry optimization was performed at B3LYP/aug-cc-pvDz energy level following by calculation of electrostatic potential on a grid of 80000 evenly distributed points at the MP2/aug-cc-pvDz level of theory. Electrostatic potentials for each molecular conformation were obtained and further included in the fitting of partial atomic charges.

The ether geometry and partial charges of two extended charges are assumed to be transferrable, and, therefore, are constrained during the fitting of partial atomic charges. They are fitted in a similar way as discussed in parameterization of partial charges Section 2.3.2 for DME using least square fitting procedure and minimizing the value of the objective function. The most populous hydrophilic and hydrophobic conformations of DMP are ttt, tgt, $t\bar{g}t$, and $tg^{+}g^{-}$ conformers[57] that were used for the fitting of partial atomic charges. 3,6-dimethyl diglyme (DMD) was also included in the fitting to get partial charge for the oxygen atom that is connecting two repeat units of PPO. The resulting value of the objective function χ^2 is 0.312. Final values for the partial charges of PPO are given in Table 6. Comparison of partial charges for PFF-X and NPFF reveals some difference. Again, oxygen atoms have positive charges as a result of charge delocalization for two-extended charge ether model. Methoxy and methylene carbons are also more negative than in NPFF, while the methyl carbon is more negative using no-extended charge model. Charges on hydrogen atoms are very similar in magnitude for both ether models.

7.2. Parameterization of intramolecular interactions

7.2.1. DMP valence parameters

Dispersion/repulsion parameters for ether/ether intermolecular interactions were taken from the quantum chemistry-based APPLE&P® polarizable force field that was found to provide a consistent description of density ρ, heat of vaporization ΔH_{vap}, and transport properties of a variety of polymers, including poly (propylene oxide).[73-,97] However, an additional set of *ab initio* calculations is carried out to parameterize the

Table 6. Assignment of partial atomic charges for 1,2-dimethoxypropane (DMP)

Atom type	DMP (PPO) - PFF	DMP (PPO) - NPFF[a]
O $(C\text{-}O\text{-}C)^{PPO}$	0.4064	-0.2348
O (C_m-O-C)	0.4949	-0.3304
C_m	-0.4042	-0.2327
H_m	0.1290	0.1400
C_e	-0.2997	-0.1618
H	0.0951	0.0957
C_α	0.1095	0.4219
H_α	0.0176	-0.0117
C_m*	-0.1092	-0.5294
H*	0.0349	0.1167
Lp	-0.2200	-

[a] NPFF, Ref. [57]

force field for PPO.

It was previously found that MP2/aug-cc-pvDz//B3LYP/aug-cc-pvDz provides accurate conformational and energetic information for DME in comparison with experiment including electron diffraction data, NMR vicinal coupling data, and IR spectra.[73]

Bond constants are transferred as obtained for similar compounds within a framework of APPLE&P® polarizable force development. Bond lengths are calculated as an average over a number of bond lengths obtained from optimized geometries of hydrophobic and hydrophilic conformers. Bending constants and angles are transferred from alkanes and ethers from APPLE&P®. Relative backbone torsional energies are calculated for DMP at the MP2/aug-cc-pvDz level of theory. Fitting of the torsional parameters to the energies from *ab initio* calculations is performed in the same ways as for DME. Good agreement of molecular mechanics is established with *ab initio* calculations (see the Appendix). The polarizable water model is described above in Section 2.2, while the ether model is described in Section 2.3. In order to complete the description of PPO/water systems within the atomistic polarizable force field framework, dispersion/repulsion parameters for intermolecular interactions between the ether and water need to be determined.

7.3. Transferability to DMP/water solutions

In order to establish transferability of DME/water force field parameters to DMP/water, a systematic investigation of DMP/water interactions is conducted in a similar way as described in Section 2.4. Conformations of DMP have also been classified

Figure 29. Schematic representation of the testing configurations is given for the calculation of DMP/water binding energies in (a), (b), and (c), respectively. DMP is in hydrophobic *ttt* (a and c) and hydrophilic $t\bar{g}t$ (b) conformations. Gray atoms represent carbons, white are hydrogens, and red are oxygen atoms. Dashed arrows indicate the directions along which the water molecule is to be shifted. Chemical structures were visualized using jmol open source software.

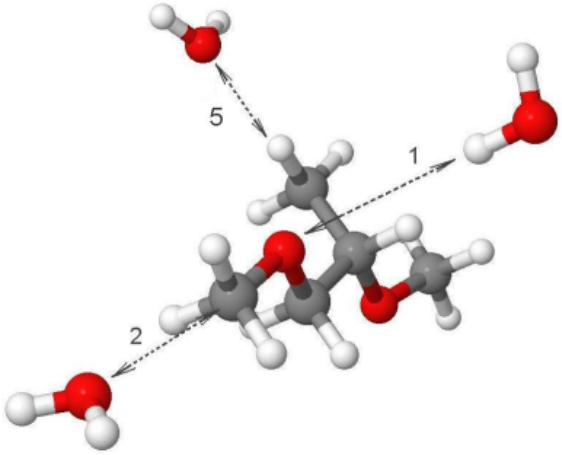

(a)

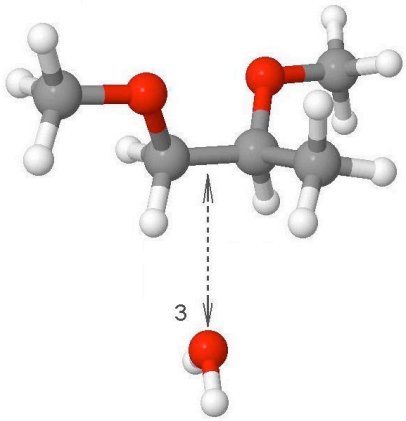

(b)

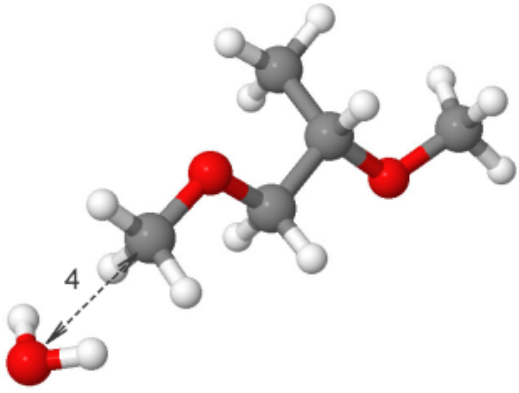

(c)

as hydrophilic and hydrophobic, which is based on their relative interactions with water.[57] Therefore, the most populous hydrophobic *ttt* and hydrophilic $t\bar{g}t$ conformations of DMP have been chosen to perform the studies of intermolecular interactions of those conformers with water.

Designed paths provide intermolecular interactions between similar groups of DME and DMP. Based on those interactions, a decision is made whether parameters are to be transferrable. For this purpose, extensive *ab initio* calculations of dimer binding energy between DMP and a single water molecule are conducted, as shown in Figure 29 (a-c). For all paths, the local optimized geometry is obtained at the B3LYP/aug-cc-pvDz level. Subsequently, the intermolecular energy of the DMP/water complex is calculated at the MP2/aug-cc-pvDz level of theory with BSSE as established in a framework of APPLE&P® force field development.[102]

Path 1 involves study of hydrogen bonding between water hydrogen atom and ether oxygen, as it was investigated for DME, for the *ttt* hydrophobic conformer. Path 2 involves interaction of water with the methyl group of the methoxy group that was also investigated for the *ttt* conformer of DME. Path 3 involves interaction of water with the "hydrophobic" side of DMP, *i.e.*, the methylene groups as opposed to the ether oxygen atoms for the $t\bar{g}t$ hydrophilic conformer. Path 4 involves interactions of water hydrogens with methoxy hydrogens. Path 5 involves interaction of water with methylene group of DMP that is not available for DME.

7.3.1. DMP/water and DME/water intermolecular interactions

Intermolecular energies for DMP/water interactions are compared with energies for DME/water interactions as obtained from *ab initio* calculations in Figure 30 (a-d). Energy dependence of DMP/water interactions as a function of separation distance is similar to the DME/water interactions for four chemically similar groups. However, intermolecular energies for hydrophilic Path 1, methoxy Path 2, and hydrophobic Path 3 are slightly more favorable for the DMP/water, see Figure 30 (a-c).

There is no difference in energies of interacting hydrogens along Path 4, see Figure 30 (d). As it can be seen, intermolecular interactions of DMP and DME with water are comparable as obtained from *ab initio* calculations. Therefore, non-bonded parameters of the polarizable force field describing DME/water intermolecular interactions are to be transferrable to DMP for the chemically similar atoms. No comparison can be made for the intermolecular interactions of water with methyl group of DMP. As a consequence, an assumption is made on transferability of non-bonded parameters obtained for the methoxy/water interactions of DME to describe methyl/water interactions of DMP. Next, comparison of molecular mechanics with *ab initio* calculations is performed for DMP/water interactions using a set of non-bonded parameters of polarizable force fields PFF-1/2/3/4 that describe DME/water intermolecular interactions.

7.4. Transferability of nonbonded parameters to DMP/water intermolecular interactions

No development of nonbonded dispersion/repulsion parameters was performed to describe intermolecular interactions of PPO with water, as a result of previous studies.

Figure 30. Comparison of interaction energies of DME and DMP compounds with water is given as obtained from *ab initio* calculations at MP2/aug-cc-pvDz//B3LYP/aug-cc-pvDz levels of theory.

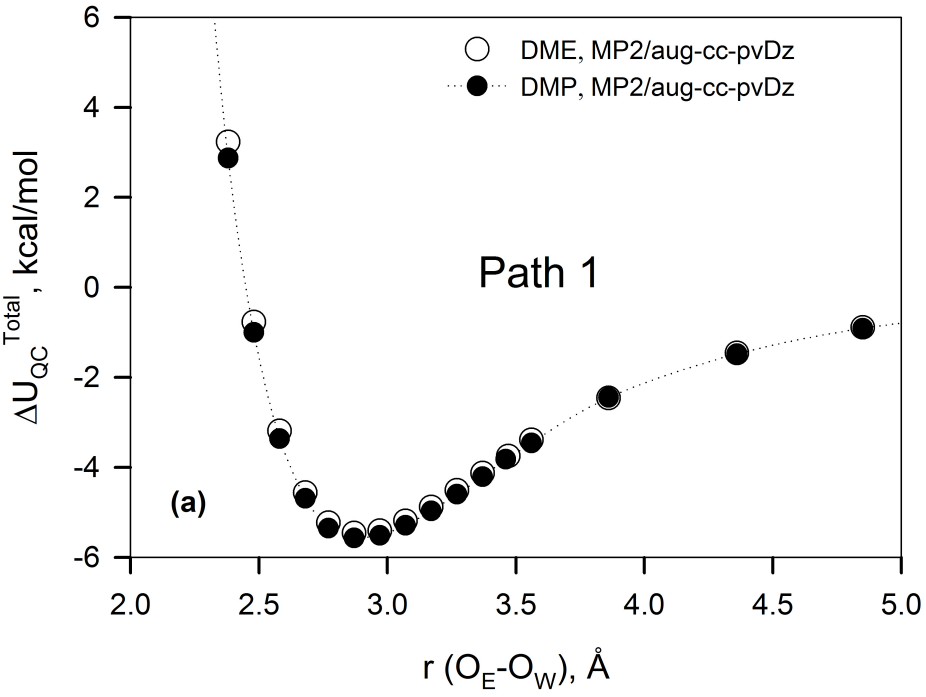
DME, MP2/aug-cc-pvDz
DMP, MP2/aug-cc-pvDz
Path 1
(a)
ΔU_{QC}^{Total}, kcal/mol
r (O_E-O_W), Å

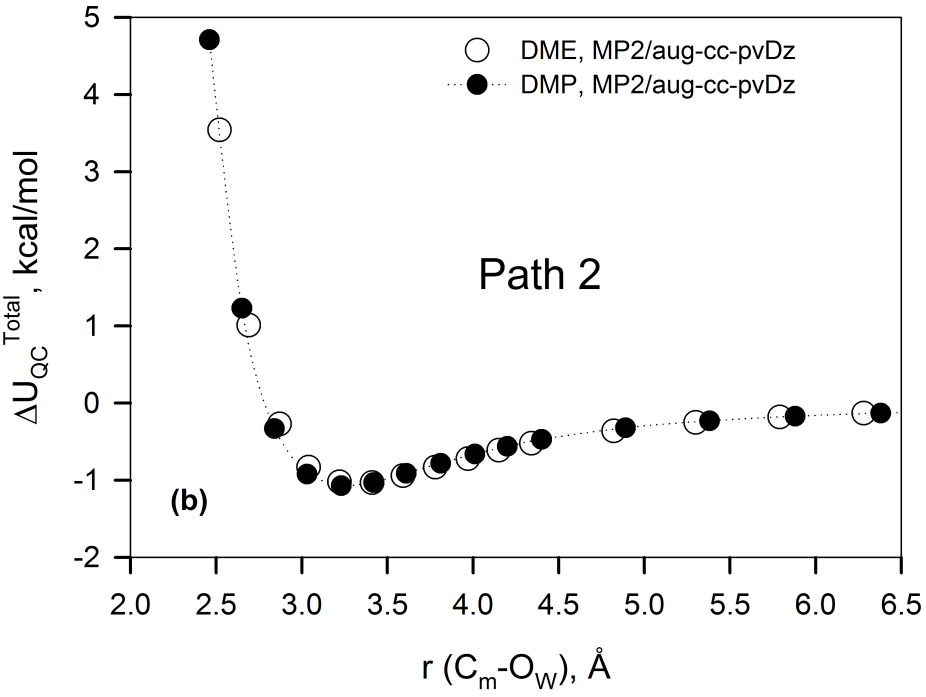
DME, MP2/aug-cc-pvDz
DMP, MP2/aug-cc-pvDz
Path 2
(b)
ΔU_{QC}^{Total}, kcal/mol
r (C_m-O_W), Å

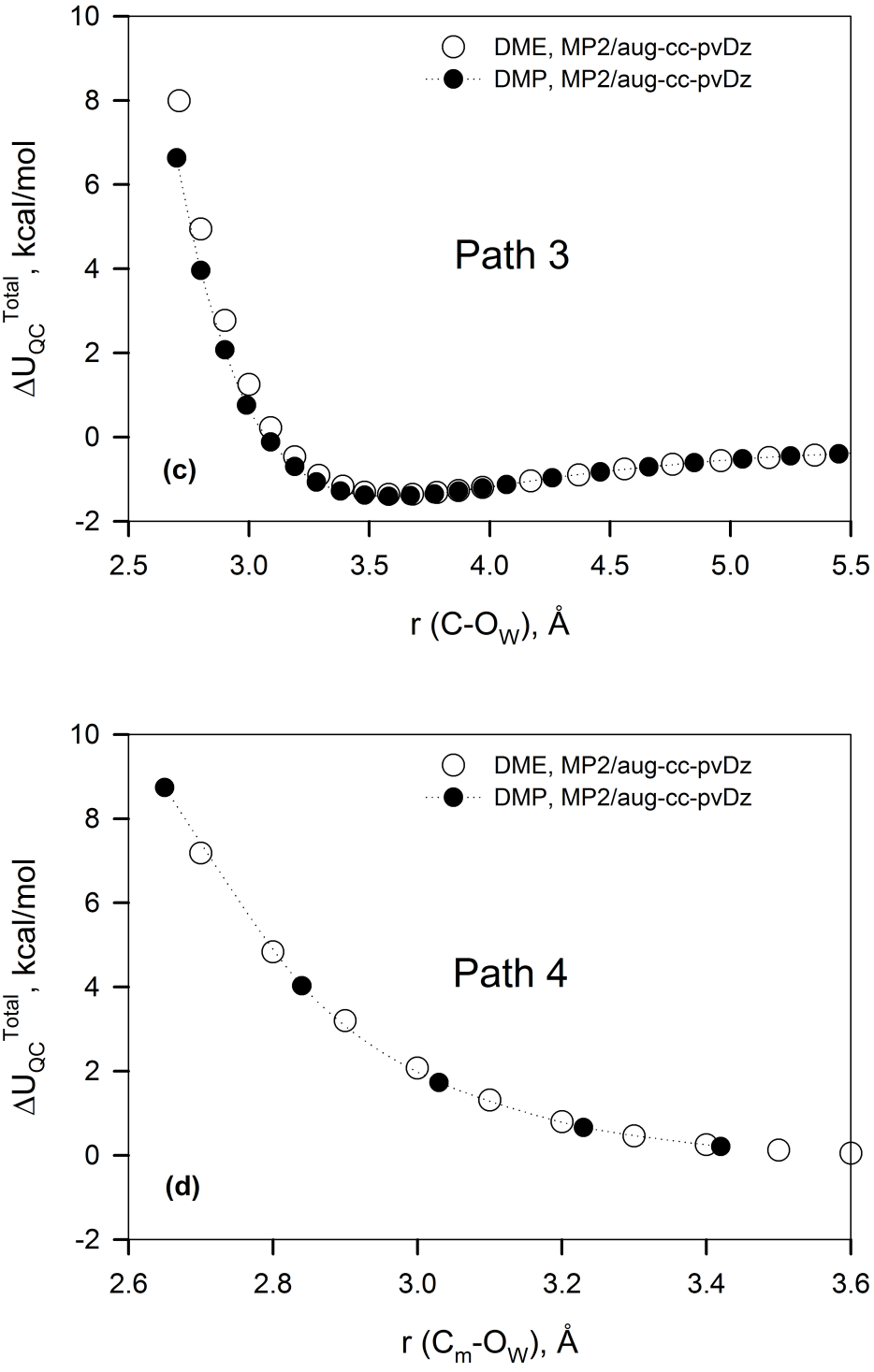

Figure 30. Continued

Nonbonded parameters developed to describe (PEO) DME/water interactions have been transferred to (PPO) DMP/water without any additional empirical adjustments. However, a comparison of molecular mechanics with *ab initio* calculation is performed to check a quality of the force fields. The *ab initio* and intermolecular energies obtained for PFF-1/3 and PFF-2/4 sets of nonbonded parameters are compared in Figure 31 (a-d).

The reproduction accuracy for DMP/water interactions is comparable with the accuracy for DME/water interactions along similar paths. Both sets of nonbonded parameters PFF-3 and PFF-4 predicted underestimation of "hydrophilic" interactions, where oxygen atom of ether is interacting with hydrogen atom of water, Path 1. Good description of interaction energies are obtained for the methoxy carbon of methoxy group with oxygen of water, Path 2, and the methylene carbon with oxygen of water, Path 3. Interactions of methoxy hydrogens with hydrogens of water resulted in more repulsive interactions at short separation distances (see Path 4). To complete a description of DMP/water interactions, it is necessary to consider interactions of methyl pendent group with water. However, there is no such group present on DME, and, therefore nonbonded parameters that describe methoxy/water interactions were transferred to the methyl/water interactions without empirical adjustments.

Figure 31. The agreement is shown for the total binding energies ΔU_{QC}^{Total} of DMP/water interactions as obtained from *ab initio* calculations and polarizable force fields.

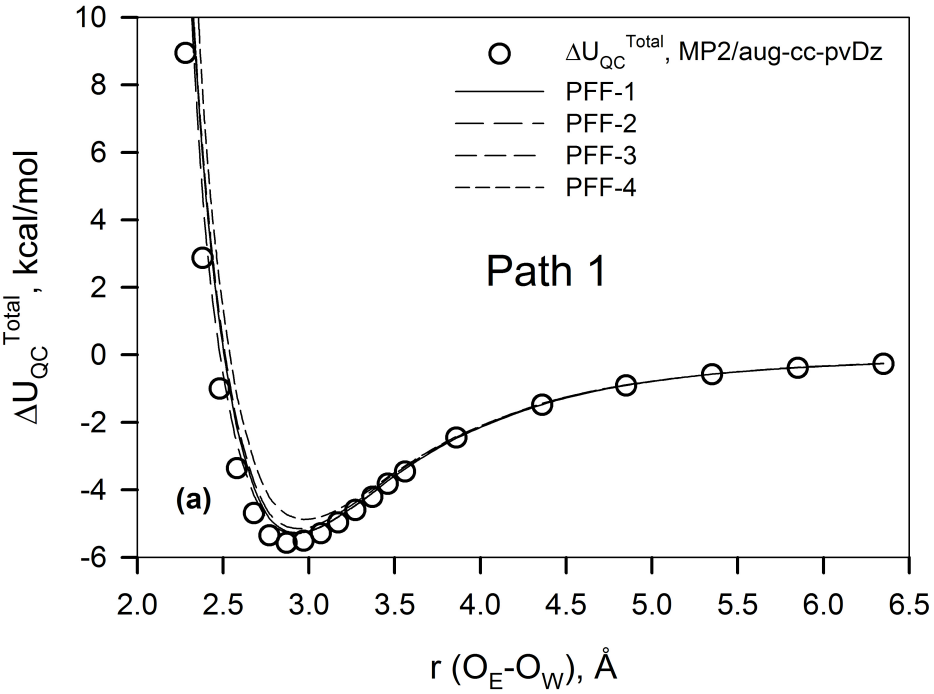
ΔU_QC^Total, MP2/aug-cc-pvDz
PFF-1
PFF-2
PFF-3
PFF-4
Path 1
(a)
ΔU_QC^Total, kcal/mol
r (O_E-O_W), Å

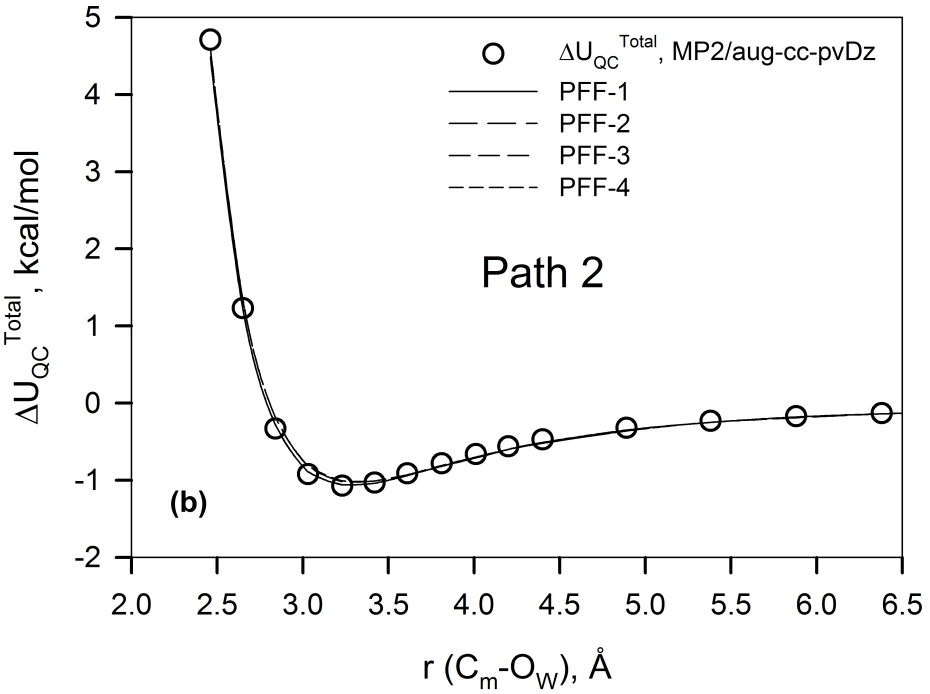
ΔU_QC^Total, MP2/aug-cc-pvDz
PFF-1
PFF-2
PFF-3
PFF-4
Path 2
(b)
ΔU_QC^Total, kcal/mol
r (C_m-O_W), Å

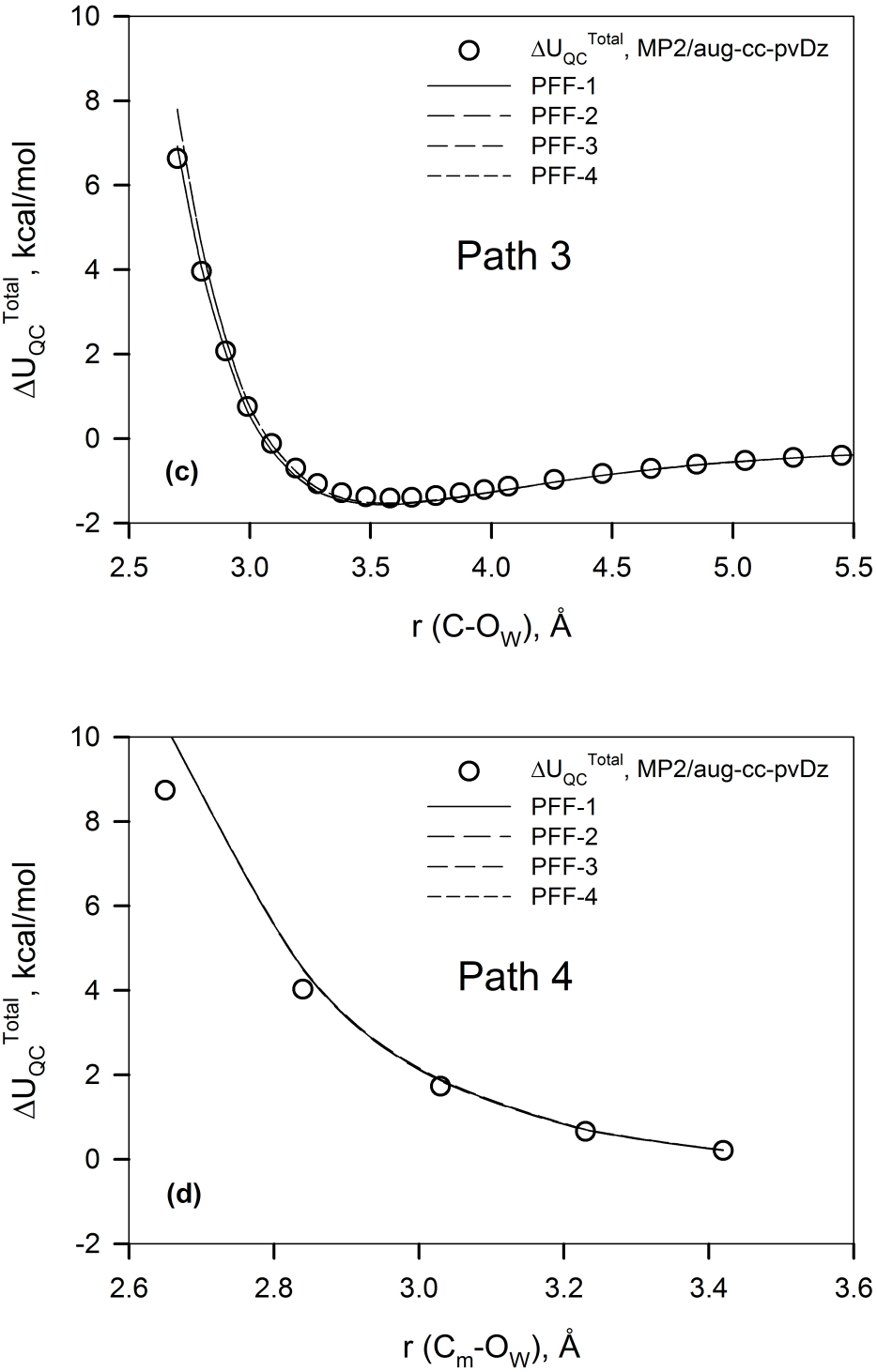

Figure 31. Continued

8. PHASE BEHAVIOR OF PPO/WATER SOLUTIONS

Each phase is enriched phase with water and becoming less enriched and more pronounced when temperature is increased for PEO/water and PPO/water solutions. It has been shown experimentally that DMP is soluble in water up to 393 K.[43] A phase diagram has been constructed for PPO/water mixtures as discussed in Section 1.2. However, available experimental data are limited to the hydroxyl-terminated chains of PPO only, which is more hydrophilic than the methyl terminated PPO. No experimental data on solvation of methyl terminated PPO in water were found in literature. Therefore, the position of the lower critical solution temperature for the methyl terminated PPO is uncertain. It is well known from experiments that replacement of the hydroxyl terminal group with other types of terminal groups results in the position of LCST being shifted.[28,29,38] These results were also confirmed by theoretical studies for PEO/water solutions.[46] However, it is anticipated that phase separation will take place for the methyl terminated PPO in water at ambient and elevated temperatures. It was found that implementing PFF-4 gives the best description of solution behavior for DMP/water and PPO/water solutions in comparison with other force fields.

8.1. Simulation methodology

To check the transferability of the two-charge ether model and nonbonded force field parameters to PPO/water solutions, a series of molecular dynamic simulations was

performed. First, molecular dynamics simulations of 125 molecules of DMP were carried out at 293 K to check the reproduction accuracy of the force field in terms of the liquid density. Good agreement with experimental data[127] was established for the density of pure DMP at 293 K. Experimental density is 0.855 g/cm^3 and density obtained from MD simulations is 0.850 g/cm^3. Second, DMP/water and PPO/water (PPO6, with CH_3 terminal groups, 395 Da) solutions were simulated at 298 K, 318 K, 363 K, 393 K, 400 K, and 448 K temperatures to study phase behavior of those solutions. Solutions were comprised of 1-72 solute molecules and 1200-100 water molecules depending upon the composition. All other parameters were similar to the parameters implemented for molecular dynamic simulations of PEO/water solutions as described in Section 3.1. Pressures of the systems were adjusted correspondingly, 20 atm above the vapor pressures of the solvent, to keep systems in a liquid state at elevated temperatures. All systems were initially equilibrated at isothermal-isobaric ensemble for 5 ns until satisfactory steady state properties (such as density of the solutions) were reached. Sampling trajectories were generated in the NPT ensemble over 20 ns. All nonbonded PEO/water parameters were transferred to PPO/water without any additional empirical adjustments. The nonbonded parameters for the methyl carbon and oxygen of water pair of PPO were taken as parameters for the methoxy carbon and oxygen of water interactions of PEO. Partial atomic charges from the fitting of the two-charge ether model for PPO are given in Table 6.

8.2. Phase behavior of DMP/water solutions

DMP/water solutions were simulated employing PFF-3/5 and PFF-4/6 force fields. A similar approach was implemented to study phase behavior of DMP aqueous solutions as it was performed for PEO12/water solutions. A series of molecular dynamics simulations were performed initially at 400 K to define a phase transition point for DMP by scaling repulsion parameter A for the "hydrogen bond" potential, eq. 10. The coordination number of O_E-O_E was determined by counting intra- and intermolecular interactions within 6 Å of intermolecular distance. $<C_n>$ is given as a function of A parameter in Figure 32 (a). Fitting was performed using sigmodal distribution function (see eq. 24). A phase transition point was determined to be at $<C_n> \approx 3.8$.

Phase analysis is performed next implementing PFF-3/5 and PFF-4/6 at 298 K, 318K, 363 K, and 393 K. The average coordination number is plotted as a function of temperature in Figure 32 (b). It can be seen that implementing empirical force fields resulted in phase separation of DMP except for force field PFF-4. No tendency for aggregation of DMP in water is observed at low and high temperatures. These results are in a good agreement with experimental data.[43] Phase separation is seen for PFF-5 and PFF-6 force fields as those force fields predict lower free energy of DME solvation than PFF-3 and PFF-4. However, PFF-6 force field is exhibiting less degree of aggregation in comparison with PFF-5. Similar results were obtained for the phase behavior of PEO12/water solutions.

Figure 32. Master curve (a) and phase diagram (b) are given for DMP as obtained from MD simulations. Dotted line in figure (b) indicates a phase transition as was obtained from phase analysis.

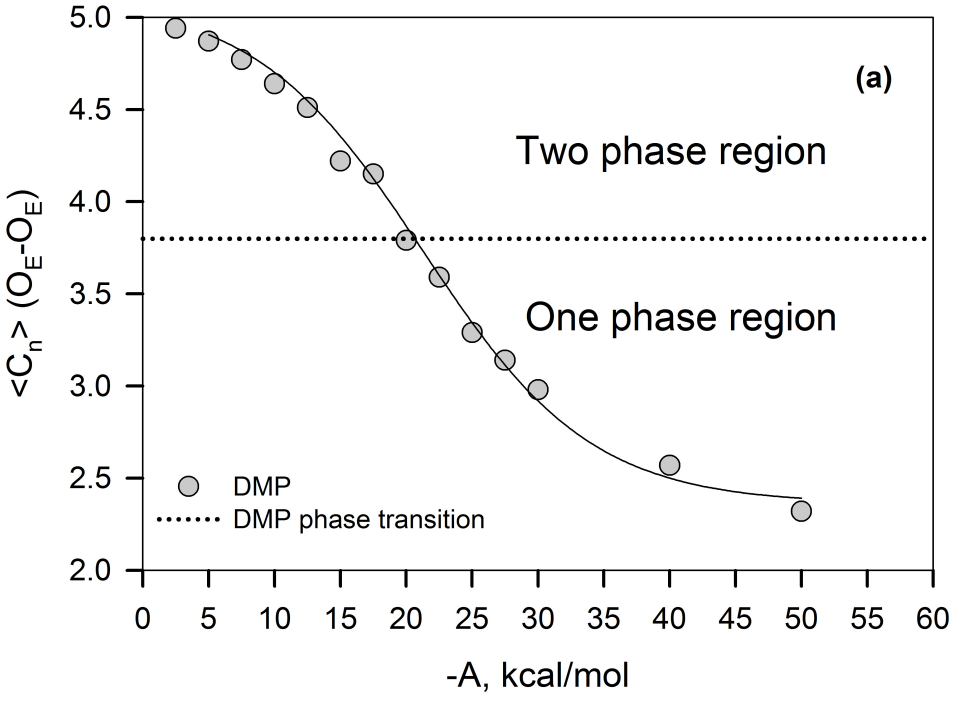
(a)
Two phase region
One phase region
DMP
DMP phase transition
<C_n> (O_E-O_E)
-A, kcal/mol
5.0
4.5
4.0
3.5
3.0
2.5
2.0
0
5
10
15
20
25
30
35
40
45
50
55
60

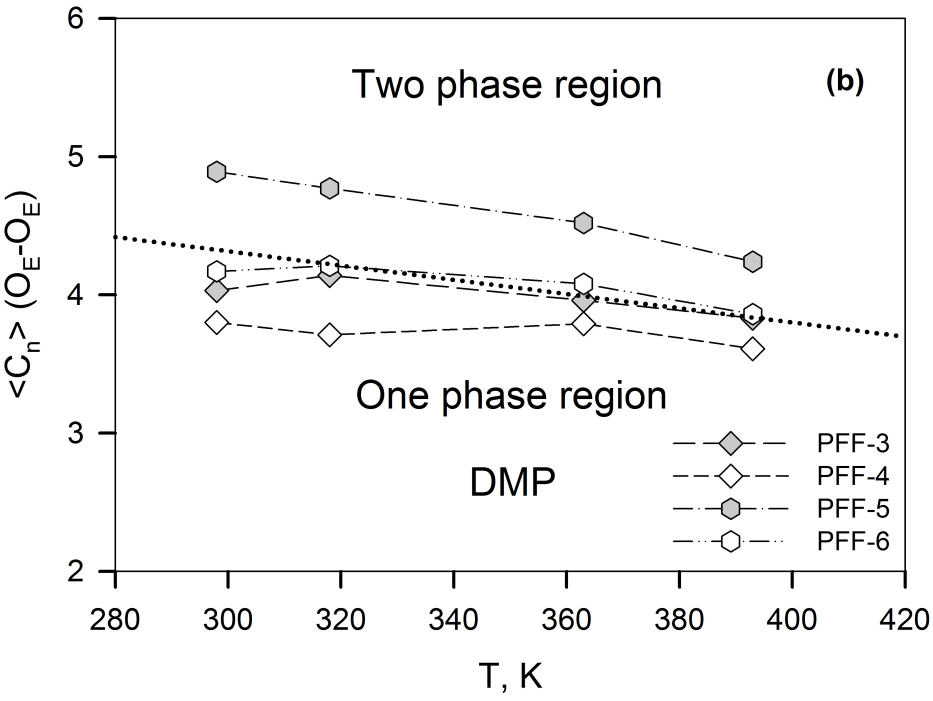
(b)
Two phase region
One phase region
DMP
PFF-3
PFF-4
PFF-5
PFF-6
<C_n> (O_E-O_E)
T, K
6
5
4
3
2
280
300
320
340
360
380
400
420

8.3. Phase behavior of PPO/water solutions

Preliminary studies of PPO6/water solutions was performed next by running a series of MD simulations at 400 K to find a phase transition point. A master curve was constructed first for PPO6/water solutions. Data are fitted to the sigmoidal distribution and phase transition point is determined to be <Cn>≈4.7. The relationship between the extent of O_E-O_E correlation and phase behavior of PPO6/water solutions is given in Figure 33 (a) where the phase transition point is represented by a dotted horizontal line. Increase in O_E-O_E intermolecular correlations is observed with decreasing the strength of ether/water interactions (see Figure 33 (a)). This trend is similar to PEO/water solutions. In addition to the structural intermolecular correlation analysis of PPO6, water density distribution is also analyzed as it was performed for PEO12/water solutions.

The water probability distribution is also expected to be Gaussian-like for the homogeneous solution where favorable intermolecular interactions take place and non-Gaussian as solution undergoes spinodal decomposition.[128] Water density distributions for the repulsion A parameters are shown in Figure 33 (b). It can also be seen that water density distribution is Gaussian for A = -50.00 kcal/mol indicating a homogeneous solution and two peak distributions for A = -25.00 kcal/mol and A = -10.00 kcal/mol. It can also be seen that distribution for A = -25.00 kcal/mol is corresponding to the phase transition point at $<C_n>\approx 4.7$ and is therefore non-Gaussian. The magnitudes of interaction parameters are much higher than for PEO indicating less solubility. Corresponding snapshots from MD simulations for PPO6/water solutions are given in Figure 34 (a-c).

Phase behavior of PPO6/water solutions is studied next for PFF-1/3/5 and PFF-2/4/6 force fields. MD simulations are carried out at 298 K, 318 K, 363 K, 400 K, and

Figure 33. Average coordination number $<C_n>$ is given for the O_E-O_E as a function of ether/water intermolecular interaction parameter A at 400 K. Solid circles indicate values obtained from MD simulations and line indicates sigmoidal fit. Water density distributions are given for the three interaction parameters A.

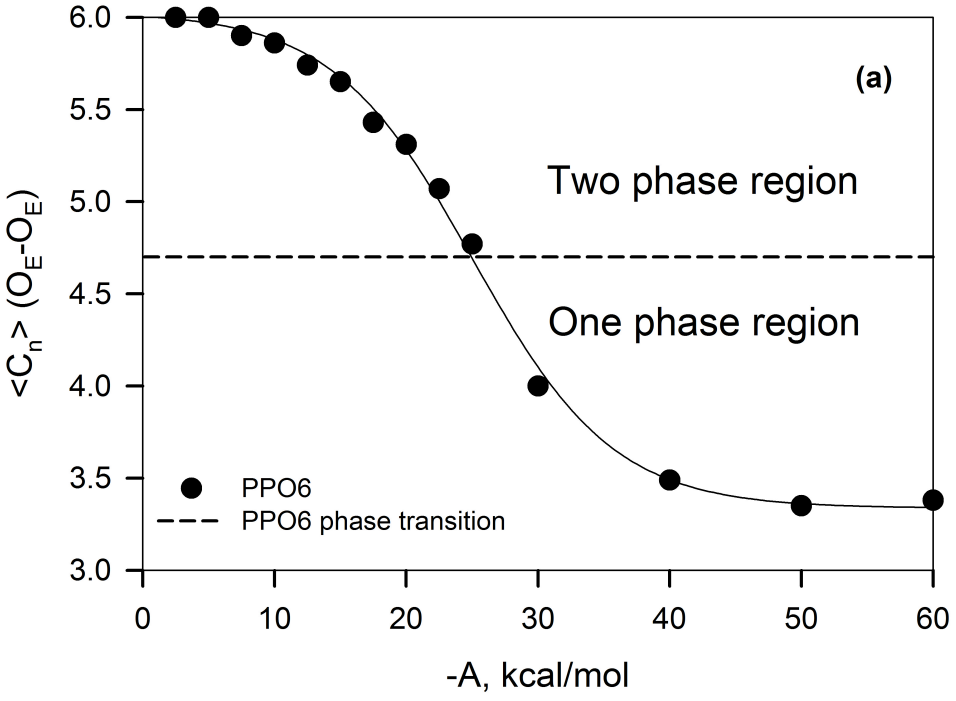
(a)
Two phase region
One phase region
PPO6
PPO6 phase transition
<C_n> (O_E-O_E)
-A, kcal/mol
6.0
5.5
5.0
4.5
4.0
3.5
3.0
0
10
20
30
40
50
60

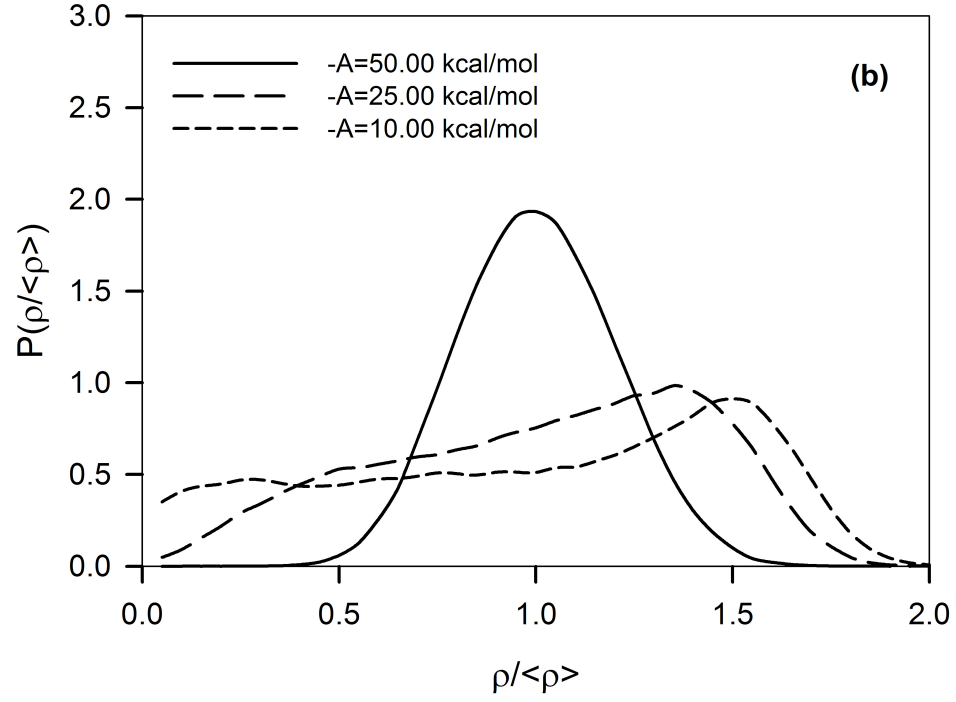
(b)
-A=50.00 kcal/mol
-A=25.00 kcal/mol
-A=10.00 kcal/mol
P(ρ/<ρ>)
ρ/<ρ>
3.0
2.5
2.0
1.5
1.0
0.5
0.0
0.0
0.5
1.0
1.5
2.0

Figure 34. Snapshots for PPO6/water solutions are given as obtained from MD simulations for the repulsion interaction parameters A. Homogeneous solution is obtained for A=-50 kcal/mol (a), phase separated system is obtained for A=-25.00 kcal/mol (b) and A=-10 kcal/mol (c).

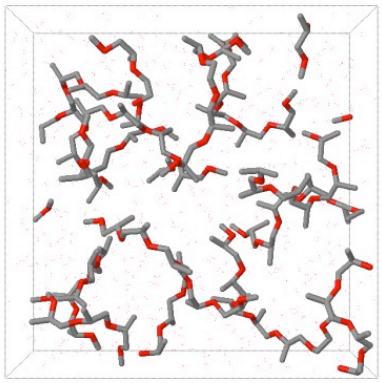

(a)

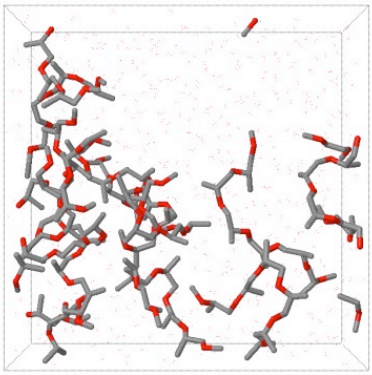

(b)

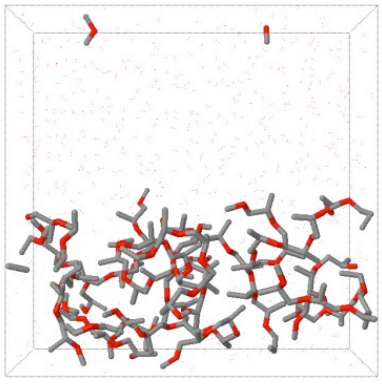

(c)

448 K. O_E-O_E pair correlation fluctuations are determined within 6.0 Å intermolecular distance. The phase diagram is constructed, which is shown in Figure 35.

Qualitatively similar behavior of O_E-O_E coordination number is obtained for the force fields PFF-3/5 and PFF-4/6. However, implementing PFF-5 force field resulted in a higher degree of aggregation than PFF-6.

All force fields predicted phase separation of PPO6 at 298 K except for PFF-2. PFF-2 force field is the most hydrophilic among six according to the free energy of DME solvation. LCST at 363 K was predicted using PFF-2 force field that is above the experimental value of ~320 K for hydroxyl terminated PPO indicating stronger O_E-H_W intermolecular interactions than for any other force fields developed. Similar tendency of C_n is observed for PEO12 with increasing of simulation temperature. O_E-O_E coordination number is above the phase transition line for PFF-3/5 and PFF-4/6 force fields. A decrease in coordination number is due to the thermal expansion at elevated temperatures. To determine LCST for CH_3 terminated PPO6 chains in water, an extra set of simulations should be performed at temperatures lower than 298 K.

Figure 35. Phase diagrams are given for PPO6/water solutions as obtained from MD simulation using PFF-1 through 6 force fields. Dotted line indicates a phase transition, as it was determined from the phase analysis.

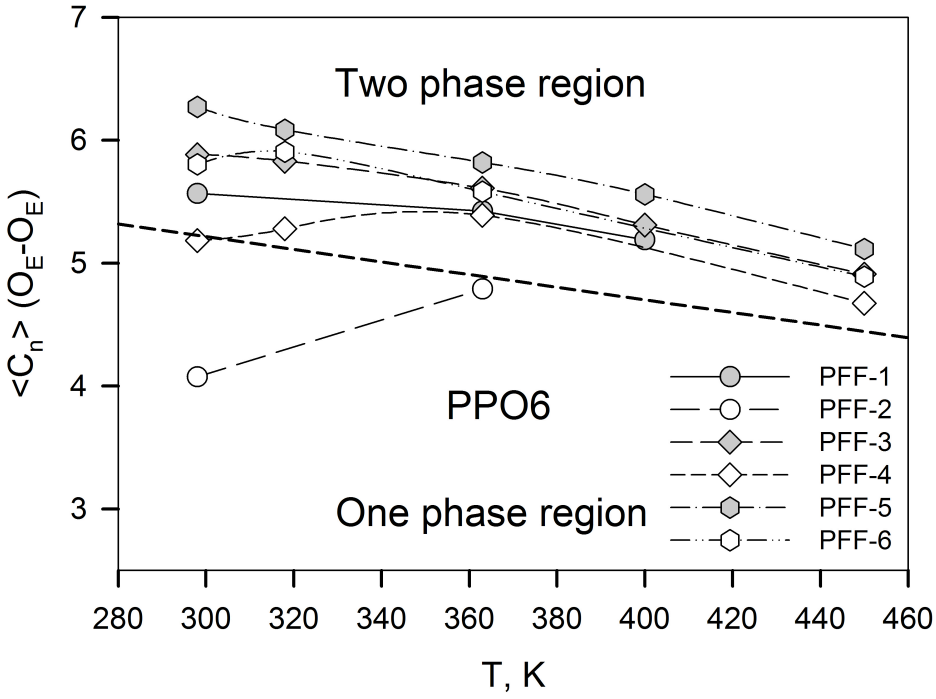
Two phase region
PPO6
One phase region
PFF-1
PFF-2
PFF-3
PFF-4
PFF-5
PFF-6
<C_n> (O_E-O_E)
T, K
7
6
5
4
3
280
300
320
340
360
380
400
420
440
460

9. COMPARISON OF PFF-3 AND PFF-4 FORCE FIELDS

The resulting potentials, PFF-3 and PFF-4, give a description of solvation thermodynamics properties in excellent agreement with experiment, as indicated in Table 5. Furthermore, both force fields accurately describe ΔH_{solv} of solvation for DME in water. Water self-diffusion coefficient D_W and excess viscosity $\Delta\eta^E$ are also well reproduced by both force fields. However, PFF-4 provides a noticeably better description of excess volume (Figure 24 (b)) and hence appears to be the superior force field. This is despite the fact that PFF-3 actually provides a better description of DME/water interactions along Path 1, as shown in Figure 21 (a). PFF-4 also predicts more accurately the self-assembly of ethers as a function of temperature, which is more consistent with theoretical predictions of PEO/water and experimental data of DMP/water solutions. From these observations, the conclusions are made that in parameterization of polymer/water potentials:

(a) parameterizing the potential to match gas phase small molecule/water interactions as obtained from high-level *ab initio* calculations is a good starting point for a potential but empirical adjustments are likely to be required

(b) empirically adjusting the potential to reproduce the free energy of solvation of small molecules in water provides an improved description of water self-diffusion coefficients and excess viscosity of other small molecule/water solution properties as well as polymer/water solution properties

(c) unfortunately there is no unique way to carry out such an empirical adjustment and variations that provide equally good descriptions of the free energy of solvation of the small molecule(s) in water can provide significantly different descriptions of other important properties

(d) empirical adjustments of potentials are usually necessary to match a single solution property. However, the ability of the empirically adjusted potential to describe an array of solution properties should be investigated.

10. CONCLUSIONS

The ability of MD simulations to accurately reproduce the properties of PEO/water and PPO/water solutions as a function of temperature requires high-quality water potential, accurate description of electrostatic potential for the ether polarizable model, and an accurate description of ether/ether and ether/water interactions. The SWM4-AD water model provides a better description of the temperature dependence of water properties than other studied potentials. This potential has been combined with polarizable two-extended charge ether potential, and water/ether nonbonded interactions have been parameterized to accurately reproduce the binding of water to DME. A strong indicator of the quality of the potential is the ability of the potential to accurately describe the free energy and energy of solvation of DME in water. New empirically adjusted polarizable potential PFF-4 provides a good description of DME/water interactions in the gas phase as provided by high-level *ab initio* calculations while at the same time accurately reproducing the thermodynamic properties of DME/water solutions. Developed polarizable ether/water force field, PFF-4, is transferrable to PPO/water solutions as justified by the ability of the force field to predict a correct phase behavior of DMP/water and PPO/water solutions as a function of temperature that is consistent with experimental results based upon preliminary simulation studies. Further studies of higher molecular weight PEO/water solutions are necessary where LCST behavior is

expected to further investigate the ability of polarizable ether/water potential to describe PEO/water phase behavior.

The observed correlation between DME/water thermodynamic properties and the phase behavior of PEO/PPO/water solutions with ΔG_{solv} for DME/water solutions provides a readily accessible method for initially evaluating the quality of an ether/water potential. For example, previously published nonpolarizable ether/water potential[42] yields ΔG_{solv} = -5.6 kcal/mol, significantly greater than the experimental value, and hence it is anticipated that this potential predicts too hydrophilic interactions between PEO and PPO with water. Similarly, the polarizable CHARMM potential[99] yields ΔG_{solv}= -3.8 kcal/mol, (similar to the PFF-5 and PFF-6 potentials), apparently too hydrophobic in description of ether/water interactions. A more recently published polarizable CHARMM potential[111] yields ΔG_{solv}= -5.6 kcal/mol, and it is anticipated that this potential will yield PEO/water and PPO/water interactions that are too favorable.

APPENDIX

A.1 Comparison of the thermodynamic properties for water models

Comparison of thermodynamic properties for TIP4P, SWM4-DP water models, and experiment are given in Table 7. The TIP4P water model exhibits high diffusion coefficient, while SWM4-DP is in perfect agreement with experiment. Higher enthalpy of vaporization is also obtained for the TIP4P model. However, better agreement with experiment in liquid density is reached. Comparison of the water surface tension γ with experiment gives better agreement for SWM4-DP. Surface tension is much lower for the nonpolarizable water model.

A.2 Interface transit method for estimation of free energy of solvation

The interface transit method (IT) is described based on the constrained force approach[129] to estimate free energy of solvation ΔG_{solv}. This method involves a partition of simulation space into two regions. One region would correspond to the vacuum space and another to the film of solvent.

DME molecule is brought from vacuum to the bulk of water. Water molecules are constantly moving between the center of the bulk and the water/vacuum interface due to thermal fluctuations in the system. Each water molecule can move freely at the interface having fewer numbers of hydrogen bonds. As DME approaches the interface, the

Table 7. Liquid state properties for selected water models

	TIP4P[a]	SWM4-DP[b]	Experiment [c]
T (K)	298.00	298.00	298.00
$D10^{-9}(m^2/s)$	2.8	2.30±0.04	2.30
Δu (kcal/mol)	-10.1	-9.93	-9.92
ΔH_{vap} (kcal/mol)	10.65	10.52	10.52
α (Å)	-	1.04252	1.44
$<\mu>$ (D)	2.18	2.456	2.9±0.6
ε_0	53±2	79±5	78.4
ε_∞	1		1.79
ρ (g/cm^3)	0.9937	1.0056	0.9970
τ_D (ps)	7±2	9.4±0.7	8.27±00.2
γ (dyn/cm)	53.6[d]	66.9±0.9	72.0

[a] Ref.[76,130];

[b] Ref.[72,82];

[c] Ref.[120];

[d] Ref.[84].

surface water molecules will rigorously bind to the solute by formation of the hydrogen bond. This interaction will change DME conformation to low energy state and will affect sampling of gas conformations. However, it is necessary to sample all available energy states for DME in gas before entering the solvent. Therefore, to avoid this problem, water/vacuum interface should be 'sharpened' to decrease interactions of a solvent with free solvent molecules when approaching the interface.

In order to sharpen the solvent/vacuum interface, two artificial walls parallel to the solvent/vacuum interface are applied (x-y plane) on the left ZL and on the right ZR sides of the film. The biasing force from the walls $F_i^{wall}(z_i)$ acting on each atom is defined as

$$F_i^{wall}(z_i) = \begin{Bmatrix} +k(z_i - z_l)^2 & z_i < z_l \\ -k(z_i - z_r)^2 & z_i > z_r \\ 0 & z_l \le z_i \le z_r \end{Bmatrix} \quad \text{(A.1)}$$

where z_i is the position of an atom i, Å; k=5 kcal/mol·Å^2 is a force constant, and z_l and z_r are the positions for the left or right walls relative to the center-of-mass of the water film, Å. To ensure that the net external force (from the walls) on the film is zero, each time step the total force from both walls was determined and then a counter force was evenly distributed between all atoms in the film. Therefore, the effective force experienced by each atom in the film is

$$F_i^{eff}(z_i) = F_i^{wall}(z_i) - \sum_{i=1}^{N} \frac{F_i^{wall}(z_i)}{N} \quad \text{(A.2)}$$

where N is the total number of atoms in the water film. As can be seen in Figure 36, application of this force sharpens the water/vacuum interface without significantly perturbing the density at the center of the film. A single DME molecule is introduced from the gas phase into the center of the solvent film maintaining bulk like conditions with the periodic separation step Δz_i. In a system with additional constrains, a narrow water/vacuum interface was reached with a constant bulk density of water. A single water molecule can be found at the distance of 5 Å away of the interface. In order to adequately thermalize the single gas-phase molecule the solute needs to experience an additional Brownian force with a friction coefficient that can be chosen empirically. The center-of-mass of the solute is kept at fixed separation distance Δz from the center-of-mass of the film, and the force required to maintain this constrain is determined every time step as

$$F_{inst} = -\frac{\Delta z_i^* m_{solute}^*}{\Delta t^2} \quad \text{(A.3)}$$

where F_{inst} is a constrained force that needs to be applied to move the solvent to its original position at t_0; Δz_i^* is a difference from the original and final positions of the center-of-mass for the solute molecule due to the external force, Å; $m_{solute}^* = \frac{m_{solute}}{m_{solute} + m_{solvent}}$ a mass ratio of solute to the total mass of the system, g; and Δt is the integration step size, fs.

Figure 36. Water bulk distribution densities are shown without constrains (no artificial walls) and with additional constrains (artificial walls applied) at the water/vacuum interface.

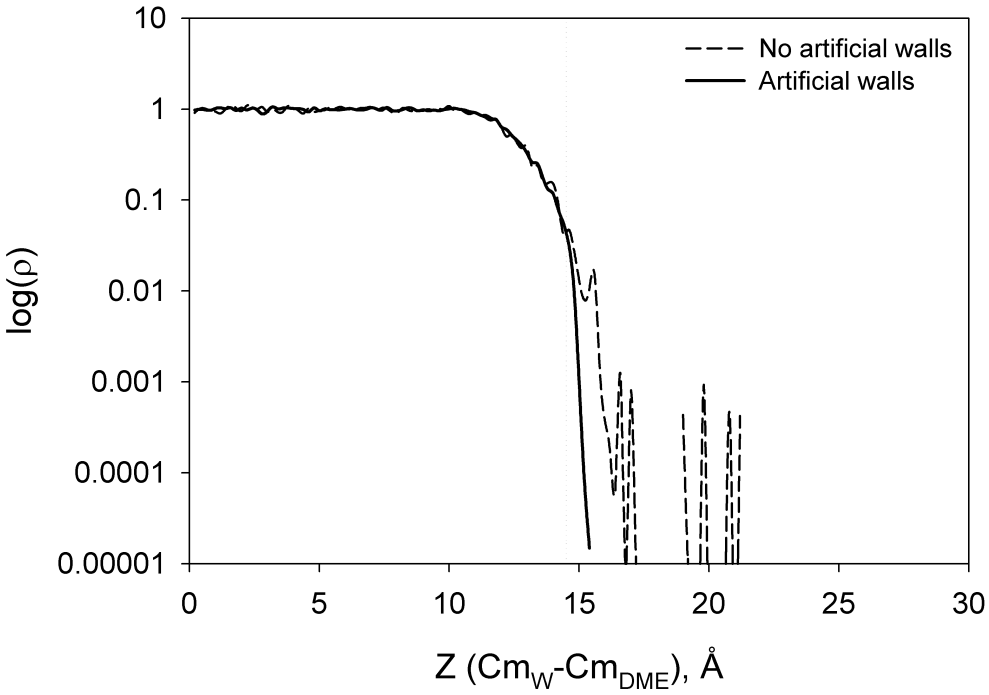
10
1
0.1
0.01
0.001
0.0001
0.00001
log(ρ)
0
5
10
15
20
25
30
Z (Cm$_W$-Cm$_{DME}$), Å
No artificial walls
Artificial walls

A.3 Method for estimation of water density distribution in a sub-box

There are several algorithms established for analysis of the phase transitions. Rovere et al.[126] have described a block density distribution technique, which is an extension of finite-size scaling techniques initially developed for the analysis of phase transitions of lattice models. A block density technique has been utilized to look for the water density fluctuations within a simulation box. Analysis was carried out by dividing a simulation box into the sub-boxes with volume $V=L^3$ (where L is the size of a sub-box) and by calculating the probability distribution function $P(\rho_w/\langle\rho_w\rangle)$ where ρ_w is the water density in the sub-box normalized by an average water density $\langle\rho_w\rangle$ in the sub-box. The sub-box size was chosen to be less than the half of the simulation box to avoid double counting and large enough to avoid finite size effects. The sub-box size of L=10 Å was defined as an optimal for calculations of probability distributions by performing a number of analyses using different sub-box sizes. In practice, the sub-box size of L=10 Å was placed in 100 random locations of simulation box. The probability distribution is expected to be Gaussian for the homogeneous solution and non-Gaussian as solution undergoes spinodal decomposition. Density distributions were fit to the Gaussian function as

$$P(c) = \frac{1}{\sqrt{2\pi\sigma^2}} \exp\left(-\frac{\left(c-\langle c\rangle\right)^2}{2\sigma^2}\right) \tag{A.4}$$

The probability of generating a value from Gaussian distribution with the mean $\langle c\rangle$ and variance σ^2 where the variance is $\sigma=\langle[c-\langle c\rangle]^2\rangle$. Analysis of the water

distributions confirms a homogeneous distribution for PFF-1/3 and PFF-2/4 force fields and non-homogenous distribution for PFF-5 and PFF-6 force fields at elevated temperatures (Figure 37 (a-f)).

A.4 Rotational isomerization for DME

Conformational energies and rotational barriers are important aspects in reproducing static and dynamic properties of PEO. DME model compound was used to calculate conformational potentials. Conformational energies were calculated at MP2/aug-cc-pvDz//B3LYP-aug-cc-pvDz level. Comparison of energies obtained from *ab initio* calculations and the force field is given in Figure 38. Good agreement with *ab initio* data is established. Local energy minima are well described by the force field. However, the barrier for Xgt rotation is underestimated by ~2 kcal/mol.

A.5 Rotational isomerization for DMP

Conformational energies and rotational barriers are also important aspects in reproducing static and dynamic properties of PPO. DMP model compound was used to study conformational transitions and energies. These conformations are expected to be different from DME due to the different chemical structure. Torsional parameters were obtained by fitting to the energies from MP2/aug-cc-pvDz//MO52X/aug-cc-pvDz levels for the most important conformers. Comparison of energies from *ab initio* calculations and PFF-force field is given in Figure 39. A good agreement is established with *ab initio* calculations.

Figure 37. Comparison of water density distributions $P(\rho_w/\langle\rho_w\rangle)$ is given for PEO/water solutions. Lines correspond to the fit to the distributions obtained from MD simulations. γ' is a standard deviation obtained from the fit.

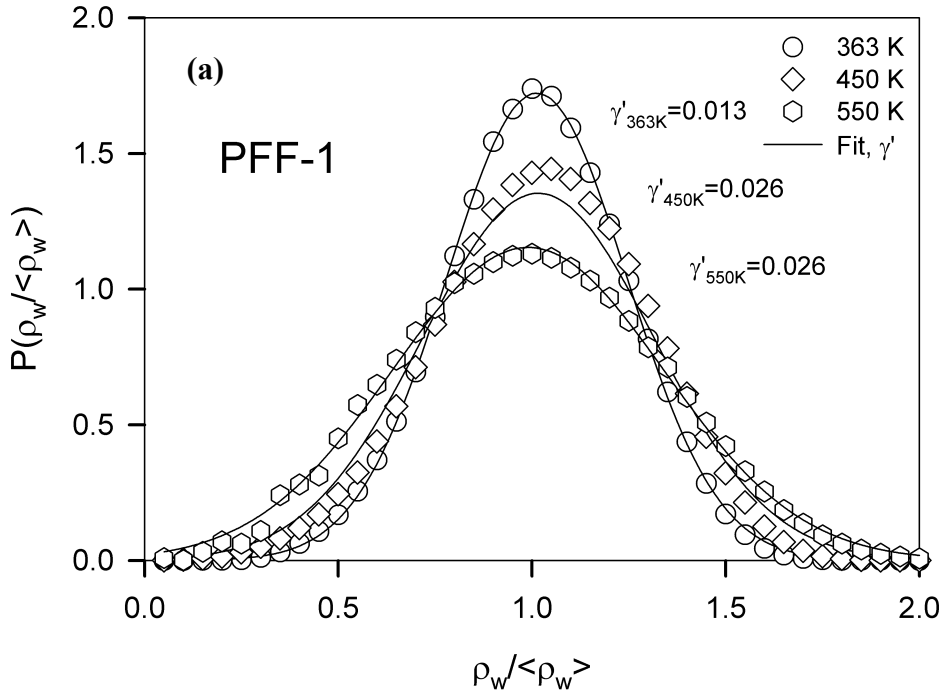
(a)
PFF-1
363 K
450 K
550 K
Fit, γ'
γ'363K=0.013
γ'450K=0.026
γ'550K=0.026
P(ρw/<ρw>)
ρw/<ρw>
0.0
0.5
1.0
1.5
2.0

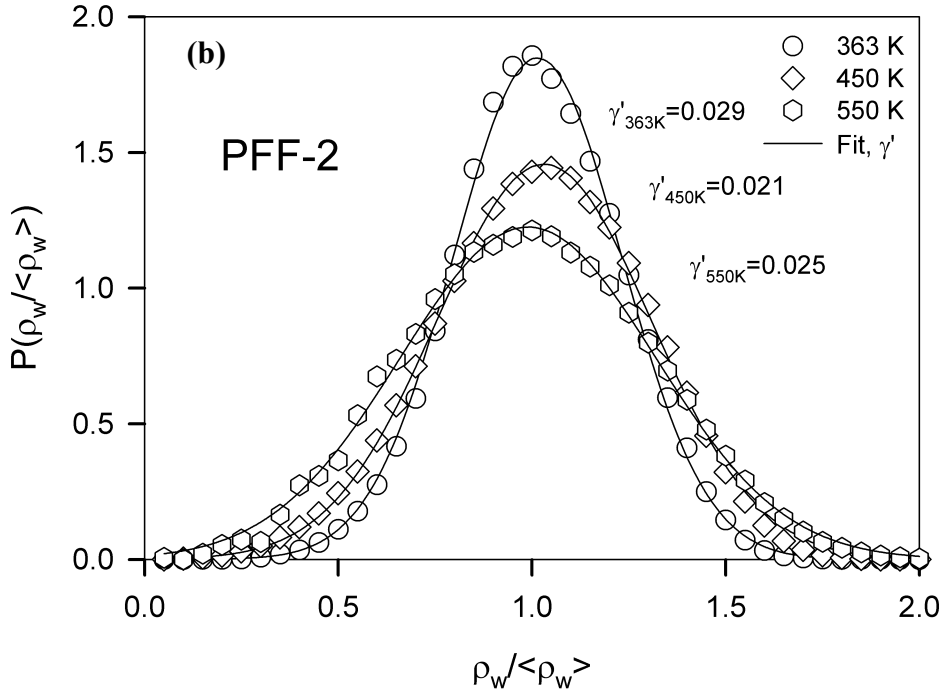
(b)
PFF-2
363 K
450 K
550 K
Fit, γ'
γ'363K=0.029
γ'450K=0.021
γ'550K=0.025
P(ρw/<ρw>)
ρw/<ρw>
0.0
0.5
1.0
1.5
2.0

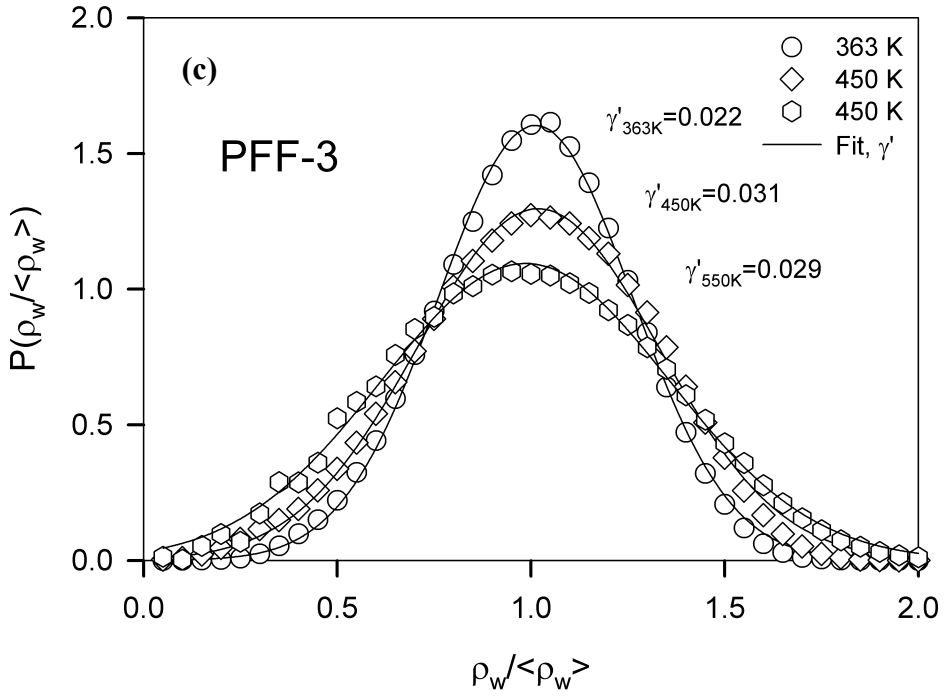

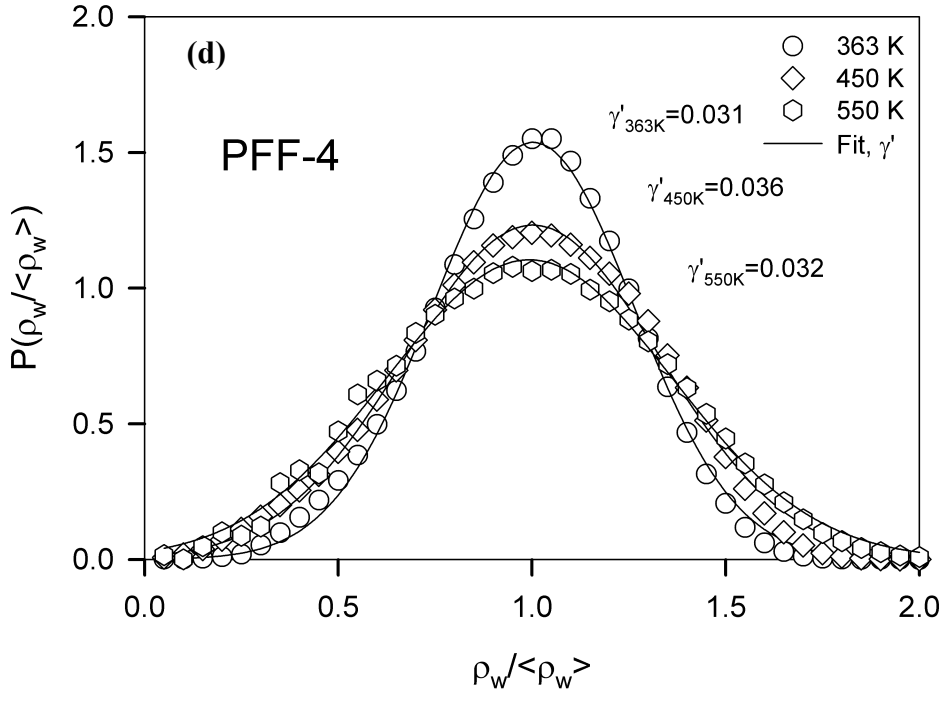

Figure 37. Continued

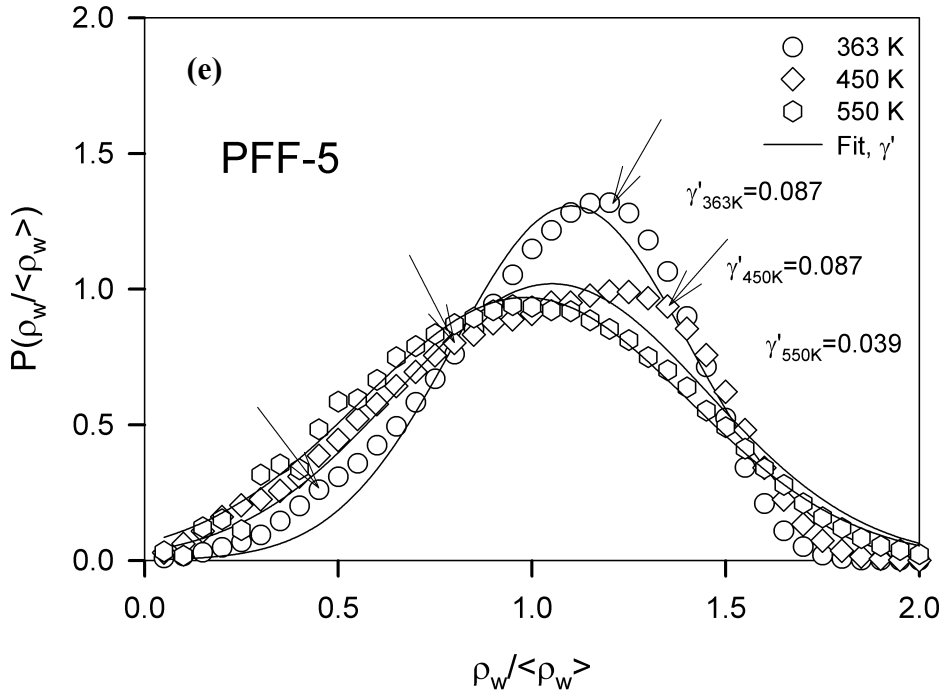

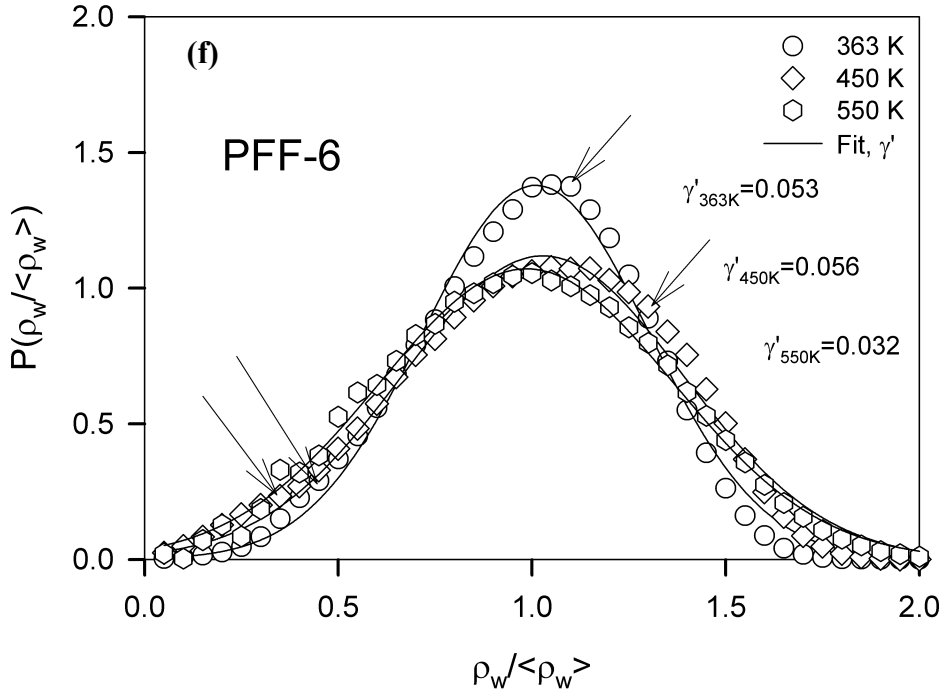

Figure 37. Continued

Figure 38. Conformational energy paths are shown for DME. Open circles indicate *ab initio* calculations and lines indicate fits as obtained for the polarizable force field.

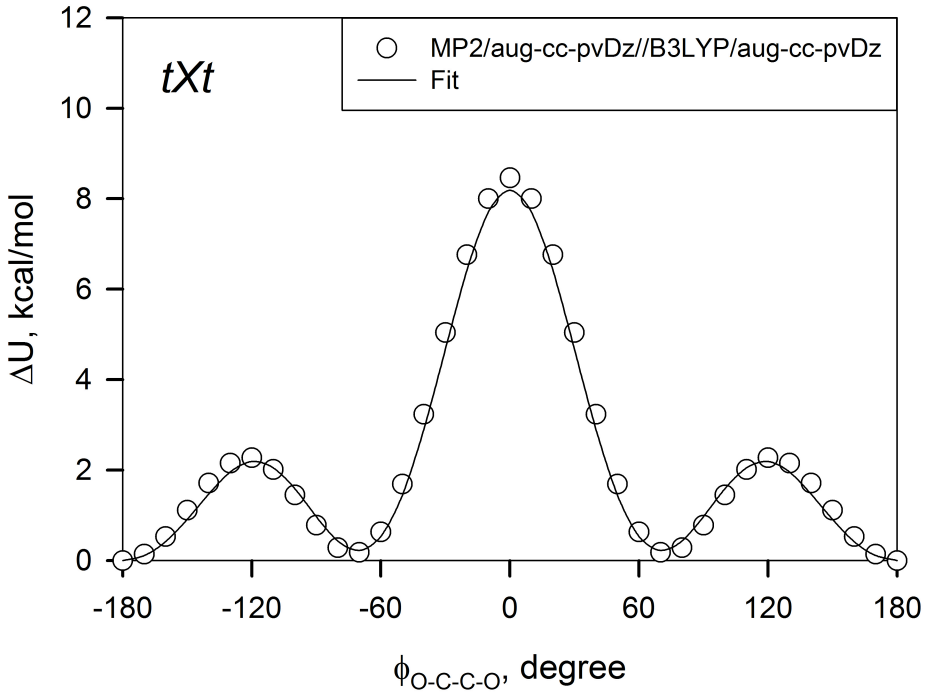
tXt
MP2/aug-cc-pvDz//B3LYP/aug-cc-pvDz
Fit
ΔU, kcal/mol
0
2
4
6
8
10
12
-180
-120
-60
0
60
120
180
ϕO-C-C-O, degree

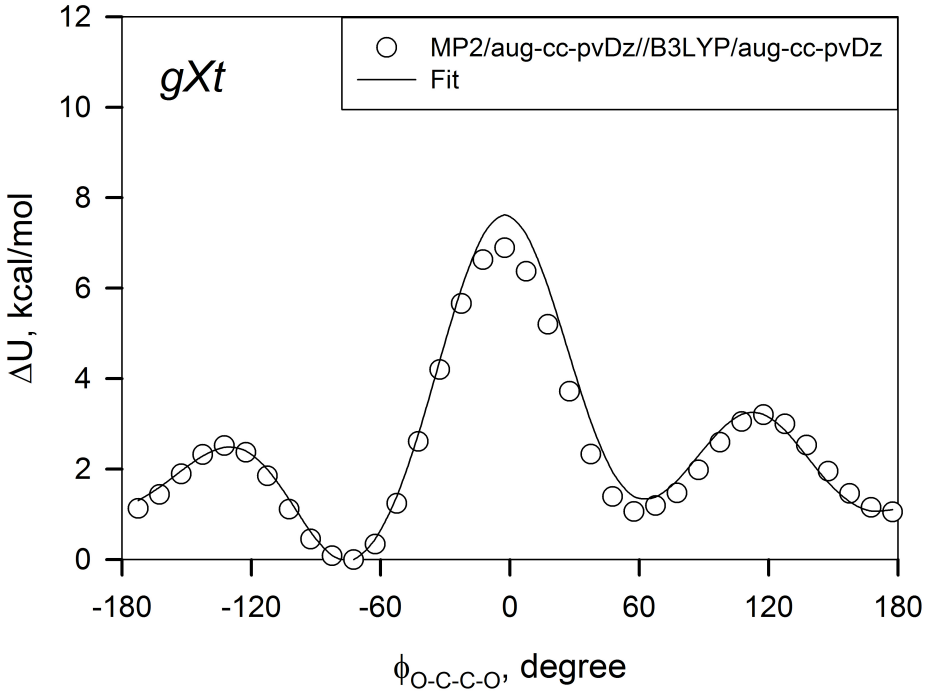
gXt
MP2/aug-cc-pvDz//B3LYP/aug-cc-pvDz
Fit
ΔU, kcal/mol
0
2
4
6
8
10
12
-180
-120
-60
0
60
120
180
ϕO-C-C-O, degree

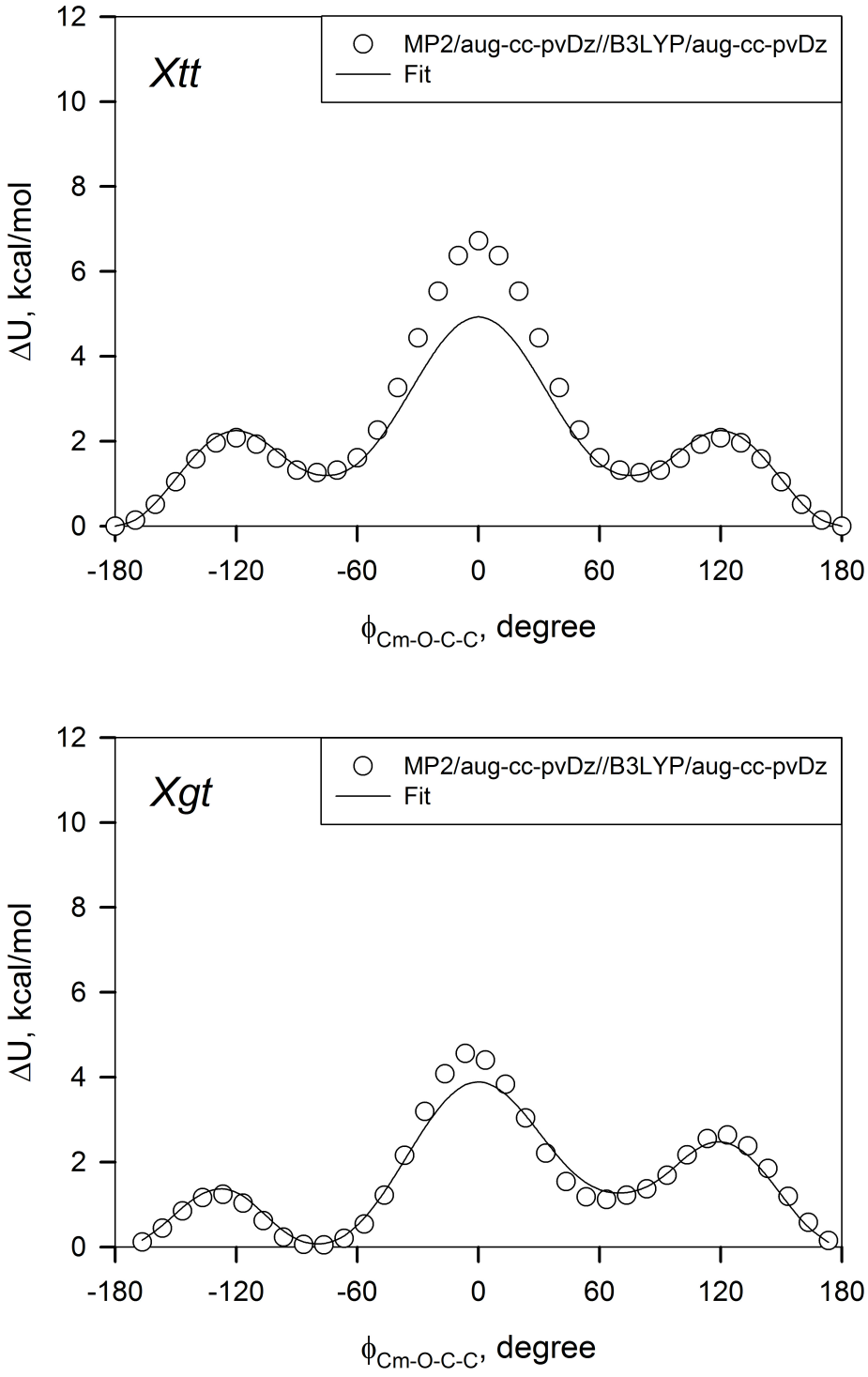

Figure 38. Continued

Figure 39. Conformational energy paths are shown for DMP. Open circles indicate *ab initio* calculations and lines indicate fits as obtained for the polarizable force field.

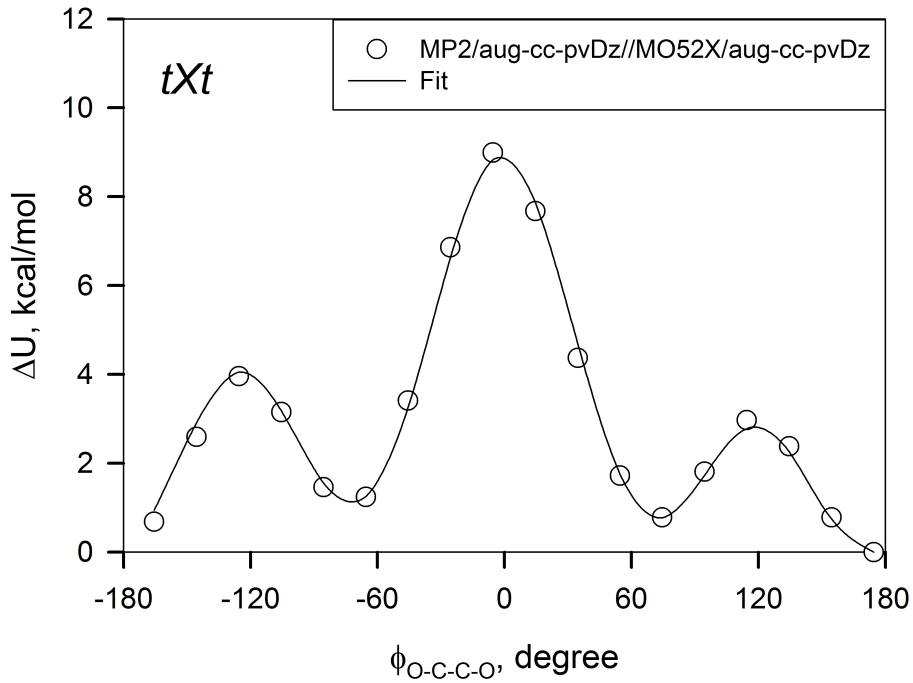
tXt
MP2/aug-cc-pvDz//MO52X/aug-cc-pvDz
Fit
ΔU, kcal/mol
0
2
4
6
8
10
12
-180
-120
-60
0
60
120
180
ϕO-C-C-O, degree

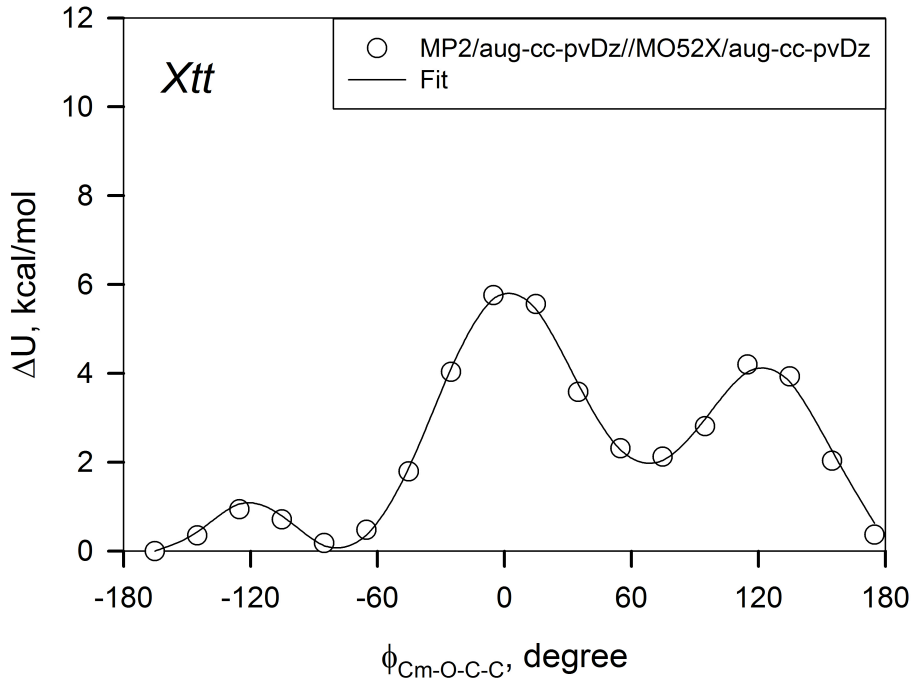
Xtt
MP2/aug-cc-pvDz//MO52X/aug-cc-pvDz
Fit
ΔU, kcal/mol
0
2
4
6
8
10
12
-180
-120
-60
0
60
120
180
ϕCm-O-C-C, degree

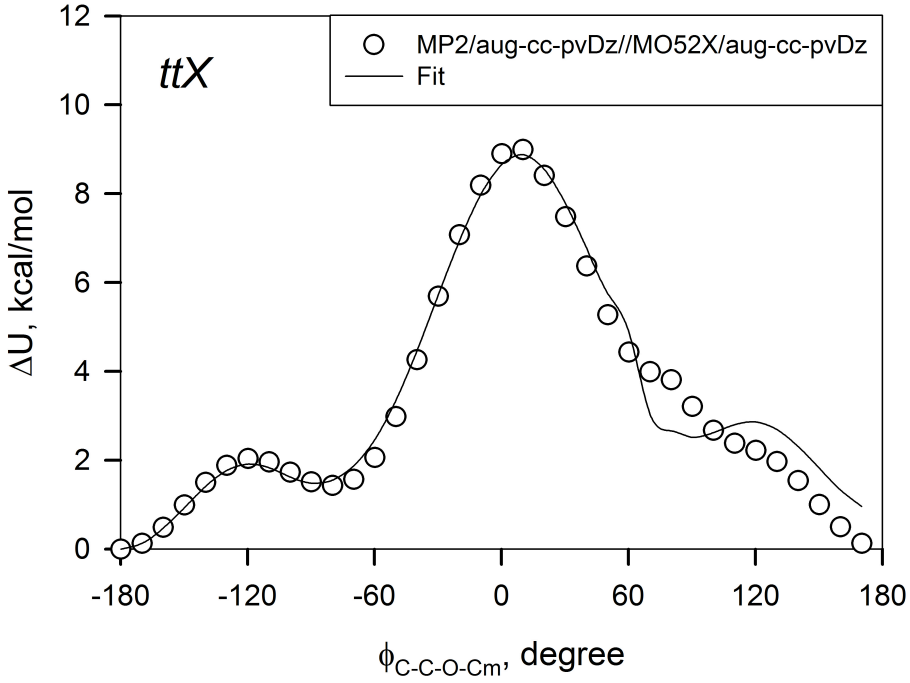

Figure 39. Continued

A.6 Conformational populations for DME in water

Previous molecular dynamics simulation studies[61] revealed *tgt* and *tgg* conformers of DME as the most populous in DME/water solutions. Low energy *ttt*, $tg\bar{g}$, and *ttg* conformations were found to be the most populous in the gas phase further defined as hydrophobic. It was also established that populations of hydrophilic conformations are increasing with dilution while hydrophobic conformations are decreasing. The analysis of those conformers is performed for PFF-1 through PFF-4 force fields. Conformational populations were estimated as a function of DME concentrations for each single conformer at 318 K. Results are compared with the most recent Raman spectroscopic data as shown in Figure 40. Qualitative agreement is established with experiment for all concentrations. Populations of hydrophilic conformations of DME are overestimated for tgt conformer at low concentrations, 0.18 mole fraction, while populations at higher concentrations are in a good agreement with experiment. Populations of hydrophilic *tgg* conformer are underestimated within all concentrations. The hydrophobic populations $tg\bar{g}$ and *ttg* are systematically underestimated for all force fields, while populations for *ttt* are overestimated.

The effect of free energy on conformational populations of DME has also been considered. Implementing PFF-4 force field resulted in an improved description of conformer populations in comparison with PFF-2. However, the effect is relatively small. These observations are in agreement with previous studies by Smith et al.[61] where the influence of DME conformations on solvation thermodynamics was investigated.

Figure 40. Populations of DME conformers as a function of concentration at 318 K.

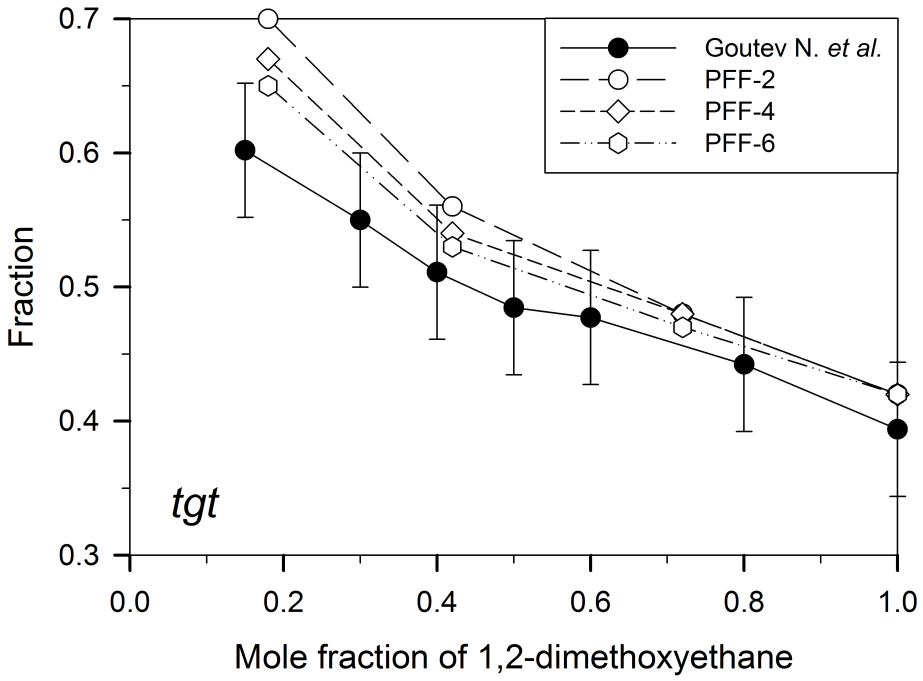
0.7
0.6
0.5
0.4
0.3
Fraction
0.0
0.2
0.4
0.6
0.8
1.0
Mole fraction of 1,2-dimethoxyethane
Goutev N. et al.
PFF-2
PFF-4
PFF-6
tgt

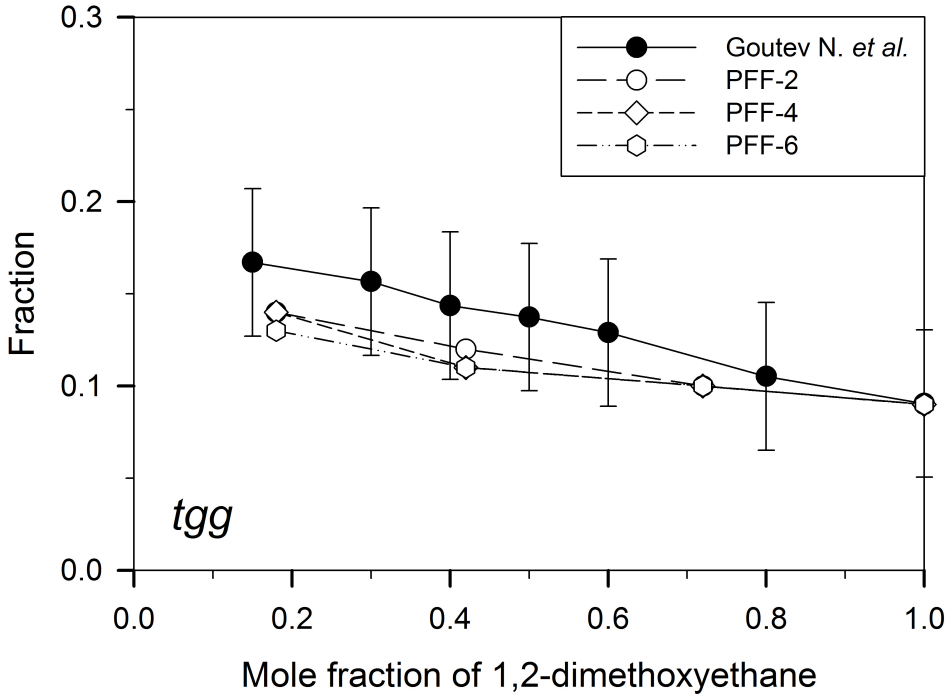
0.3
0.2
0.1
0.0
Fraction
0.0
0.2
0.4
0.6
0.8
1.0
Mole fraction of 1,2-dimethoxyethane
Goutev N. et al.
PFF-2
PFF-4
PFF-6
tgg

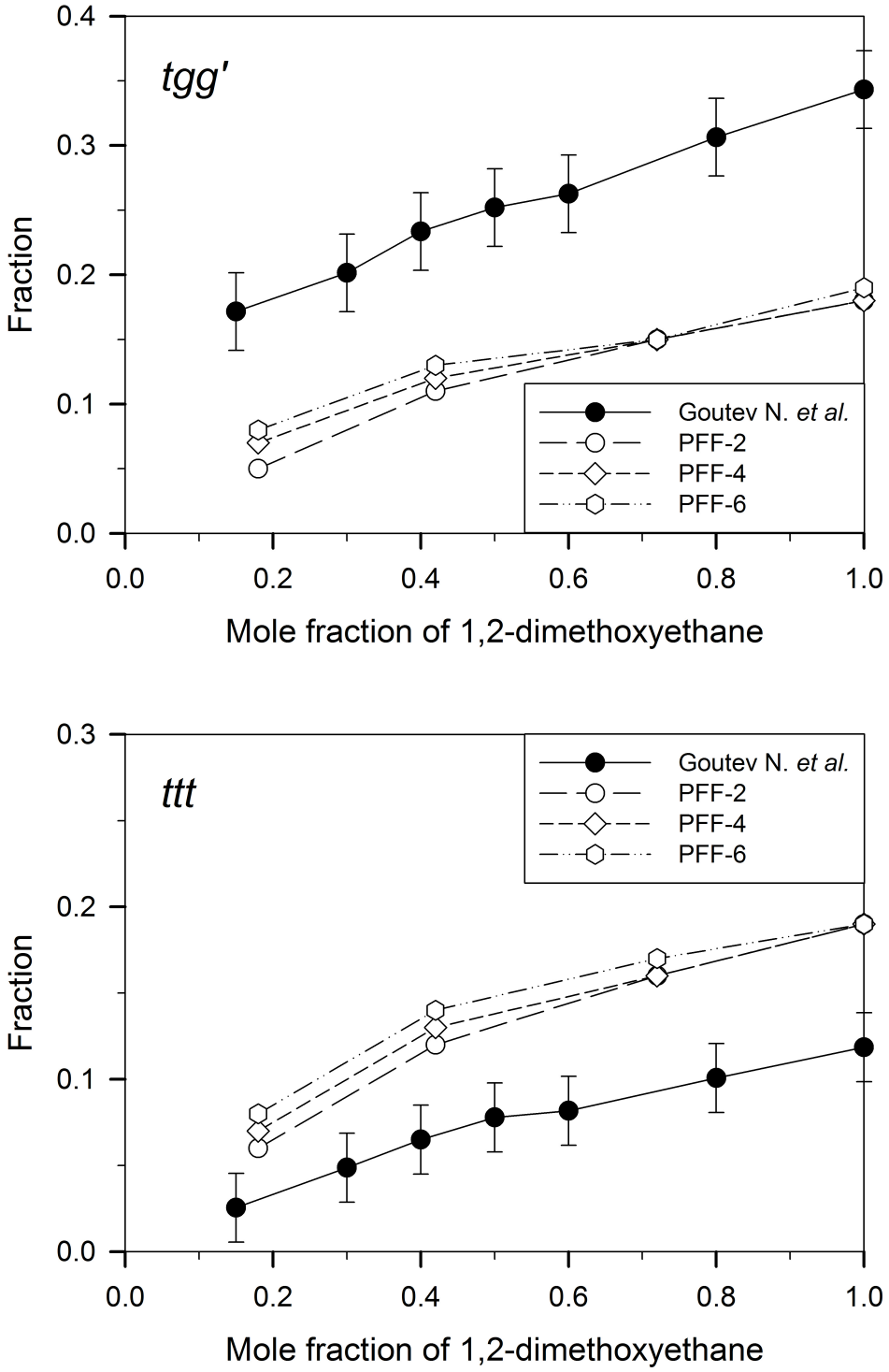

Figure 40. Continued

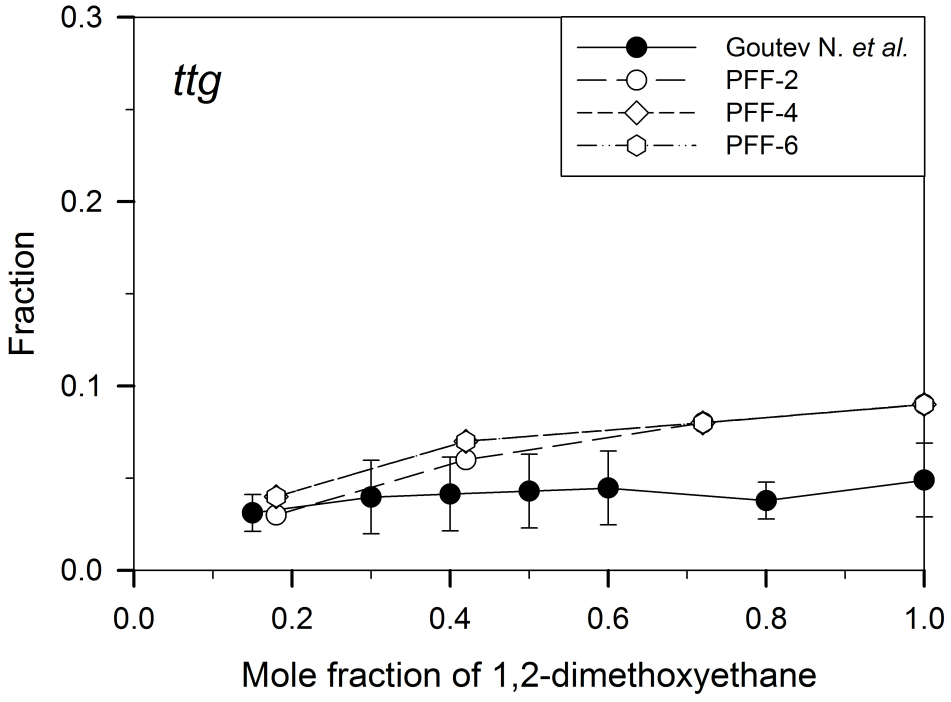

Figure 40. Continued

REFERENCES

(1) Franks, F. *Water A Comprehensive Treatise: Aqueous Solutions of Amphiphiles and Macromoleculaes.*; Plenum Press: London, 1975; p 8.

(2) Yaminsky, V. V.; Vogler, E. A. *Curr Opin Colloid In* **2001**, *6*, 342.

(3) Matsen, M. W.; Bates, F. S. *Macromolecules* **1996**, *29*, 7641.

(4) Blume, A. In *Self-assembly*; Robinson, B. H., Ed.; IOS Press: Amsterdam, 2003; p 389.

(5) Scholtz, J. M.; Baldwin, R. L. *Annual Review of Biophysics and Biomolecular Structure* **1992**, *21*, 95.

(6) Chakrabartty, A.; Baldwin, R. *Advances in Protein Chemistry* **1995**, *46*, 141.

(7) Bae, Y. C.; Lambert, S. M.; Soane, D. S.; Prausnitz, J. M. *Macromolecules* **1991**, *24*, 4403.

(8) Saeki, S.; Kuwahara, N.; Nakata, M.; Kaneko, M. *Polymer* **1976**, *17*, 685.

(9) Yallapu, M. M.; Reddy, M. K.; Labhasetwar, V. *Biomedical Applications of Nanotechnology;* John Wiley & Sons: New Jersey, 2007; p 131.

(10) Hadjichristidis, N.; Pispas, S.; Floudas, G. *A Block Copolymers Synthetic Strategies, Physical Properties, and Applications*; John Wiley & Sons: New Jersey, 2003; p 290.

(11) Uglea, C. V. *Oligomer Technology and Applications*; Taylor & Francis Inc.: New York, 1998; p 249.

(12) Hamley, I. W. In *The Physics of Block Copolymers*; Oxford University Press, Inc.: New York, 1998; p 295.

(13) Fusco, S.; Borzacchiello, A.; Netti, P. A. *Bioactive and Compatible Polymers.* **2006**, *21*, 149.

(14) www.basf.com/group/corporate/en/brand/PLURONIC

(15) Malmsten, M.; Linse, P.; Zhang, K. W. *Macromolecules* **1993**, *26*, 2905

(16) Linse, P. *Macromolecules* **1993**, *26*, 4437.

(17) Alexandridis, P.; Holzwarth, J. F.; Hatton, T. A. *Macromolecules* **1994**, *27*, 2414.

(18) Goldmints, I.; Holzwarth, J. F.; Smith, K. A.; Hatton, T. A. *Langmuir* **1997**, *13*, 6130.

(19) Panagiotopoulos, A. Z.; Floriano, M. A.; Kumar, S. K. *Langmuir* **2002**, *18*, 2940.

(20) Senkow, S.; Mehta, S. K.; Douheret, G.; Roux, A. H.; Roux-Desgranges, G. *Phys Chem Chem Phys* **2002**, *4*, 4472.

(21) Sommer, C.; Pedersen, J. S.; Stein, P. C. *J Phys Chem B* **2004**, *108*, 6242.

(22) Yardimci, H.; Chung, B.; Harden, J. L.; Leheny, R. L. *J Chem Phys* **2005**, *123*.

(23) Lisi, D. R.; Lazzara, G.; Milioto, S.; Muratore, N. *J Chem Therm* **2006**, *38*, 1344.

(24) Jebari, M. M.; Ghaouar, N.; Aschi, A.; Gharbi, A. *Polym Int* **2006**, *55*, 176.

(25) Goldmints, I.; vonGottberg, F. K.; Smith, K. A.; Hatton, T. A. *Langmuir* **1997**, *13*, 3659.

(26) Mortensen, K. *J Phys Cond Matter* **1996**, *8*, A103.

(27) Mortensen, K.; Brown, W. *Macromolecules* **1993**, *26*, 4128.

(28) Malcolm, G. N.; Rowlinson, J. S. *J Chem Soc Faraday Trans* **1957**, *53*, 921.

(29) Bilimova, Y. S.; Gladkovskii, G. A.; Golubev, V. M.; Medved, Z. N. *Polymer Science U.S.S.R* **1980**, *22*, 2456.

(30) Das, B.; Roy, M. N.; Hazra, D. K. *Indian Journal of Chemical Technology* **1994**, *1*, 93.

(31) Biros, J.; Pouchly, J.; Zivny, A. *Die Makromolekulare Chemie* **1986**, *188*, 379.

(32) Zivny, A.; Biros, J.; Pouchly, J. *Die Makromolekulare Chemie* **1989**, *190*, 1345.

(33) Dohnal, V.; Roux, A. H.; Hynek, V. *J Sol Chem* **1994**, *23*, 889.

(34) Kustov, A. V.; Antonova, O. A.; Korolev, V. P. *J Sol Chem* **2002**, *31*, 671.

(35) Trouw, F.; Bedrov, D.; Borodin, O.; Smith, G. D. *J Chem Phys* **2000**, 01.

(36) Bieze, T. W. N.; Barnes, A. C.; Huige, C. J. M.; Enderby, J. E.; Leyte, J. C. *J Phys Chem* **1994**, *98*, 6568.

(37) Crowther, N. J.; Eagland, D. *J Chem Soc Faraday Trans* **1996**, *92*, 1859.

(38) Medved, Z. N.; Petrova, N. I.; Tarakanov, O. G. *Vysokomoleculrnie Soedinineniya* **1982**, *24*, 674.

(39) Teixeira, J.; Bellissent-Funel, M.-C.; Chen, S. H.; Dianoux, A. J. *Phys Rev A* **1985**, *31*, 1913.

(40) Mills, R. *Molecular Motions in Liquids* **1974**, 391.

(41) Holtz, M.; Heil, S. R.; Sacco, A. *Phys Chem Chem Phys* **2000**, *2*, 4740.

(42) Smith, G. D.; Borodin, O.; Bedrov, D. *J Comput Chem* **2002**, *23*, 1480.

(43) Stephenson, R. M. *J Chem Eng Data* **1993**, *38*, 134.

(44) Carlsson, M.; Hallen, D.; Linse, P. *J Chem Soc Faraday Trans* **1995**, *91*, 2081.

(45) Bekiranov, S.; Bruinsma, R.; Pincus, P. *Phys Rev E* **1997**, *55*, 577.

(46) Dormidontova, E. E. *Macromolecules* **2004**, *37*, 7747.

(47) Karlstrom, G. *J Phys Chem* **1984**, *89*, 4962.

(48) Matsuyama, A.; Tanaka, F. *Phys Rev Lett* **1990**, *65*, 341.

(49) Dormidontova, E. E. *Macromolecules* **2002**, *35*, 987.

(50) Flory, P. J. *Principles of Polymer Chemistry*; Ithaca: Cornell University Press, 1953; p 495.

(51) Jaffe, R. L.; Smith, G. D.; Yoon, D. Y. *J Phys Chem* **1993**, *97*, 12745.

(52) Smith, G. D.; Crain, K.; Jaffe, R. L. *J Phys Chem A* **1997**, *101*, 3152.

(53) Smith, G. D.; Jaffe, R. L.; Yoon, D. Y. *J Phys Chem* **1993**, *97*, 12752.

(54) Smith, G. D.; Jaffe, R. L.; Yoon, D. Y. *J Am Chem Soc* **1995**, *117*, 530.

(55) Smith, G. D.; Yoon, D. Y.; Jaffe, R. L.; Colby, R. H.; Krishnamoorti, R.; Fetters, L. J. *Macromolecules* **1996**, *29*, 3462.

(56) Smith, G. D.; Borodin, O.; Pekny, M.; Annis, B.; Londono, D.; Jaffe, R. L. *Spectrochim Acta A* **1997**, *53*, 1273.

(57) Smith, G. D.; Borodin, O.; Bedrov, D. *J Phys Chem A* **1998**, *102*, 10318.

(58) Bedrov, D.; Borodin, O.; Smith, G. D. *J Phys Chem B* **1998**, *102*, 9565.

(59) Bedrov, D.; Smith, G. D. *J Chem Phys* **1998**, *109*, 8118.

(60) Smith, G. D.; Bedrov, D.; Borodin, O. *J Am Chem Soc* **2000**, *122*, 9548.

(61) Smith, G. D.; Bedrov, D. *J Phys Chem A* **2001**, *105*, 1283.

(62) Bedrov, D.; Smith, G. D. *J Chem Phys* **2003**, *118*, 6656.

(63) Bedrov, D.; Smith, G. D. *J Phys Chem B* **1999**, *103*, 10001.

(64) Smith, G. D.; Bedrov, D. *Macromolecules* **2002**, *35*, 5712.

(65) Smith, G. D.; Bedrov, D. *J Phys Chem B* **2003**, *107*, 3095.

(66) Smith, G. D.; Bedrov, D.; Borodin, O. *Phys Rev Lett* **2000**, *85*, 5583.

(67) Borodin, O.; Trouw, F.; Bedrov, D.; Smith, G. D. *J Phys Chem B* **2002**, *106*, 5184.

(68) Borodin, O.; Bedrov, D.; Smith, G. D. *J Phys Chem B* **2002**, *106*, 5194.

(69) Bedrov, D.; Pekny, M.; Smith, G. D. *J Phys Chem B* **1998**, *102*, 996.

(70) Bedrov, D.; Smith, G. D. *J Phys Chem B* **1999**, *103*, 3791.

(71) Bedrov, D.; Borodin, O.; Smith, G. D.; Trouw, F.; Mayne, C. *J Phys Chem B* **2000**, *104*, 5151.

(72) Lamoureux, G.; MacKerell, A. D.; Roux, B. *J Chem Phys* **2003**, *119*, 5185.

(73) Borodin, O.; Smith, G. D. *J Phys Chem B* **2003**, *107*, 6801.

(74) Borodin, O.; Smith, G. D. *J Phys Chem B* **2006**, *110*, 6279.

(75) http://www.eng.utah/~gsmith/lucretius.html

(76) Jorgensen, W. L.; Chandrasekar, J.; Madura, J. D.; Impey, R. W.; Klein, M. L. *J Chem Phys* **1983**, *79*, 926.

(77) Yu, H.; Hansson, T.; van Gunsteren, W. F. *J Chem Phys* **2003**, *118*, 221.

(78) Yu, H.; van Gunsteren, W. F. *J Chem Phys* **2004**, *121*, 9549.

(79) Rick, S. W.; Stuart, S. J.; Berne, B. J. *J Chem Phys* **1994**, *101*, 6141.

(80) Rick, S. W. *J Chem Phys* **2001**, *114*, 2276.

(81) Stern, H. A.; Rittner, F.; Berne, B. J.; Friesner, R. A. *J Chem Phys* **2001**, *115*, 2237.

(82) Lamoureux, G.; Harder, E.; Vorobyov, I. V.; Roux, B.; MacKerell, A. D. *Chem Phys Lett* **2006**, *418*, 245.

(83) English, N. J. *Mol Phys* **2005**, *103*, 1945.

(84) Ismail, A. E.; Grest, G. S.; Stevens, M. J. *J Chem Phys* **2006**, *125*, 014702(1.

(85) Guillot, B. *J Mol Liq* **2002**, *101*, 219.

(86) Ryckaert, J. P.; Ciccotti, G.; Berendsen, H. J. C. *J Comput Phys* **1977**, *23*.

(87) Allen, M. P.; Tildesley, D. J. *Computer Simulation of Liquids*; Oxford University Press: New York, 1987; p 33.

(88) Martyna, G. J.; Tuckerman, M. E.; Tobias, D. J.; Klein, M. L. *Mol Phys* **1996**, *87*, 1117.

(89) Gunsteren, W. F.; Berendsen, H. J. C. *Mol Phys* **1982**, *45*, 637.

(90) Bedrov, D.; Borodin, O.; Smith, G. D. *J Phys Chem B* **1998**, *102*, 5683.

(91) Gaussian 03, R. E., M. J. Frisch, G. W. Trucks, H. B. Schlegel, G. E. Scuseria, M. A. Robb, J. R. Cheeseman, J. A. Montgomery, Jr., T. Vreven, K. N. Kudin, J. C. Burant, J. M. Millam, S. S. Iyengar, J. Tomasi, V. Barone, B. Mennucci, M. Cossi, G. Scalmani, N. Rega, G. A. Petersson, H. Nakatsuji, M. Hada, M. Ehara, K. Toyota, R. Fukuda, J. Hasegawa, M. Ishida, T. Nakajima, Y. Honda, O. Kitao, H. Nakai, M. Klene, X. Li, J. E. Knox, H. P. Hratchian, J. B. Cross, V. Bakken, C. Adamo, J. Jaramillo, R. Gomperts, R. E. Stratmann, O. Yazyev, A. J. Austin, R. Cammi, C. Pomelli, J. W. Ochterski, P. Y. Ayala, K. Morokuma, G. A. Voth, P. Salvador, J. J. Dannenberg, V. G. Zakrzewski, S. Dapprich, A. D. Daniels, M. C. Strain, O. Farkas, D. K. Malick, A. D. Rabuck, K. Raghavachari, J. B. Foresman, J. V. Ortiz, Q. Cui, A. G. Baboul, S. Clifford, J. Cioslowski, B. B. Stefanov, G. Liu, A. Liashenko, P. Piskorz, I. Komaromi, R. L. Martin, D. J. Fox, T. Keith, M. A. Al-Laham, C. Y. Peng, A. Nanayakkara, M. Challacombe, P. M. W. Gill, B.

Johnson, W. Chen, M. W. Wong, C. Gonzalez, and J. A. Pople, Gaussian, Inc., Wallingford CT, 2004.

(92) Becke, A. D. *Phys Rev A* **1988**, *38*, 3098.

(93) Becke, A. D. *J Chem Phys* **1992**, *98*, 1372.

(94) Becke, A. D. *J Chem Phys* **1992**, *98*, 5648.

(95) Lee, C.; Yang, W.; Parr, R. G. *Phys Rev B* **1988**, *37*, 785.

(96) Kendall, R. A.; Dunning, T. H. *J Chem Phys* **1992**, *96*, 6796.

(97) Borodin, O. *J Phys Chem B* **2009**, *113*, 11463.

(98) Smith, G. D.; Borodin, O. In *Molecular Simulations Methods for Predicting Polymer Properties.*; Galiatsatos, V., Ed.; John Wiley & Sons, Inc.: New Jersey, 2005; p 47.

(99) Vorobyov, I.; Anisimov, V. M.; Greene, S.; Venable, R. M.; Moser, A.; Pastor, R. W.; MacKerell, A. D. *J Chem Theory Comput* **2007**, *3*, 1120.

(100) Yu, H.; van Gunsteren, W. F. *Comp Phys Commun* **2005**, *172*, 69.

(101) Cieplak, P.; Dupradeau, F. Y.; Duan, Y.; Wang, J. *J Phys Cond Matter* **2009**, *21*, 1.

(102) www.wasatchmolecular.com.

(103) Moore, W. J. *Physical Chemistry*; Prentice-Hall, Inc., Englewood Cliffs: New Jersey, 1972; p 913.

(104) Borodin, O.; Smith, G. D. *J Phys Chem B* **2009**, *113*, 1763.

(105) Boys, S. F.; Bernardi, F. *Mol Phys* **1970**, *19*, 553.

(106) Waldman, M.; Hagler, A. T. *J Comp Chem* **1993**, *14*, 1077.

(107) Lennard-Jones, J. E.; S., F. R.; Devonshire, A. F. *Proceedings of the Royal Society of London* **1937**, 53.

(108) Lennard-Jones, J. E.; F.R.S.; Devonshire, A. F. *Proceedings of the Royal Society of London* **1937**, *CLXV*, 1.

(109) Buckingham, R. A. *Proceedings of the Royal Society of London* **1938**, *168*, 264.

(110) Simkin, B. Y.; Sheikhet, I. I. In *Quantum Chemical and Statistical Theory of Solutions: A Computational Approach.*; Ellis Horwood Limited: New York, 1995; p 155.

(111) Baker, C. M.; MacKerell, A. D. *J Mol Model* **2009**, *16*, 567.

(112) Hanke, E.; Schulz, U.; Kaatze, U. *Chem Phys Chem* **2007**, *8*, 553.

(113) Sandell, L. S.; Goring, D. A. I. *Die Makromolekulare Chemie* **1970**, *138*, 77.

(114) Kjellander, R.; Florin, E. *J Chem Soc Faraday Trans* **1980**, *77*, 2053.

(115) Ben-Naim, A.; Marcus, Y. *J Chem Phys* **1984**, *81*, 2016.

(116) Ben-Naim, A. *Molecular Theory of Solutions;* Oxford University Press: New York, 2006; p 203.

(117) Jorgensen, W. L.; Blake, J. F.; Buckner, J. K. *Chem Phys* **1989**, *129*, 193.

(118) Li, L. W.; Davande, H.; Bedrov, D.; Smith, G. D. *J Phys Chem B* **2007**, *111*, 4067.

(119) Bedrov, D.; Smith, G. D.; Davande, H.; Li, L. W. *J Phys Chem B* **2008**, *112*, 2078.

(120) *CRC Handbook of Chemistry and Physics*, Lide, D. R., Ed.; CRC Press: Boca Raton, 2003; p 2616.

(121) Daivis, P. J.; Evans, D. J. *J Chem Phys* **1994**, *100*, 541.

(122) Mondello, M.; Grest, G. S. *J Chem Phys* **1997**, *106*, 9327.

(123) Cabani, S.; Gianni, P.; Mollica, V.; Lepori, L. *J Sol Chem* **1981**, *10*, 563.

(124) Cabani, S.; Mollica, V. *J Chem Soc Faraday Trans* **1978**, *74*, 2667.

(125) Kelly, C. P.; Cramer, C. J.; Truhlar, D. G. *J Chem Theory Comput* **2005**, *1*, 1133.

(126) Rovere, M.; Heermann, W.; Binder, K. *J Phys Cond Matter* **1990**, *2*, 7009.

(127) Sigma-Aldrich Regulatory & Safety Data, w. s. c., 1(1), 213B.

(128) Cahn, J. W.; Hilliard, J. E. *J Chem Phys* **1958**, *28*, 258.

(129) Mülders, T.; Krüger, P.; Swegat, W.; Schlitter, J. *J Chem Phys* **1995**, *104*, 4869.

(130) Jorgensen, W. L.; Jenson, C. *J Comput Chem* **1998**, *19*, 1179.